ABSTRACT

A PRECIPITATION ORGANIZATION CLIMATOLOGY FOR NORTH CAROLINA: DEVELOPMENT AND GIS-BASED ANALYSIS

by

Christopher M. Zarzar

July 2014

Director of Thesis: Dr. Tom Rickenbach

Major Department: Geography, Planning, and Environment

A climatology of precipitation organization is developed for the Southeast United States and is analyzed in a GIS framework. This climatology is created using four years (2009-2012) of daily-averaged data from the NOAA high-resolution multi-sensor precipitation estimation (MPE) dataset, specifically the radar-based quantitative precipitation estimation (QPE) product and the mosaic reflectivity. The analysis associates precipitation at each pixel with the spatial scale of precipitation organization, either a mesoscale precipitation feature (MPF) or isolated storm. While the long-term averaged precipitation totals of these systems may be similar, their hydrological and climatological impacts are very different, especially at a local scale. The classification of these modes of precipitation organization in the current precipitation climatology provides information beyond standard precipitation climatologies that will benefit a range of hydrological and climatological applications.

This study focuses on North Carolina and takes advantage of a GIS framework to examine hydrological responses to different modes of precipitation organization. Specifically, the following questions are addressed: First, what are the discharge response characteristics to precipitation events in different watersheds across the state, from the mountains to the coastal plain? Second, what are the different impacts on watershed discharge between MPF precipitation and isolated precipitation? We first present seasonal and annual composites of precipitation and duration of MPF and isolated storms across three regions of North Carolina: the western mountains, the central Piedmont, and the eastern coastal plain. Further analysis in a GIS framework provides information about the impacts this seasonal and geographic variability in precipitation has on watershed discharge. This analysis defines five watersheds in North Carolina based on five North Carolina river basins using ArcGIS watershed delineation techniques. The amount of precipitation that comes from MPF and isolated convection in each watershed is estimated using ArcGIS and QPE data from a climatology of precipitation organization. Comparing these estimates to USGS streamflow data provides information about the impact different modes of precipitation organization have on watershed discharge in North Carolina.

It was found that precipitation from MPF and isolated events had substantial spatial and temporal variability. While MPF average daily precipitation was greatest in the winter, isolated average daily precipitation was greatest in the summer. This resulted in seasonal and spatial variations in precipitation-discharge correlations. Precipitation originating from MPF events produced stronger precipitation-discharge correlations in the winter and fall than in the summer and spring, while most isolated

precipitation-discharge correlations were relatively weak. Additionally, the watersheds in the western mountains experienced stronger correlations with a shorter time lag than coastal watersheds. It was determined that much of this spatial variability in precipitation-discharge correlations could be explained by watershed characteristics. Overall, it was found that MPF precipitation is the main mode of precipitation organization that drives daily watershed discharge, and differences in watershed precipitation-discharge lag times can be best explained by the watershed characteristics.

A PRECIPITATION ORGANIZATION CLIMATOLOGY FOR NORTH CAROLINA: DEVELOPMENT AND GIS-BASED ANALYSIS

A Thesis

Presented To the Faculty of the Department of Geography, Planning, and Environment

East Carolina University

In Partial Fulfillment

of the Requirements for the Degree

Master of Arts in Geography

by

Christopher M. Zarzar

July 2014

A PRECIPITATION ORGANIZATION CLIMATOLOGY FOR NORTH CAROLINA:

DEVELOPMENT AND GIS-BASED ANALYSIS

by

Christopher M. Zarzar

July 2014

APPROVED BY:

DIRECTOR OF
DISSERTATION/THESIS: _____
(Thomas M. Rickenbach, PhD)

COMMITTEE MEMBER: _____
(Thomas W. Crawford, PhD)

COMMITTEE MEMBER: _____
(Rosana Nieto Ferreira, PhD)

CHAIR OF THE DEPARTMENT
OF GEOGRAPHY, ENVIRONMENT, AND PLANNING: _____
(Burrell E. Montz, PhD)

DEAN OF THE
GRADUATE SCHOOL: _____
(Paul J. Gemperline, PhD)

ACKNOWLEDGEMENTS

This study was funded in part by a grant (AGS-1118141) from the National Science Foundation's Division of Atmospheric and Geospatial Science, specifically the Climate and Large-Scale Dynamics program and the Physical and Dynamic Meteorology program.

Most importantly, I need to thank my family, Michael, Krista and Katie, who make so much possible for me. Their support, help, and guidance in all aspects of my life have been vital to my achievements and I cannot thank them enough for all that they do. I would like to thank my advisor, Dr. Tom Rickenbach, for his tremendous support and guidance along the way. I was extremely lucky to have him as my mentor and I have learned an incredible amount under his advisement. I would also like to thank my committee members, Dr. Rosana Nieto Ferreira and Dr. Tom Crawford, who always made time to help me and to share ideas. A special thank you to Dr. Burrell Montz who somehow created time to help whenever I needed assistance. Thank you to all the Department of Geography, Environment, and Planning. I could not have asked for a better experience. The department is a close-knit community and the friends I have made along the way have become lifelong friends. Their support and help in my work and in the simple enjoyments of life are things I will never forget, and for all of this I am grateful. Lastly, thank you to my dog Leila. Everyone who knows her understands how much of a gift she is to have around.

TABLE OF CONTENTS

LIST OF TABLES xi

Introduction 1

Review of Literature 3

2.1 Midlatitude Cyclones 3

2.2 Precipitation Modes of Organization 7

2.3 Precipitation Climatologies 11

2.4 Precipitation Organization Climatologies 14

2.5 Surface Influences on Precipitation and Hydrology 16

2.5.1 Factors Influencing Discharge 19

2.6 Spatial Analysis 23

2.7 Purpose 26

Data and Methods 28

3.1 Climatology Development 28

3.1.1 Radar Data 29

3.1.2 Precipitation Organization Identification 31

3.2 Analysis of the Climatology 32

3.2.1 Regional and Local Analyses 32

3.2.2 Study Area 33

3.2.4 North Carolina River Basins 36

3.3 USGS Stream Gauge Data 53
3.4 ArcGIS 55
3.4.1 Data Conversion 55
3.4.2 Watershed Delineation 56
3.4.3 Local Statistics of Precipitation within the Watersheds 60
3.5 Watershed Precipitation and Discharge Correlations 62
3.6 Precipitation Pattern Analysis 64
Results 66
4.2 Precipitation and Hydrology Connections 72
4.2.1 Visual Assessment 73
4.3 Precipitation-discharge Correlations 79
4.3.1 Four Year Annual Correlations 97
4.3.2 Four Year Seasonal Correlations 98
4.3.3 Event-based Correlations 101
4.3.4 Annual Event-based Correlations 102
4.3.5 Seasonal Event-based Correlations 103
Discussion 105
5.1 Watershed Characteristics 105
5.2 Seasonal Precipitation Distributions 107
5.3 Precipitation Organization Characteristics 110

Conclusions..... 112

References.....117

APPENDIX A: ArcGIS Tools Developed.....127

APPENDIX B: Event Based Analysis Dates.....129

LIST OF TABLES

1. River basin attributes 39
2. Watershed attributes 39
3. Percentages of land cover types 38
4. USGS selected stream gauge stations 51
5. 4-year precipitation-discharge correlations for all rain events. 78
6. 4-year precipitation-discharge correlations for MPF rain events. 79
7. 4-year precipitation-discharge correlations for Isolated rain events 80
8. 4-year seasonal precipitation-discharge correlations for French Broad 84
9. 4-year seasonal precipitation-discharge correlations for Broad 85
10. 4-year seasonal precipitation-discharge correlations for Yadkin-Pee Dee 86
11. 4-year seasonal precipitation-discharge correlations for Lumber 87
12. 4-year seasonal precipitation-discharge correlations for Neuse 88
13. Event-based precipitation-discharge correlations for all rain events 89
14. Event-based precipitation-discharge correlations for MCS rain events. 87
15. Event-based precipitation-discharge correlations for isolated rain events. 88
16. Event-based seasonal precipitation-discharge correlations for French Broad. ... 89
17. Event-based seasonal precipitation-discharge correlations for Broad 90
18. Event-based seasonal precipitation-discharge correlations for Yadkin-Pee Dee 91
19. Event-based seasonal precipitation-discharge correlations for Lumber 92
20. Event-based seasonal precipitation-discharge correlations for Neuse. 93
21. Number of all rain events included in event-based analysis 99

LIST OF FIGURES

1. The life stages of a midlatitude cyclone 4
2. Differences (%) between LPJmL estimations 22
3. Southeast U.S. study region. 30
4. Data collection process flowchart. 31
5. Precipitation organization identification algorithm diagram 32
6. Regions of North Carolina 33
7. Relief map of North Carolina. 34
8. North Carolina river basins 36
9. Land cover map of the French Broad watershed 40
10. Land cover map of the Broad watershed 43
11. Land cover map of the Yadkin-Pee Dee watershed 46
12. Land cover map of the Lumber watershed 49
13. Land cover map of the Neuse watershed. 52
14. The five river basins and the five watershed regions 57
15. Diagram of flow accumulation raster 58
16. Daily averaged seasonal precipitation 61
17. Preparation of data flowchart. 62
18. Southeast seasonal composite reflectivity 67
19. North Carolina seasonal composite reflectivity. 69
20. Seasonal composite precipitation across North Carolina 71
21. Hydrograph for the French Broad watershed. 74
22. Hydrograph for the Broad watershed 75

23. Hydrograph for the Yadkin-Pee Dee watershed 76
24. Hydrograph for the Lumber watershed 77
25. Hydrograph for the Neuse watershed 78
26. Example events selected from each watershed 80
27. Weighted seasonal composites 108

Chapter 1

Introduction

Due to changes in land use, increasing population (U.S. Census Bureau 2013), and climate change (IPCC 2007), knowledge of how water reaches the Earth's surface is essential to determining how best to manage water resources and mitigate hydrological hazards. Water can reach Earth's surface in a number of ways. Mesoscale precipitation features (MPFs) are widespread, long-lived precipitation events that encompass all widespread convective rain/snow and stratiform rain/snow events. A well-known subset of MPFs are mesoscale convective systems (MCSs). Typically, MCS events are characterized by a line of intense convective precipitation and a region of widespread light to moderate stratiform precipitation (Parker and Johnson 2000). In contrast, isolated convective cells may be short-lived, but these cells can produce intense convective precipitation and localized flood hazards (Wilhelmi and Morss 2013). Tropical cyclones transport large amounts of momentum, heat, and precipitation from the tropics to the polar regions (Emanuel 2003) and have the potential to initiate large-scale flood events (Ashley and Ashley 2008). Frozen precipitation can stay in a single location for long periods creating hazardous conditions before melting and continuing in the hydrological cycle (Graybeal and Leather 2006). A clear accounting of regional, seasonal, and interannual changes in these different precipitation modes of organization will lead to improved water management practices, agriculture planning, hydrologic prediction, climate prediction, and hazards mitigation.

Previous work will help demonstrate why it is important to gain a better understanding of the regional, seasonal, and interannual changes in these different

precipitation modes of organization. In the following review, the synoptic scale environments in which the different precipitation modes of organization originate will be described. Next, the characteristics of the different mesoscale precipitation modes of organization will be defined and then followed by the different methods employed to study these events. The different techniques used to develop precipitation climatologies for research are then discussed. Following this, the local factors influencing precipitation and hydrology will be discussed. Additionally, the importance of integrating GIS into atmospheric research will be expressed by examining work that has used GIS to conduct spatial inquiries. This section concludes with a summary of the goals of the current study.

Chapter 2

Review of Literature

2.1 Midlatitude Cyclones

First defined by Bjerknes (1919), midlatitude cyclones, also known as extratropical cyclones, are driven by temperature gradients between the subtropics and polar regions, and can be fundamentally defined as a weather system with frontal boundaries extending from a central low pressure. The structure of these systems and the associated precipitation characteristics of these cyclones have been well-documented (Cunningham 1951; Carlson 1980; Houze and Hobbs 1982; Rutledge and Hobbs 1983; Shultz and Mass 1993; Browning and Roberts 1994; Field and Wood 2007; Wallace and Hobbs 2006).

One of the most distinct characteristics of these midlatitude disturbances is the comma cloud pattern produced by the airflow through extratropical cyclones (Carlson 1980). The main wind-flows of a midlatitude cyclone that produce this unique cloud structure include the northward moving warm air and southward moving cold air (Fig. 1).

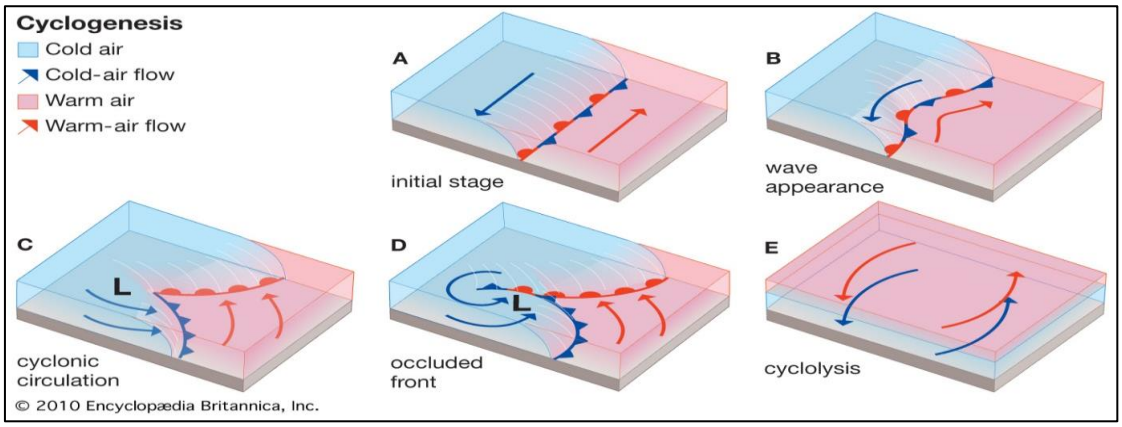

Figure 1. The life stages of a midlatitude cyclone. The red shaded region indicates the warm sector while the blue shaded region behind the cold front indicates the cold sector.

Typically, an extratropical cyclone will have a region of stratiform precipitation near the leading warm front. This precipitation is driven by a "seeder-feeder" process where ice crystals aloft descend through the lower level stratiform cloud shield and aggregate until they fall as stratiform precipitation (Cunningham 1951; Houze and Hobbs 1982; Rutledge and Hobbs 1983). Following the passage of this warm front, the warm sector, as defined by Wallace and Hobbs (2006), is the region between the leading warm front and the trailing cold front (Fig. 1). Houze and Hobbs (1982) discuss the wide variability of precipitation organization and intensity in the warm sector. This region of the cyclone has been a focus of research because of the hazardous weather phenomena produced in the warm sector (Browning and Roberts 1994; Carlson 1980; Schultz and Mass 1992).

Browning (1985) explains that in the Northern Hemisphere, a low level jet, also called the ‘warm conveyor belt’, is the main precipitation-producing wind feature in an extratropical cyclone. This warm conveyor belt begins south of the midlatitude cyclone and flows northward along the length of the surface cold front. It provides low-level moisture and lift that can produce a line of heavy rain that coincides with the surface cold front and a broad region of vertically oriented light to moderate rain in the region adjacent to the surface cold front (Browning 1985). However, Browning (1985) points out that the most vigorous convection does not coincide with the cold front; rather, this convection takes place 200-300 km ahead of the cold frontal boundary. After the passage of the cold front, cold continental polar air begins to flow southward within the

cold sector of an extratropical cyclone. This region is typically the coolest region of an extratropical cyclone and is characterized by northerly winds, clearing skies, and low dewpoints.

While case studies have led to the development of extratropical cyclone conceptual models, this method of research is dependent upon the author's selection of the event. As a result, these case studies tend to focus on abnormally strong systems and explosive cyclones (Browning and Roberts 1994). More recently, research has taken advantage of multisensor datasets and the National Center for Environmental Prediction (NCEP) reanalysis dataset—a global, 2.5° x 24-hr horizontal resolution dataset that integrates past observations and numerical weather prediction (NWP) models (Kalnay et al. 1996)—to study the trends and evolution of extratropical cyclones (McCabe et al. 2000; Mote et al. 1996; Nguyen and DeGaetano 2011). For example, McCabe et al. (2000) created a 39-year (1959-1997) extratropical cyclone dataset for Northern Hemisphere winters using sea level pressure (SLP) fields from NCEP reanalysis data. They discovered that from 1959-97, the frequency of extratropical cyclones affecting the midlatitudes decreased, but the frequency of extratropical cyclones affecting higher latitudes increased. In addition, they found that for both the mid and high latitudes, winter extratropical cyclones have become more intense since 1959. Nguyen and DeGaetano (2011) also found that closed-low (defined as a 30 meter closed contour at 500 hPa) frequency, average precipitation, and extreme precipitation associated with closed-lows have increased in the Northeastern United States. However, Curtis (2006) developed a 38-year (1961-98) climatology of cold season extratropical cyclones that affect the Southeast United States (SE U.S.) using NCEP

reanalysis and found that ENSO (the El Niño/Southern Oscillation) has a significant impact on the frequency of extratropical cyclones. Curtis (2006) discovered that the number of extratropical cyclones as well as the number of different genesis regions of these cyclones increased during El Niño years compared to La Niña and neutral years. However, no significant trend for all extratropical cyclones over the period was determined.

Davis and Dolan (1993) determined that it was important to classify extratropical cyclones based on their region of genesis because extratropical cyclones form along baroclinic zones and require the support of the jet stream. Their results suggest that there is a strong relationship between the location of extratropical cyclone genesis and extratropical cyclone intensity. Similarly, Senkbeil et al. (2012) classified extratropical cyclones affecting the Southeast U.S. based on five regions of origin including the Rio Grande, Gulf of Mexico, Great Plains, Southeast U.S., and Florida, and found the resulting precipitation pattern of systems varied greatly across the SE U.S. with the greatest precipitation totals coming from storms that originated in the Gulf of Mexico. To determine the general precipitation patterns associated with each extratropical cyclone, Senkbeil et al. (2012) used 24-hr cumulative precipitation data from the NOAA/National Climatic Data Center's (NCDC's) station locator webpage. Another method, applied by Nieto-Ferreira et al. (2013), used NCEP reanalysis data from 1998-2010 and identified a midlatitude cyclone when eastern North Carolina (NC) experienced at least a 2 mb pressure drop over a 24-hr period. They used high-resolution National Aeronautics and Space Administration's Tropical Rainfall Measuring Mission (NASA TRMM) daily precipitation data to analyze the precipitation distribution

associated with the passage of midlatitude systems. While the results of Senkbeil et al. (2012) agree with those of Curtis (2006), Nieto-Ferreira et al. (2013) found a similar frequency of extratropical cyclones across the SE U.S. during all ENSO phases. These contradicting results demonstrate the variation of extratropical cyclone activity due to a range of physical, locational, periodical, and methodological factors.

2.2 Precipitation Modes of Organization

The importance of identifying precipitation features associated with large scale dynamical forcing was presented in the early work of Leary and Houze (1979). They coined the term mesoscale precipitation feature (MPF) to generalize six precipitation features whose maximum horizontal dimensions ranged 190-580 km and were associated with synoptic scale dynamical forcing. Since then, studies have defined a subset of an MPF as a mesoscale convective system (MCS) if it is of convective origin, exceeds a length scale extent of 100 km (Houze et al. 1990), and persists for more than three hours (Parker and Johnson 2000). MCSs have been a focus of research because they often produce severe weather and make a significant contribution to total precipitation in the tropics (Nesbitt et al. 2006, Rickenbach and Rutledge 1998) and over land (Nesbitt et al. 2006, Rickenbach et al. 2012). Geerts (1998) surveyed MCSs across the SE U.S. using radar composites from 1994-1995, finding that while these systems occur year around, they tend to be larger and longer-lived in the winter than the summer, but are more frequent in the summer months. Using an array of sensing techniques including radar composites, National Weather Service (NWS) rawinsonde observations, the NOAA profiler network, and the NCEP gridded reanalysis, Parker and Johnson (2000) analyzed the characteristics and synoptic environments of MCSs and

found that there are three main precipitation configurations possible in MCSs: leading stratiform (LS), parallel stratiform (PS) and trailing stratiform (TS). No matter the configuration of these systems, research has found that MCSs tend to occur within the warm sector of an extratropical cyclone and have a line of intense convective precipitation and a large stratiform precipitation shield (Houze et al. 1990; Kane et al. 1987; Parker and Johnson 2000).

It is important to distinguish between regions of stratiform and convective precipitation because the heating and hydrological impacts associated with these two types of precipitation are very different (Houze 1989; Houze 1997; Sui et al. 2007; Yang and Smith 2008). Stratiform precipitation can be characterized by light-to-moderate precipitation rates. Stratiform precipitation tends to have a homogenous appearance in radar imagery with a 'bright band' signature depicting the location of the melting layer in the feature (Houze 1989; Steiner et al. 1995; Houze 1997). While stratiform precipitation may be less intense than convective precipitation, it is important to categorize stratiform precipitation independently because its areal coverage makes a significant contribution to the overall hydrological cycle and produces a much different vertical heating profile than convective precipitation (Houze 1989).

Convective precipitation tends to be associated with high rain rates and has strong radar reflectivity gradients. Churchill and Houze (1984) identified regions of convection as areas with precipitation rates that double the precipitation rate in the surrounding area. Another convection identification method has used a 40 dBZ radar reflectivity threshold to identify regions of convection (Sui et al. 2007; Churchill and Houze 1984; Houze 1993). More recently, Zhang et al. (2011) developed a National

Mosaic and Multi-Sensor QPE (NMQ) system that identifies a radar reflectivity pixel as convective precipitation if it meets at least one of the following three requirements: 1) reflectivity at any height in the column is greater than 50 dBZ, 2) reflectivity is greater than 30 dBZ at the −10°C height or above, or 3) one or more cloud-to-ground lightning flashes occurred in the vicinity of the pixel within the last 5 min (Zhang et al. 2011, p. 1328).

Because convective precipitation delivers a significant amount of water to a localized area, it tends to produce more immediate hydrological hazards than stratiform precipitation (Brooks and Stensrud 2000; Curriero et al. 2001; Wilhelmi and Morss 2013). For example, Curriero et al. (2001) found a correlation between extreme convective precipitation and waterborne disease outbreaks due to increased rates of runoff allowing for the transport of hazardous microbes. Wilhelmi and Morss (2013) described how flash floods associated with convective precipitation have the potential to be life threatening due to the intensity and rapid onset of flash flooding.

Convective precipitation tends to be studied within the context of MCSs, but convective precipitation often occurs as isolated “popcorn” storms during the warm season. These isolated cells can occur independent of the typical synoptic environment associated with convection. In fact, Nieto-Ferreira (2013) found that in the Carolinas, about 30% of summertime precipitation is associated with a midlatitude cyclone compared to more than 70% in the winter months. During the warm season, these isolated cells often arise due to local forcing mechanisms, such as orographic lift and localized heating. This precipitation organization is not emphasized in past research because it was thought to be a small player in the annual mean precipitation; however,

these isolated cells can make significant contributions to seasonal precipitation (Rickenbach and Rutledge 1998; Rickenbach et al. 2014). While studying oceanic convection over the warm pool of the Western Pacific, Rickenbach and Rutledge (1998) found that while the majority of precipitation was associated with MCSs, isolated convective cells still made a significant contribution (12%) to overall precipitation. They suggest that while MCSs tend to be the mesoscale precipitation system focused on in research, isolated convective cells make a significant contribution to precipitation production, and attention should be given to both MCSs and isolated convective cells.

Tropical cyclones (TCs) occur less often than other mesoscale precipitating events, but TCs have been a focus of research because they transport large amounts of water and heat northward from the tropics and have the potential to initiate large-scale flood events (Ashley and Ashley 2008). These systems develop in a number of different ocean basins and in a range of different environments. In the North Atlantic Ocean, TCs develop from tropical cloud clusters (TCCs), which are typically (60% of cases) produced by easterly moving waves off the African coast (Chen et al. 2008). While these systems affect the Southeast U.S. less often than other precipitation systems, they make a significant contribution to overall precipitation. Using 8 years of satellite-derived precipitation data, Shepherd et al. (2007) estimated that from 1998-2006, TCs contributed about 8% of the SE U.S. warm season precipitation. More recently, Prat and Nelson (2013) used twelve years (1998-2009) of TRMM precipitation data to assess the precipitation contribution of tropical cyclones in the SE U.S. They found that precipitation contributions from tropical cyclones are 8%-12% for inland areas and up to 15%-20% for coastal areas. Knight and Davis (2009) found similar contributions from

TCs using surface rain gauge data from 1972-2007. They found that TCs have made an increased contribution of 5%-10% per decade to extreme precipitation while no significant trends were found in other mesoscale precipitation events. While their results were intriguing, Knight and Davis (2009) acknowledge that it is challenging to capture the true distribution of precipitation for a TC without remote sensing techniques because of the TC's large areal extent, embedded convection, and high winds.

The physical state of precipitation can have very different hydrological impacts. As previously noted, frozen precipitation can stay in a single location for long periods before melting and continuing in the hydrological cycle. Winter weather events can have substantial impacts on daily life and can pose risks to public safety including the loss of power and dangerous road conditions (Rauber et. al 2001). Devastating floods can also occur if this frozen precipitation melts at high rates (Graybeal and Leather 2006). Graybeal and Leathers (2006) quantified the risk of snowmelt flooding for the Appalachia region using data from official weather stations on seasonal time scales from 1971-2000. They found that flooding influenced by snowmelt occurs on average every two years for Pennsylvania and West Virginia and about every ten years for the North Carolina mountains. Overall, a better understanding of these precipitation regimes will improve how they are represented in numerical weather prediction models and climate simulations, which will in turn help forecast accuracy and hazard mitigation.

2.3 Precipitation Climatologies

The utilization of precipitation climatologies has proved to be useful for analyzing trends in precipitation frequencies and intensities. These climatologies have been created using a range of methods and observational techniques. Epstein and Barnston

(1990) created a precipitation climatology from 36 years of rain gauge data from 146 stations scattered around the United States. Their climatology categorized the frequency of days with measurable precipitation within 5-day periods from 1948-1983. Brooks and Stensrud (1999) discussed the need for precipitation climatologies with shorter timescales (< 24 hr) to study flash flood events. Using the Hourly Precipitation Dataset (HPD), they created a climatology of heavy rains on a 3-hr timescale. While Brooks and Stensrud (1999) found that the evolution of their heavy precipitation climatology was comparable to the observed flash flood events, they determined that the 50 km resolution of the data was still too low and missed most of the large precipitation events.

Data voids are unavoidable when using surface observations and can have significant impacts on the accuracy of research attempting to describe precipitation systems with intense precipitation and high spatial variability (Gourley et al. 2009; Knight and Davis 2009). For example, Knight and Davis (2009) found that tropical cyclones make a significant contribution to warm season extreme precipitation in the Southeastern U.S.; however, they note the challenges of representing the true precipitation distribution in a TC with rain gauge data because of spatial limitations and errors introduced by physical factors such as high wind speeds and small-scale embedded convection. To resolve these issues, Brooks and Stensrud (1999) suggest that radar precipitation measurements could be used to develop higher resolution precipitation datasets, but that the development of a radar-derived precipitation dataset that spans a long period will be a significant challenge.

Remote sensing methods have been another approach for developing precipitation climatologies. Although previously limited due to computing and data storage limitations, precipitation climatologies developed from radar data (e.g. Steiner et al. 1995; Overeem et al. 2009) resolve the data voids found in rain gauge climatologies. Radar is a preferred method for the investigation of precipitation characteristics because it can better capture heavy precipitation variability within a system while presenting accurate precipitation estimates (Austin 1987; Gourley et al. 2009; Krajewski and Smith 2002; Wu et al. 2012). As previously mentioned, radar allows the user to identify regions of stratiform precipitation and regions of convective precipitation. In addition, radar allows for the reconstruction of a storm's vertical profile and makes it possible to better analyze embedded features (e.g. hail cores) in a precipitating system (Steiner et al. 1995).

More recently, precipitation climatologies have originated from spaceborne remote sensing techniques (Guirguis and Avissar 2008; Yang and Smith 2008). Using satellite data to develop precipitation climatologies has become increasingly popular since the launch of TRMM and the start of the Global Precipitation Monitoring (GPM) mission (Nesbitt et al. 2006). The passive and active microwave sensors aboard polar orbiting satellites allow for the development of long-term global precipitation climatologies. A recent intercomparison of precipitation estimates from radar, satellite, gauge, and multisensor datasets presented by Gourley et al. (2009) demonstrated the improvements in satellite-derived precipitation estimates. A seasonal comparison between the unadjusted radar and unadjusted satellites data indicated that before quality control measures, precipitation estimates from satellite are superior to the

unadjusted radar. However, it is important to note that the unadjusted radar includes beam blockage and biological target errors, and results will likely vary if quality control measures are applied. While satellite precipitation estimations are continuously improving, precipitation estimates from satellite are still inferior to corrected radar reflectivity estimates as demonstrated by the use of radar precipitation estimates as reference estimates for the validation of numerical models and satellite precipitation estimates (Vasic et al. 2007).

2.4 Precipitation Organization Climatologies

Using composite radar reflectivity data from 1994-95, Geerts (1998) analyzed 398 MCSs and found that MCSs occur most frequently in the summer but persist for a longer period in the winter. While this information has made an important contribution to the literature, a drawback to this type of study is the tendency to focus on specific types of precipitation systems. Except for a rare few, these studies were limited to this type of focused analysis partly due to the lack of accessibility to the computing power necessary to work with large quantities of radar data. Palecki et al. (2005) acknowledged that while past precipitation climatologies provide useful information regarding the general patterns and trends of precipitation and certain convective organization trends, improving our understanding of the global hydrological cycle and numerical modeling will come from climatologies that provide information about all storm precipitation characteristics. Palecki et al. (2005) claim to have made the first attempt at creating an extensive climatology of individual storm precipitation characteristics. Initial results from this climatology indicated decreases in storm total precipitation and duration but increases in storm frequency for the Western U.S. from 1971-2002. In

addition, it was discovered that the eastern U.S. has experienced an increasing trend in storm total precipitation and duration during the winter months from 1971-2002. Although the climatology developed by Palecki et al. (2005) represents important progress toward our understanding of precipitating events, the authors acknowledge the limitations of their work due to the use of rain gauge data and the quality and consistency of rain gauge data. Additionally, rain gauge data limited the authors to a few storm characteristic variables making it impossible to classify the type of mesoscale convective mode that delivered the precipitation.

As expressed by Rickenbach and Rutledge (1998), better understanding of the structure and tendencies of precipitating systems will come from datasets containing the full extent of mesoscale convective modes. In their study, Rickenbach and Rutledge (1998) used 80 days of shipboard radar data collected during the Tropical Ocean Global Atmosphere Coupled Ocean Atmosphere Response Experiment (TOGA COARE) to produce a climatology of mesoscale modes of organization for the equatorial Western Pacific. This study found that linear MCSs were responsible for the majority (80%) of precipitation during the study period. Non-MCS isolated convection occurred the majority (48%) of the time and made a significant contribution (12%) to total precipitation during the study period. This result is intriguing because very little research has investigated the structure and precipitation characteristics of isolated, small-scale convection. However, Rickenbach and Rutledge (1998) showed that these modes of organization have significant impacts to the hydrologic cycle. Therefore, a more complete precipitation climatology would require the integration of the methods applied by Rickenbach and Rutledge (1998) and Palecki et al. (2005).

2.5 Surface Influences on Precipitation and Hydrology

The global hydrological cycle attempts to explain all aspects of water and its transportation across the globe (Oki and Kanae 2006). There are numerous factors and properties we do not fully understand in the global hydrological cycle. For some places, like in North Carolina, gaining a better understanding of these factors is especially important because the majority of rivers in the state originate in North Carolina, and thus all of North Carolina's water resources ultimately derive from precipitation falling within the state. Therefore, it is imperative that we work toward improving our understanding of precipitation delivery so that we can better manage water resources and mitigate hydrologic hazards in a period of rapid population growth, changing landscapes, and a changing climate (Amatya et al. 2006; Qi et al. 2009; Zachary Bean et al. 2007).

One factor that the current study works to gain a better grasp of is the impact that Earth's surface has on the global hydrological cycle. It is known that interactions between Earth's surface and the atmosphere can have important implications for precipitation and hydrology. For example, the topography of the surface can alter precipitation distribution due to orographic lift in mountainous regions (Bleasdale and Chang 1972; Basist et al. 1994; Konrad 1996; Prudhomme and Reed 1998; Rowe et al. 2008). Basist et al. 1994 studied the relationships between topography and mean annual precipitation using four variables: elevation, slope, orientation, and exposure in linear bivariate and multivariate analyses. Where Bleasdale and Chan (1972) previously determined that slope and elevation best explained precipitation variability in mountainous regions, Basist et al. (1994) suggested that the orientation and exposure of the topographic feature to the prevailing wind best explained the interaction of

topography and mean annual precipitation distribution. However, Konrad (1996) acknowledged that seasonal variations and the type of precipitation event are important considerations when investigating the relationship between topography and precipitation. Therefore, Konrad (1996) separated cool and warm season months as well as precipitation intensity when analyzing the relationship between topography and precipitation events in the Southern Blue Ridge Mountains. In the cool season, Konrad (1996) found that elevation and northwest exposure of a feature best explained light precipitation events. This result is consistent with the common northwest flow snow events that occur in the Southern Appalachians after the passage of a midlatitude cyclone (Keighton et al. 2009; Miller 2012). While a moderate relationship existed between light precipitation and exposure in the warm season, elevation explained the greatest variance in light and moderate precipitation events occurring during the warm season months. Most interesting was the drastic change in results when the relationship was analyzed using annual precipitation totals. Konrad (1996) discovered that the strong relationships previously discovered by the separation of cool and warm months were lost in the annual precipitation analysis, reinforcing the importance of analyzing precipitation on seasonal rather than annual timescales.

While studying convective episodes across North Carolina using nine years (1996-2000 & 2002-2005) of composited radar data, Parker and Ahijevych (2007) discovered that the majority of convective episodes originated during the warm season months in the high elevations of the Blue Ridge Mountains. Those systems typically (88% of the time) propagated eastward, often tracking across the full state of North Carolina. They also discovered some (12% of the time) convective systems propagated

westward. While less typical, these systems represent the contributions to convective episodes made by the coastal sea breeze and tropical cyclones (Parker and Ahijevych 2007). Parker and Ahijevych (2007) also suggest that the steep topography of the Blue Ridge Mountains act as an obstacle, finding that only 10% of cases developing west of the mountains successfully crossed into the central and eastern portions of North Carolina.

Other studies have found that land use changes, especially urbanization, can have noticeable impacts on precipitation distribution, frequency, and intensity. Chen and Avissar (1994) used the Regional Atmospheric Modeling System (RAMS) at the Colorado State University (CSU) to model and understand the effects that surface moisture has on precipitation. They found that it is necessary to include surface information in numerical models, including large-scale and regional models, because the horizontal surface moisture distribution had substantial implications for precipitation onset, intensity, and distribution (Chen and Avissar 1994; Thielen et al. 2000). Carlson and Arthur (2000) further analyzed the influence land use has on precipitation and found that if 30% of a 1 km^2 parcel of agricultural land were urbanized, the surface temperature would increase by 58%. If that parcel of land were located near a large body of water, the surface temperature would increase by 138% resulting in a 14% decrease in moisture, likely due to increased evaporation.

Baik et al. (2001) used the Advanced Regional Prediction System (ARPS), a three-dimensional, nonhydrostatic, fully compressible, finite-difference model, to simulate interactions between urban heat islands and convection. Simulations suggested that anomalous warming from urban land-use could initiate convection and

enhance precipitation downwind of urban areas. Shepherd et al. (2002) confirmed the simulations of Baik et al. (2001) using three years (1998-2000) of data from the precipitation radar (PR) on the TRMM satellite. They found that urban heating increased precipitation 30-60 km downwind of the urban center (Shepherd et al. 2002; Shepherd and Burian 2003) by 28% compared to areas upwind from the urban area.

2.5.1 Factors Influencing Discharge

River discharge is defined by USGS as “the volume of water moving down a stream or river per unit time.” Factors like soils characteristics, relief, land use, precipitation, and antecedent precipitation influence how much water is discharged from a stream at any given time. Therefore, the influences on precipitation due to surface interactions have important implication for watershed hydrology and potential hydrologic hazards. In general, more rain means more water that can either infiltrate the surface or runoff into the river system. However, in reality there is more complexity in this relationship because the resulting discharge can be quite different depending on the type, duration, and intensity of the precipitation (Córdova and Rodríguez-Iturbe 1985; Goel et al. 2000; Kao and Govindaraju 2007; Kurothe et al. 1997). Hewlett et al. (1977) separated out five storm variables—storm precipitation, antecedent flow, season, duration, and intensity—and used a 30 year rain gauge based precipitation record to assess their contributions to storm flow in a forested watershed. They found that storm intensity was responsible for only 4.7 percent of the total variation in peak flow whereas the other four variables were responsible for 72 percent of the total variation. Therefore, Hewlett et al. (1977) came to the conclusion that while it is obvious that precipitation intensity may have an important influence on storm flow for compacted fields,

impervious surfaces, and local regions of saturated ground, it is not an important contributor when assessing storm flow for an entire forested watershed (Hewlett et al. 1977; Hewlett et al. 1984).

As suggested by Hewlett et al. (1977), studies have used numerical modeling to show that the separation of precipitation intensity and duration is an important consideration when assessing discharge for smaller or urbanized watersheds. Using a bivariate exponential distribution model that defined precipitation intensity and duration as marginal variables, Córdova and Rodríguez-Iturbe (1985) showed that precipitation intensity and duration are not independent of each other; rather, they are actually negatively correlated. With this in mind, Kurothe et al. (1997) developed a stochastic precipitation model that accounted for the negative correlation between precipitation intensity and duration. They ran this model for the Davison watershed in North Carolina and found that including the intensity-duration correlation in their model produced much different impacts on stream discharge than previous studies that did not take this relationship into account.

More recent studies have shifted their focus toward what may happen to watershed discharge in future climate conditions. From numerical model simulations in the Trent river basin in North Carolina, Sun et al. (2009) found that when air temperature was increased by 1.11°C each day, the resulting water yield decreased by 6% due to changes in evapotranspiration. More impressive was the extreme sensitivity streamflow had to changes in precipitation. When simulated precipitation was increased by 10%, evapotranspiration was increased by about 4% while streamflow was increased by 23%. Knowing how sensitive watershed discharge can be to increases or decreases

in precipitation is important because it demonstrates how important accurate precipitation measurements are for the correct calculations of streamflow for ungauged rivers (Biemans et al. 2009; Curtis et al. 2007). While quantifying the uncertainty of discharge calculations due to uncertainty in seven globally gridded precipitation datasets, Biemans et al. (2009) discovered that there was an average uncertainty of 30% in the precipitation datasets which led to as much as 90% uncertainty for some of the discharge calculations from the 294 river basins they analyzed worldwide (Fig. 2).

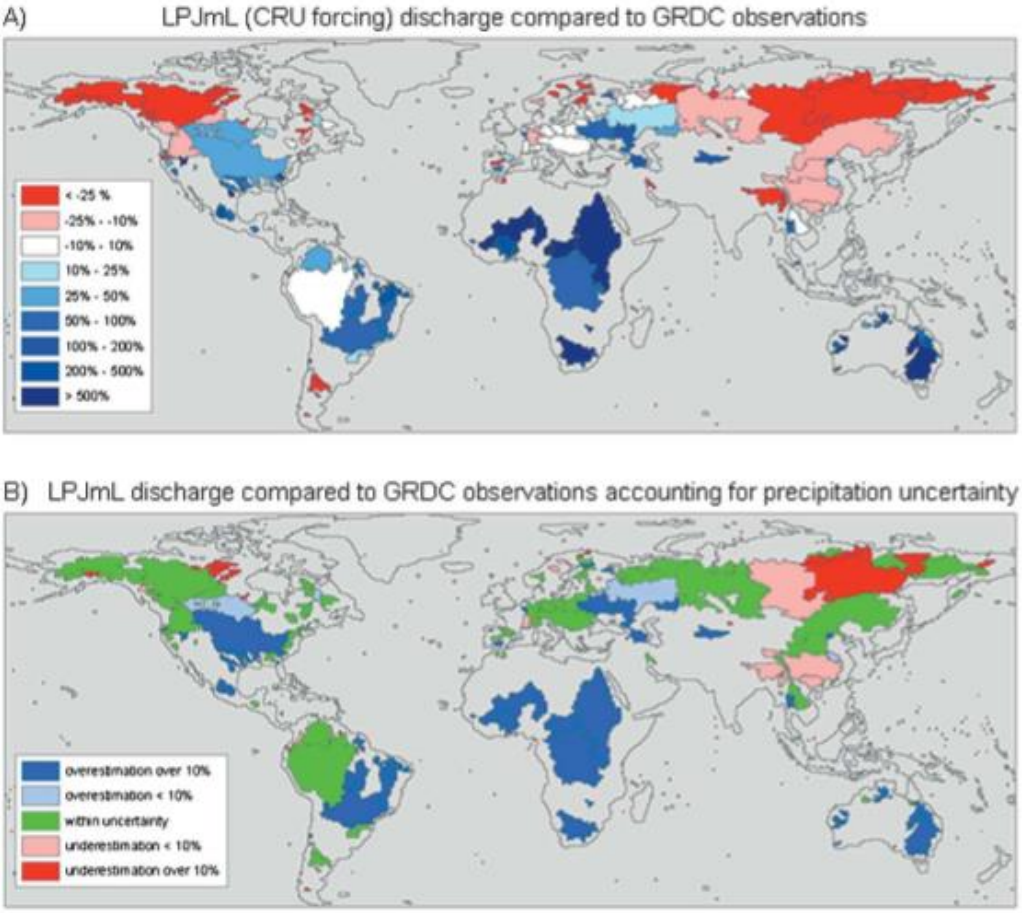

Figure 2. Borrowed from Biemans et al. 2009. (a) Differences (%) between Lund–Potsdam–Jena managed land (LPJmL) model estimations of discharge based on CRU climatic forcing and GRDC streamflow observations. (b) Basins for which the observed discharge lies either within or outside of the simulated range under the different precipitation datasets.

While surface characteristics can indirectly impact streamflow through the altering of precipitation, other surface factors like soils characteristics, relief, and land use have direct implications to the resulting streamflow. Sandier soils tend to be more permeable and allow for more rain water infiltration and water absorption which leads to less storm runoff and lower stream discharge rates (USDA NRCS 2005). More impermeable rocks and clay soils resist rainwater infiltration, leading to greater storm runoff and higher stream discharge rates. The relief of an area can have substantial impacts on the stream discharge characteristics. Steeper terrain will aid in the

acceleration of the water due to gravity, meaning that rain water will have less time to infiltrate the surface before it moves into the river system. Therefore, terrain has a greater influence on runoff response in mountainous watersheds than in flatter coastal watersheds where soil composition dominates the runoff response (La Torre Torres et al. 2011; Markewich et al. 1990).

Land use can have some of the greatest impacts on a stream's discharge rates. Homogenous landscapes created by agricultural activities decrease surface friction allowing water to reach the stream quicker (USDA NRCS 1986). Urban areas have impervious surfaces (e.g. roads, rooftops, and sidewalks) that make it impossible for water to infiltrate the surface and diverts water straight into the river system (Hollis 1975). While in a heavily forested area, an average of 70% of annual precipitation can be lost through evapotranspiration in low relief, heavily forested watersheds leaving the remaining 30% of the initial precipitation available to either infiltrate the ground water or contribute to the peak river discharge (Amatya et al. 2002; La Torre Torres et al. 2011; Lu et al. 2005; Sun et al. 2010). Therefore, the lack of vegetation in these rural and urban regions leads to a loss in absorption of the water by flora and less evapotranspiration of the water, leading to greater stream discharge. Hollis (1975) assessed that the increased stream discharge due to urbanization in general can increase the frequency of small floods and can even double areas impacted by 100 year flood events if the paved area of a basin is increased by 30%.

2.6 Spatial Analysis

A Geographic Information System (GIS) is a powerful tool that has the ability to synthesize data from multiple sources and effectively display and analyze the combined

information (Gunes et al. 2000). While the sophisticated mapping capabilities of a GIS are popular in the atmospheric sciences, the advanced spatial analysis tools available in a GIS have been underutilized in the atmospheric community (Yuan 2005). However, the numerous advantages that would result from the use of GIS in atmospheric sciences research are gaining recognition. Where previous GIS applications were too slow for meteorological purposes, increased access to high performance workstations have helped to make GIS a more useful framework for meteorological inquiries (Shipley 2005).

Wilhelmi and Brunskill (2003) outline these advantages as they revisit a GIS workshop conducted at the National Center for Atmospheric Research (NCAR). This workshop brought representatives of the GIS and atmospheric sciences communities together to discuss the benefits, limitations, and future prospects of GIS in atmospheric sciences research. An array of benefits from GIS, including downscaling-techniques and the increased access and usability of weather and climate data outside the atmospheric community, greatly outweighed the limitations of the platform. Overall, the ability to couple and analyze surface and atmospheric data led those in attendance at the NCAR GIS workshop to conclude that it is imperative to integrate GIS into atmospheric research.

The greatest examples integrating atmospheric data into a GIS come from the emergency management community. GIS is an invaluable tool to emergency management mitigation, response, and recovery operations because of the precise geographic accuracy required in hazard mitigation (Gunes et al. 2000; Cova 1999). To assist in hydrological hazard mitigation, Gunes et al. (2000) developed a GIS tool that

helps emergency managers visualize and determine areas at the greatest risk of flooding so they can better prepare and respond to the natural hazard. The hydrometeorology community has also discovered the advanced capabilities of GIS. It is advantageous to conduct hydrometeorological research within a GIS platform because it simplifies such applications as flood modeling (Adler et al. 2011; Nunes Correia et al. 1998). For example, in a GIS platform, it is possible to combine elevation, census, land use, and remotely sensed precipitation data to run a hydrological model and examine the impacts that may result from a hydrological hazard.

For precipitation research applications, GIS offers an array of spatial analysis tools that can be used to analyze precipitation variability (Baigorria et al. 2007; Munroe et al. 2013), assess radar beam blockage (Kucera et al. 2004), interpolate rain gauge data (Zhang and Srinivasan 2009), and develop precipitation climatologies (Squires 2010; Xie et al. 2005). Through the creation of a GIS snowstorm database using the Global Historical Climatology Network (GHCN) data, Squires (2010) found that using GIS to develop a snowstorm climatology made the data more suitable for societal impacts and forecasting applications. For example, this integration made it possible to compare the economic and societal impacts of a snowstorm by overlaying census and transportation data with the snowfall data. Xie et al. (2005) used GIS to develop an automated utility that preprocesses raw Next Generation Weather Radar (NEXRAD) Stage III precipitation data, brings the data into a GIS, and conducts a statistical analysis on precipitation for a region of interest. They found that using GIS to process and analyze the raw NEXRAD data decreased the analysis time from months of manual work to a few days. Additionally, using GIS to downscale allowed for the analysis of the

precipitation data on the watershed scale, a very important application for hydrological research.

2.7 Purpose

This study will use the NMQ radar reflectivity dataset to develop and analyze a precipitation organization climatology for the Southeast United States. The current study will expand on the work of Palecki et al. (2005) using similar methods employed by Rickenbach and Rutledge (1998) to develop the precipitation organization climatology. The data will be integrated into a GIS platform allowing for a more detailed, local investigation of precipitation mode of organization variability and the impacts this variability may have on regional hydrology. The questions pursued in the current study include:

a. How do precipitation modes of organization vary across North Carolina?
    i. Are there seasonal and/or regional differences in the precipitation modes of organization across North Carolina?
b. How do variations in the frequency and distribution of precipitation modes of organization across North Carolina affect the regional hydrology in the state?
    i. Do MPF and isolated systems influence watershed discharge differently across North Carolina watersheds?

The information from this work will be beneficial to many different applications. This clear accounting of regional, seasonal, and interannual changes in these different precipitation modes of organization will aid in the precipitation parameterization of

climate models. The availability of this radar data in GIS format will also assist in hydrological modeling applications. Additionally, the precipitation-discharge GIS-based analysis will be a valuable resource for the improvement of agriculture crop forecasting, water resources applications, and hazards response through the improved understanding of precipitation-discharge correlations.

Chapter 3

Data and Methods

This study sets out to 1) develop a precipitation organization climatology, 2) analyze precipitation modes of organization across the Southeast U.S., 3) integrate the precipitation organization climatology into a GIS platform, 4) analyze the spatial and temporal variability of precipitation modes of organization across North Carolina, and 5) investigate correlations between precipitation modes of organization and hydrology in North Carolina.

The following section will describe the methods employed to achieve the goals of this study. First, initial data collection methods will be explained, followed by the steps taken to identify the different precipitation modes of organization from the NMQ datasets for the creation of the precipitation organization climatology. The process of integrating the precipitation organization climatology into a GIS platform will be followed by a summary of the methods employed to analyze the interactions of the precipitation modes of organization and hydrology in North Carolina.

3.1 Climatology Development

The current project developed a precipitation organization climatology for the Southeast U.S. using four years (2009-2012) of data from the NMQ radar and precipitation datasets, constructed by NCDC specifically for our project.

3.1.1 Radar Data

The Next-generation Doppler Radar (NEXRAD) network has provided continuous national radar coverage since the early 1990s. This NEXRAD data is ported and stored at NCDC where, until recently, the ability to work with NEXRAD data had been limited because of the large data storage space and advanced computing power needed to work with raw NEXRAD data. The NMQ “Mosaic 3D” radar reflectivity and the NMQ “Q2” precipitation datasets developed by NOAA, NSSL, and The University of Oklahoma (Zhang et al. 2011) consist of a merged, three-dimensional multi-sensor national radar product that allows for the study of modes of precipitation organization. Notable features of the NMQ Q2 data include snow versus rain identification as well as convective versus stratiform identification.

For use in this study, NCDC has merged the NEXRAD data across the Southeast United States and used an algorithm similar to the Q2 algorithm developed by NSSL and others to create NMQ “Mosaic 3D” and NMQ Q2 datasets for the Southeast U.S. (Fig. 3).

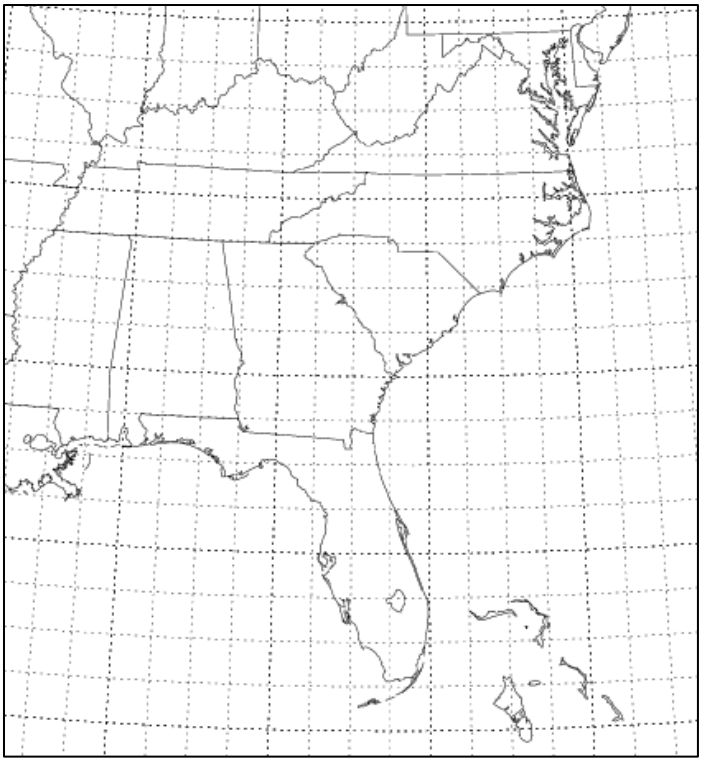

Figure 3. Southeast U.S. study region.

We acquired four years of data (2009-2012) from NCDC. At East Carolina University (ECU), a precipitation organization identification algorithm, explained in detail in the following section, was used to track and identify precipitation systems from the NMQ Mosaic 3D radar reflectivity and the NMQ Q2 precipitation datasets. The steps taken in this data assimilation process are summarized in Figure 4.

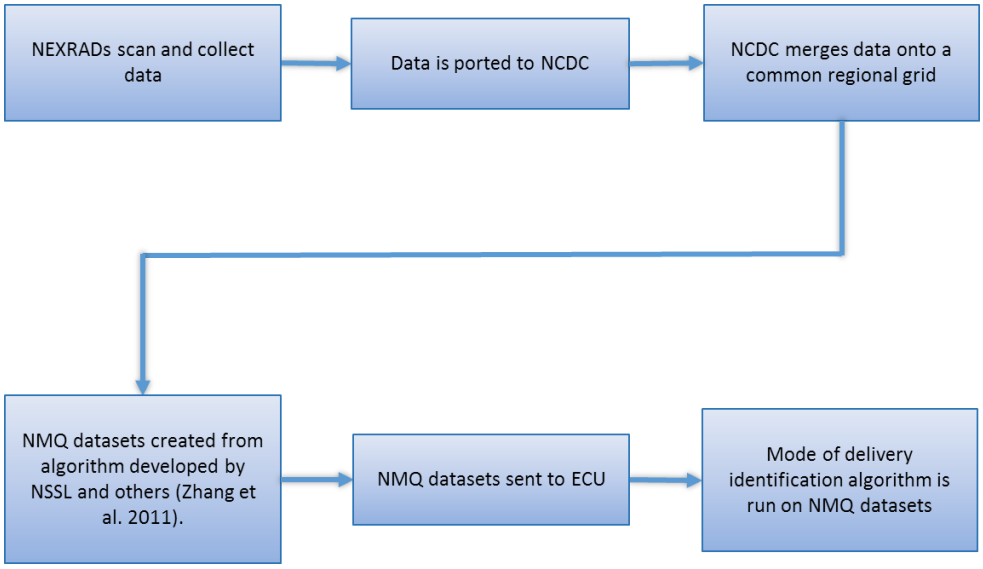

Figure 4. Flowchart summarizing the data collection process.

3.1.2 Precipitation Organization Identification

A variety of precipitating weather events occurred within the period (2009-2012) of the dataset. Some memorable weather events that impacted the Southeast U.S. during the period of this study included the widespread flood event in September 2009, the post-Christmas snow of 2010, the severe weather outbreak in April 2011, and Hurricanes Irene (2011), Isaac (2012), and Sandy (2012). Each of these events had significant impacts on the Southeast region; however, their impacts varied greatly due to the different precipitation characteristics of each system. Therefore, this project associates precipitation at each pixel with a certain precipitation organization system. This study adopts a precipitation organization identification framework based on two predetermined precipitation organization categories:

1. Mesoscale precipitation features: A precipitation system with a minimum length scale 100 km (Houze et al. 1990)
2. Isolated storms: Raining systems that do not exceed the 100 km threshold for an MPF (Rickenbach and Rutledge 1998)

This identification framework will be implemented using the algorithm summarized in Figure 5.

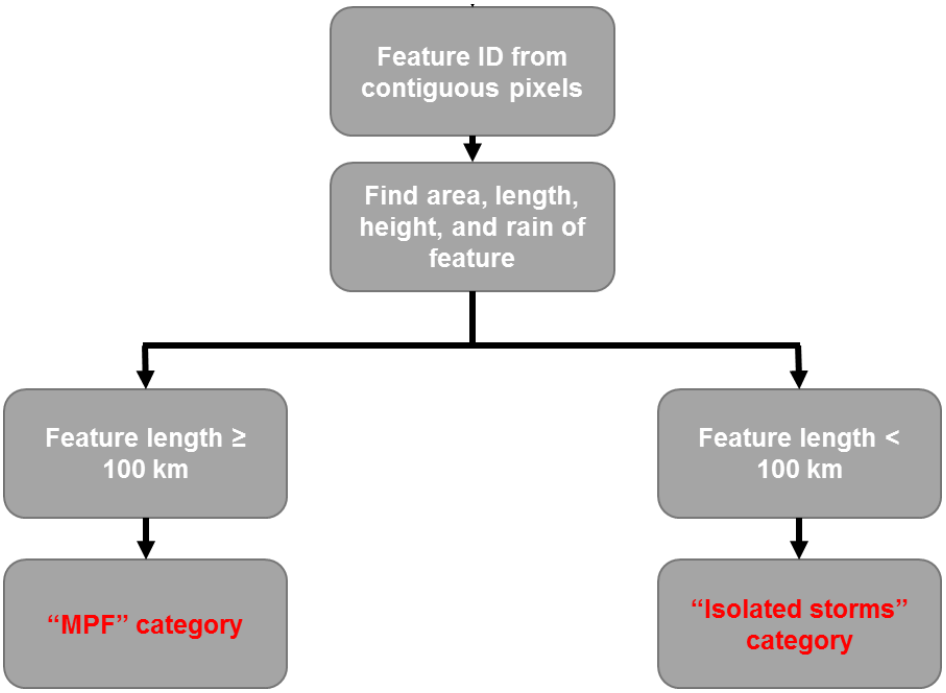

Figure 5. Diagram summarizing the precipitation organization identification algorithm. The decision tree is initiated for each file in the dataset.

3.2 Analysis of the Climatology

3.2.1 Regional and Local Analyses

After the implementation of this algorithm, the resulting precipitation organization climatology product and a programming language, the Interactive Data Language (IDL), were used to calculate the daily average precipitation contributions from each mode of

precipitation organization. These results were seasonally composited and mapped across the Southeast U.S. Using the same daily average precipitation data from the regional analysis, a second analysis was conducted for North Carolina within a GIS platform called ArcGIS to demonstrate how GIS will assist in the application of the precipitation organization climatology.

3.2.2 Study Area

North Carolina is a unique natural laboratory for researching precipitation characteristics because of the wide variety of precipitation modes of organizations that impact the state. Modes of precipitation organization in North Carolina range from tropical cyclones to blizzards. In North Carolina, there are three natural geographic regions--Western North Carolina, Eastern North Carolina, and Central North Carolina (Fig. 6)--characterized by differences in topography (Fig. 7), land surface type (Figs. 9-13), and climate.

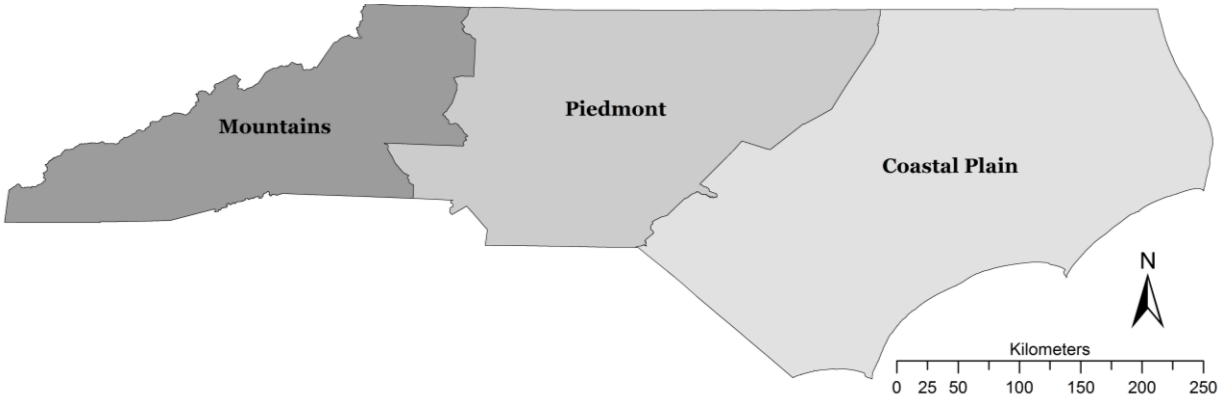

Figure 6. Regions of North Carolina. Dark gray is WNC, moderate gray is CNC, and light gray is ENC.

Western North Carolina (WNC)

Also known as the Mountains, this southern portion of the Appalachian Mountain chain resides in this region. It is home to Mount Mitchell, the highest peak east of the Mississippi River at 6,684 feet, and over 140 other mountain peaks that extend higher than 5000 feet (North Carolina Department of Public Instruction). This region typically receives the most snowfall of the three North Carolina regions primarily due to the high elevation of the landscape. After the passage of a midlatitude cyclone, winds from the Northwest lift over the mountainous terrain and, in the wintertime, the air condenses producing snowfall downwind. Similar processes generate short-lived isolated convection in the summertime due to orographic lift produced by the rough terrain.

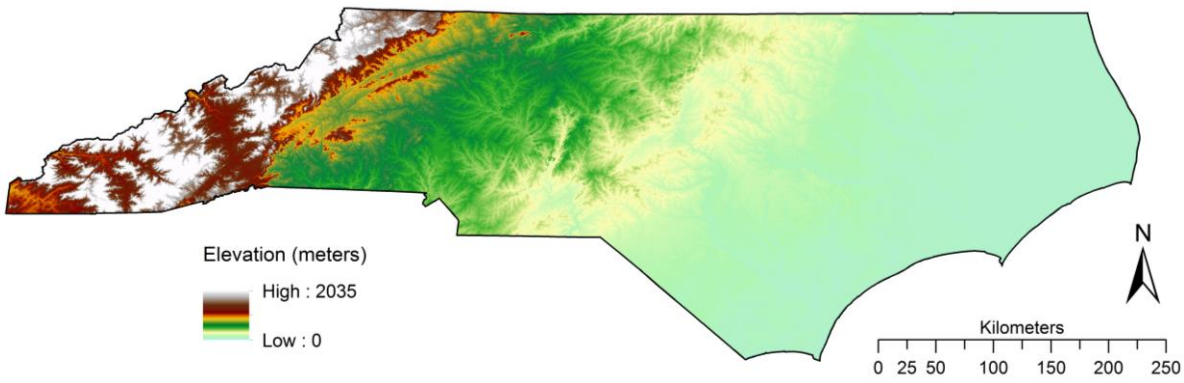

Figure 7. Relief map of North Carolina.

These are the oldest mountains in the United States and therefore have eroded creating loose and rocky soils across WNC. This mountainous region is covered by dense vegetation, mostly composed of deciduous forests and boreal conifer forests with thick underbrush (Horton 2012). Some portions of WNC, such as Transylvania County, receive the highest annual precipitation totals in North Carolina (Boyles and Raman

2003). While less common than the other two regions, severe weather and tropical systems do impact this region.

Central North Carolina (CNC)

Central North Carolina, also known as the Piedmont, experiences the greatest diversity of hydrometeorological phenomena of the three regions. This region often experiences snow in the winter, severe weather in the spring, and tropical cyclones in the summer. Unique to this region and the foothills of the mountains are Cold Air Damming (CAD) events (Wallace and Hobbs 2006). These events occur when cold air flowing westward is blocked by the mountains in WNC and disperses in the lower levels of the atmosphere creating a cold dome of air across CNC. Therefore, rain that occurs during these events freezes as it falls through the cold dome, creating hazardous conditions for CNC as large quantities of sleet and freezing rain create dangerous icing conditions for the Piedmont. Because it is in-between the Mountains and the Coastal Plain, the Piedmont region has a mixture of vegetation typically found in those other two regions including the deciduous and conifer forests found in the Mountains and the hardwood swamp forests typical in the Coastal Plains (Horton 2012). With the highest population density and fastest population growth of the three regions (U.S. Census Bureau 2013), knowledge of the hydrological characteristics of this region is extremely important to ensure the best water management and hazard mitigation practices.

Eastern North Carolina (ENC)

The Coastal Plains region is home to a unique coastline protected by a chain of barrier islands known as the Outer Banks. While snowfall is a less common occurrence

in ENC, this region of North Carolina is accustomed to severe weather and tropical cyclones. Unique to this region is a coastal sea breeze that develops because of strong daytime temperature gradients between the land and ocean. This coastal feature creates lift in the atmosphere that can initiate localized convection as it progresses inland. This region's vegetation is dominated by marsh and dune vegetation types, although hardwood swamp forests and Conifer forests are found further inland (Horton 2012).

3.2.4 North Carolina River Basins

The North Carolina Department of Environment and Natural Resources (NCDENR) identifies 17 river basins across North Carolina (Fig. 8).

Figure 8. North Carolina river basins. Bold gray lines represent the three main regions of North Carolina—Western North Carolina, Central North Carolina, and Eastern North Carolina.

Each river basin is defined by the main river into which all the water discharge in a region flows. From these 17 river basins, five were focused on in the current study: the

French Broad, Broad, Yadkin-Pee Dee, Lumber, and Neuse. These five were selected for two main reasons. First, there is up-to-date stream gauge discharge data for the time period of the climatology. Second, at least one river basin was selected from each region allowing for the representation of the three main regions of North Carolina. From these five river basins, sub-regions of these river basins, from here on referred to as watersheds, were created to better represent the data. The process of creating these watersheds will be explained in detail later. The following section will provide a general overview of the five river basins selected in this study and will provide a more detailed look into the watershed regions extracted from the five main river basins.

French Broad River Basin

The French Broad River Basin is situated in Western North Carolina and is home to 485,140 permanent residents (U.S Census Bureau 2011, Table 1). This 2829 square miles basin is made up of 3985 miles of streams that provide water to the 8 counties in the basin (N.C.DENR Office of Environmental Education and Public Affairs). This is the only river basin in the study that empties into the Gulf of Mexico. The French Broad River begins from the Court House Falls, a 50 foot waterfall in Transylvania County (N.C.DENR Office of Environmental Education and Public Affairs). This waterfall feeds into the North Fork, and forms the French Broad River once it merges with the West, Middle, and East forks. The river then flows west and is fed by three main North Carolina tributaries, the Mills, Davison, and Swannanoa rivers. The French Broad River is also joined by the Pigeon and Nolichucky rivers after it flows west into Tennessee. The French Broad River Basin has steep terrain (Fig. 7) and rocky soils resulting in low

water infiltration, high runoff rates, and high peak discharge rates (Missouri Stream Team Program 2009).

French Broad Watershed

This watershed of the French Broad River Basin was created to provide a more accurate analysis of precipitation and discharge correlations in the current study. The French Broad watershed includes 82% of the total population in the French Broad River Basin (Table 2). While there is a decrease in the population represented in the watershed, the population density actually increases (Table 1 & 2). This is because the region included in the French Broad watershed is a more developed portion of the basin (Fig. 9). This watershed has a high vegetation density (73%, Table 3) which contributes to increased water storage in the basin because it can slow the rate of runoff due to surface friction allowing time for absorption and transpiration by the flora in the basin. An interesting characteristic of this watershed, illustrated in Figure 9, is the enhanced urbanization along the river. This is an important consideration because these developed areas introduce many impervious surfaces that enhance the speed and amount of storm runoff into the stream. Between 1982 and 1997, the French Broad river basin as a whole experienced an 85 percent increase in urban and developed areas (N.C.DENR Office of Environmental Education and Public Affairs). The ongoing population growth and urbanization of this river basin creates changes in the natural areas which can enhance storm runoff and affect stream discharge.

River Basin	Cumulative Stream Length (km)	Discharge Area (km^2)	Population	Population Density (km^{-2})
French Broad	6413	7327	485140	66
Broad	2435	3921	204803	52
Yadkin-Pee Dee	9434	18702	1675937	90
Lumber	3616	8622	472276	55
Neuse	5486	15701	1687462	107

Table 1. River basin attributes

Watershed	Discharge Area (km^2)	Population	Population Density (km^{-2})
French Broad	4272.83	397842	93
Broad	2154.82	101637	47
Yadkin-Pee Dee	16865.34	1647345	98
Lumber	3184.04	190225	60
Neuse	10256.72	1555472	152

Table 2. Watershed attributes

Data Sources: NCDENR: River basin stream length and discharge area. U.S. Census Bureau: Population Data

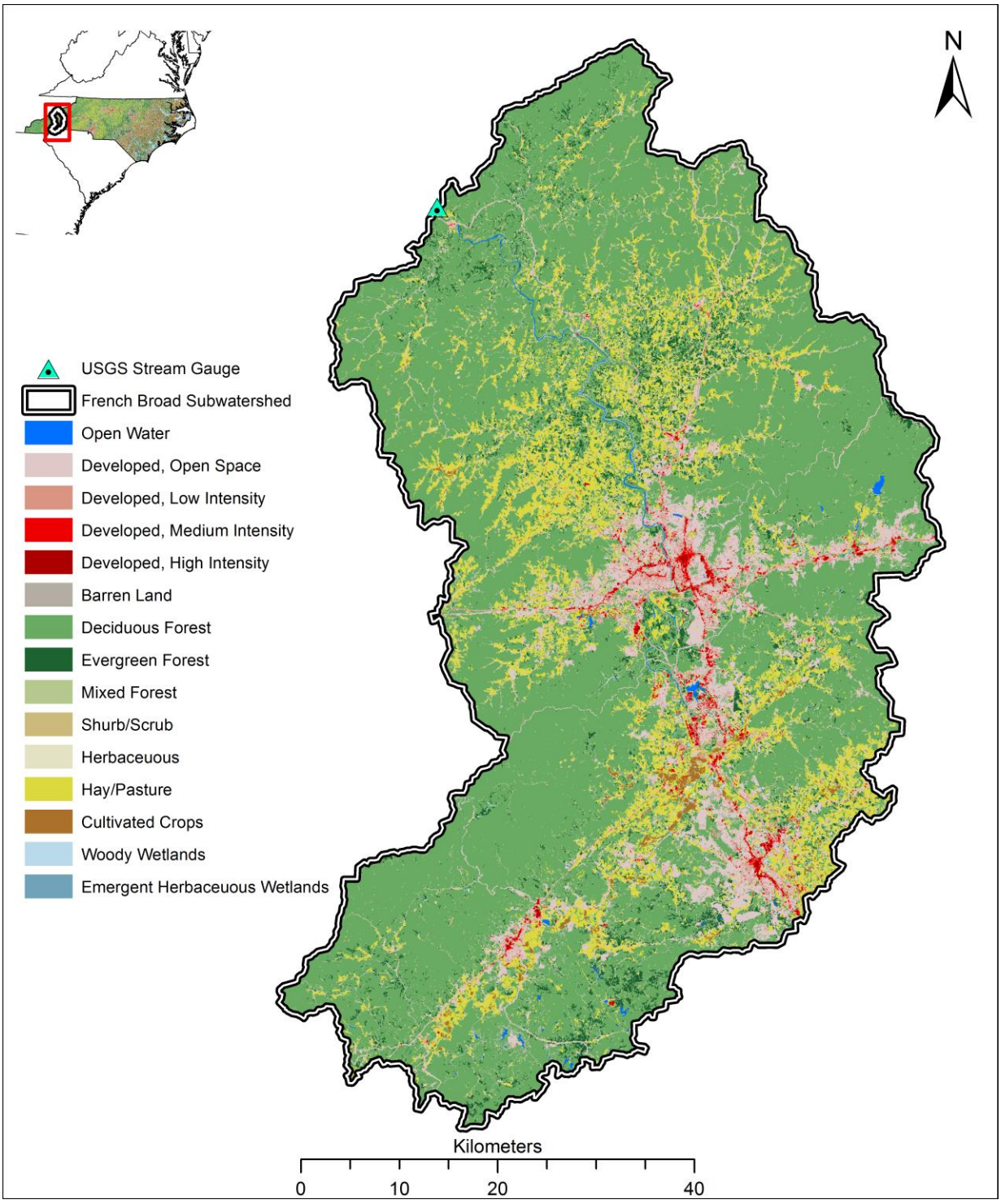

Figure 9. Land cover map of the French Broad watershed. Shades of Red indicate developed lands, shades of green indicate forested lands, browns and yellows represent shrubs or agricultural lands, and blues represent water systems. Teal triangles indicate the locations of the USGS stream gauge stations selected in this study.

Watershed	Urban (%)	Agriculture (%)	Natural Vegetation (%)	Wetlands (%)	Water (%)	Barren Land (%)
French Broad	13	13	73	< 1	< 1	< 1
Broad	8	13	77	< 1	< 1	< 1
Yadkin-Pee Dee	13	25	60	< 1	1	< 1
Lumber	8	30	38	23	1	< 1
Neuse	15	32	39	12	2	< 1

Data Source: USGS Land Cover Inventory (MRLC Consortium)

Table 3. Percentages of land cover types in the five watersheds. Urban includes any developed lands; Agriculture includes pastures, hay, or other cultivated croplands; Natural Vegetation includes deciduous forests, evergreen forests, mixed forests, shrubs, and natural herbaceous growth; Wetlands include woody wetlands and emergent herbaceous wetlands; Water includes any open water; Barren land simply includes barren land.

Broad River Basin

The Broad River Basin has similar characteristics to the French Broad River Basin because it is also located in the WNC region. The headwaters of the Broad River also begin in the mountains, but these waters flow southeast into the Piedmont of North Carolina before continuing into South Carolina (N.C.DENR Office of Environmental Education and Public Affairs). Along the way, the Broad River is joined by the Green, First Broad, Second Broad, and the North Pacolet rivers. In total, the streams that make up the Broad River Basin span 2435 kilometers across the 3921 square kilometer basin (Table 1). Some important reservoirs fed by the Broad River include Lake Lure, Lake Adger, and King Mountain Reservoir. The Broad River Basin is less developed and is home to only 204,803 residents (U.S Census Bureau 2011). This river basin is located closer to the foothills of the Appalachian Mountains which translates to less dramatic relief compared to the French Broad river basin (Fig. 7).

Broad Watershed

This subset of the Broad River Basin is heavily forested (77%) and does not include some of the more developed regions of the full river basin (Table 3, Fig. 10). The Broad watershed includes only about 50% of the total population (Table 2), and only about 8 percent of this watershed is categorized as urban (Table 3). This all corresponds to a decrease in the population density from the full river basin meaning that this river basin will provide some extra insight about precipitation and discharge correlations in heavily forested mountainous regions.

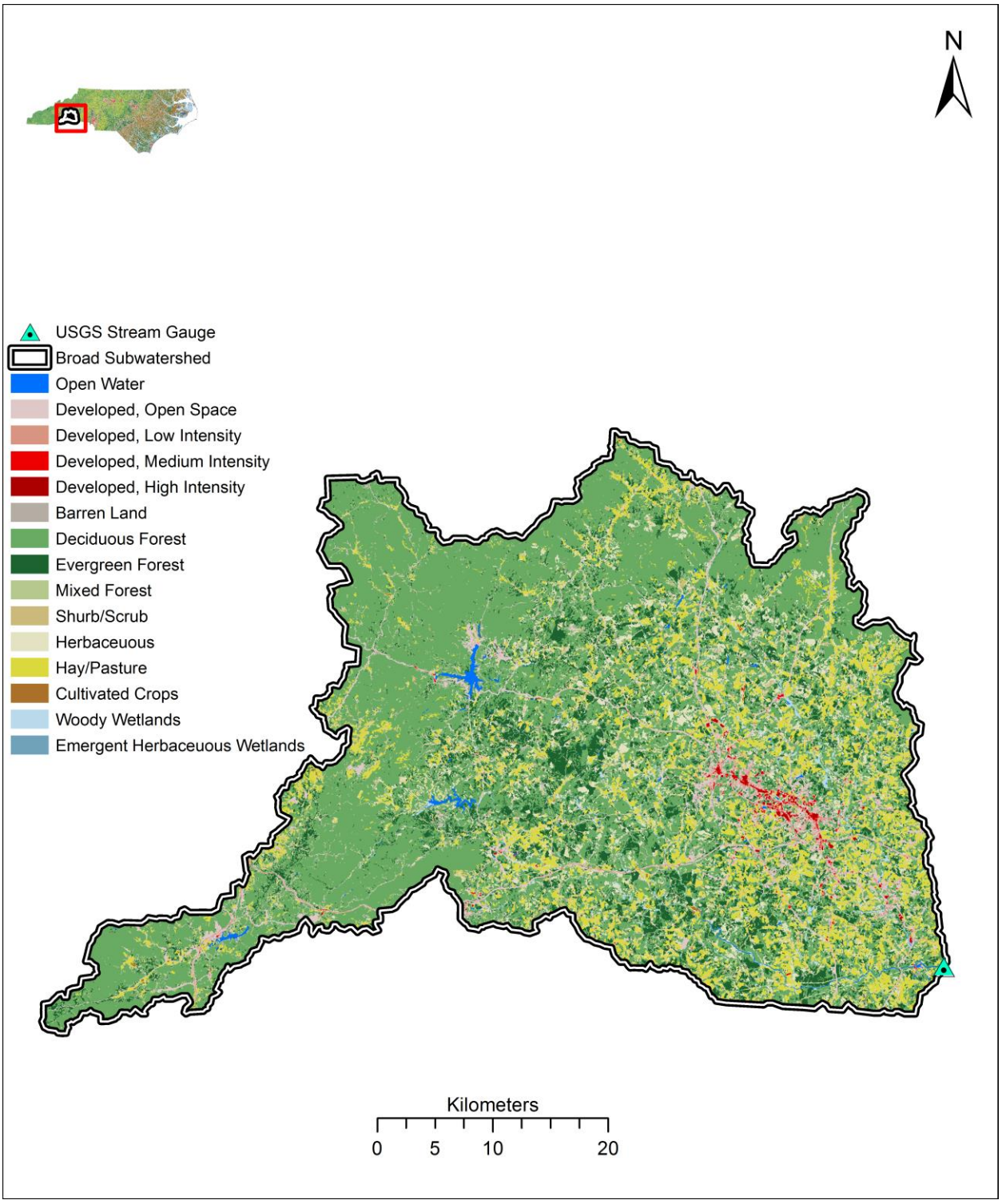

Figure 10. Land cover map of the Broad watershed. Shades of Red indicate developed lands, shades of green indicate forested lands, browns and yellows represent shrubs or agricultural lands, and blues represent water systems. Teal triangles indicate the locations of the USGS stream gauge stations selected in this study.

Yadkin-Pee Dee Basin

The main rivers in this basin include the Yadkin and the Pee Dee. The Yadkin River flows east and then south from its start in Blowing Rock. It flows through a variety of forested areas, farmlands, and urbanized landscapes while also feeding seven man-made reservoirs before its name changes to the Pee Dee near the border of North Carolina and South Carolina (N.C.DENR Office of Environmental Education and Public Affairs). These two rivers are fed by seven main tributaries including the Mitchell, Ararat, Uwharrie, and Rocky rivers, and the Dutchmans, Long, and Abbotts creeks. As the largest river basin in the study (18702 km^2), these streams span a total distance of 9434 kilometers (Table 1). While a small portion of the Yadkin-Pee Dee can be found in WNC (Fig. 8), the majority of this river basin is situated in CNC, meaning less extreme topography. The northern portion of the river basin is similar in soil characteristics to WNC as much of it is made up of igneous and metamorphic rocks, but toward the south and eastern portions of the Piedmont there is a higher concentration of clay and sands in the soil (Fish et al. 1957). This river basin houses 1,675,937 residents (U.S Census Bureau 2011), many of whom are settled in one of the multiple larger cities in the Yadkin-Pee Dee River Basin including Winston-Salem, Statesville, Greensboro, High Point and portions of Charlotte.

Yadkin-Pee Dee Watershed

Figure 11 shows an illustration of the watershed extracted from the main Yadkin-Pee Dee River Basin. From Figure 11, it is apparent that the Yadkin-Pee Dee

watershed includes the high density of the urbanized cities found in the Yadkin-Pee Dee River Basin. In fact, there is nearly a solid band of developed lands from the outskirts of Charlotte, bottom left of the Yadkin-Pee Dee watershed, to High Point, although the most developed region in the Yadkin watershed is the town of Winston-Salem which sits just north of High Point. Being the largest watershed in this study, the Yadkin-Pee Dee watershed is nearly a direct representation of the full population of the entire Yadkin-Pee Dee River Basin (Tables 1 & 2). This translates to a higher percent of urban (13%) and agricultural (25%) lands than in the mountainous watersheds (Table 3). The combination of impervious surfaces and relatively high concentrations of clay in the soils leads to a lower chance for rainwater infiltration but a greater chance for high runoff rates, resulting in higher peak stream discharge rates in the Yadkin-Pee Dee watershed.

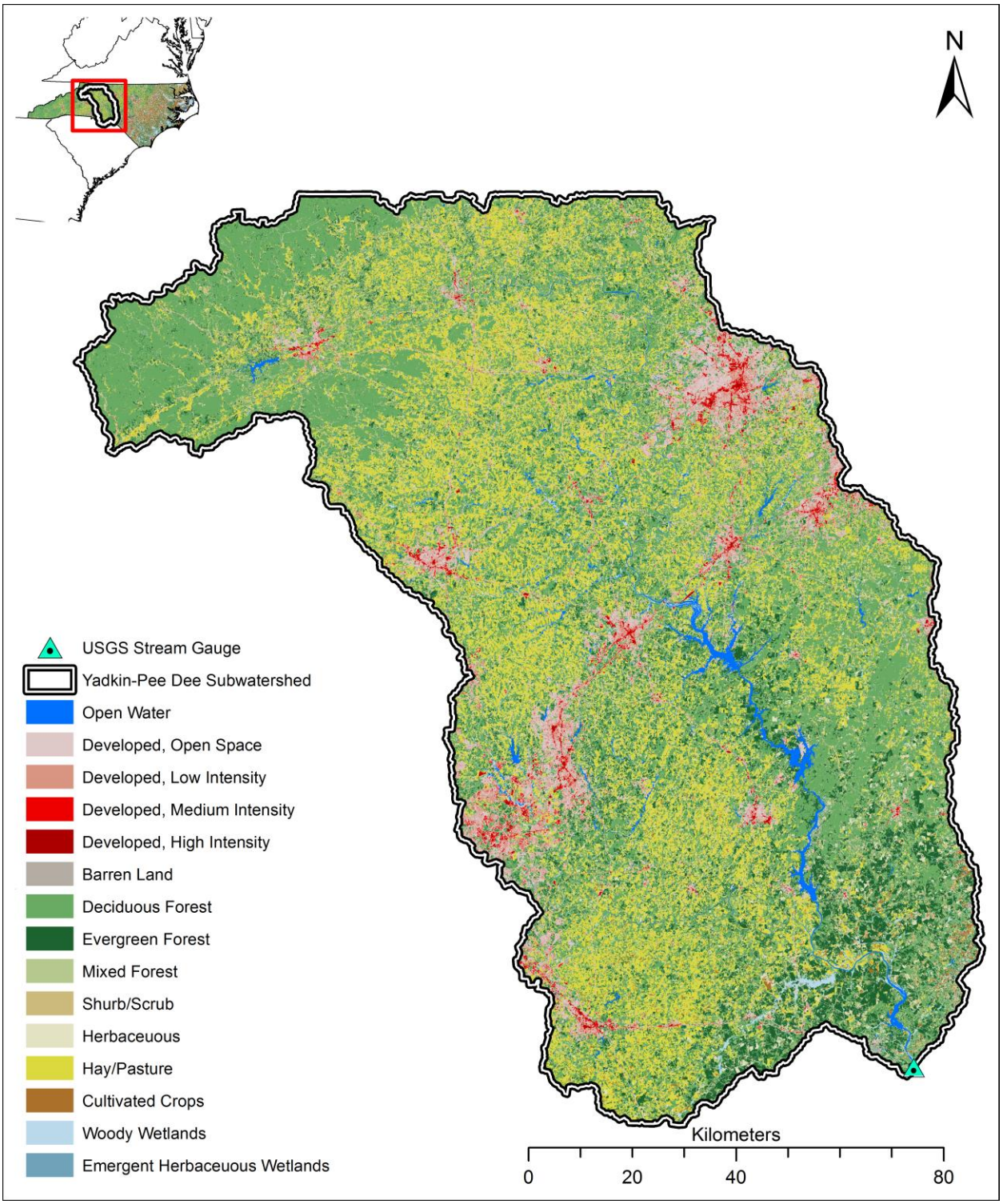

Figure 11. Land cover map of the Yadkin watershed. Shades of Red indicate developed lands, shades of green indicate forested lands, browns and yellows represent shrubs or agricultural lands, and blues represent water systems. Teal triangles indicate the locations of the USGS stream gauge stations selected in this study.

Lumber River Basin

The Lumber River Basin is actually composed of the Lumber River, the Waccamaw River, the headwaters of the Little Pee Dee River, and a small system of coastal rivers (N.C.DENR Office of Environmental Education and Public Affairs). The total distance spanned by the streams in this basin is only 3616 kilometers, much less than the French Broad River Basin (Table 1). This is partly due to the unique hydrologic characteristics of the Lumber River Basin: the numerous Carolina bays, which are a special wetland composed of elliptical depressions and collected rainwater throughout the year, and the dominance of swamp forests. In fact, about 90 percent of water in the Lumber River Basin are swamp waters (N.C.DENR Office of Environmental Education and Public Affairs), which means that much of the water flows at very slow rates. Most of the Lumber River Basin is found in ENC, but a small portion does reside in the Piedmont region (Fig. 8). The terrain of this basin is relatively flat compared to the river basins previously described (Fig. 7). The soil in the Lumber River Basin transitions to much sandier soil contributing to greater rainwater infiltration and less runoff compared to those river basins found in WNC and CNC.

Lumber Watershed

Characteristic of both the entire Lumber River Basin and the Lumber watershed in this study are the higher proportions of natural and agricultural lands than urbanized lands (Fig. 12 & Table 3). Something unique to this watershed is the higher proportion of wetlands (23%) than other watersheds in the study. This is consistent with the low-lying lands and swamp forests that dominate the region (N.C.DENR Office of

Environmental Education and Public Affairs). With much of the 190,225 people in this watershed living in rural towns, this fairly undeveloped watershed will provide important insight into how discharge rates respond to different modes of precipitation organization in relatively flat, but highly vegetated regions.

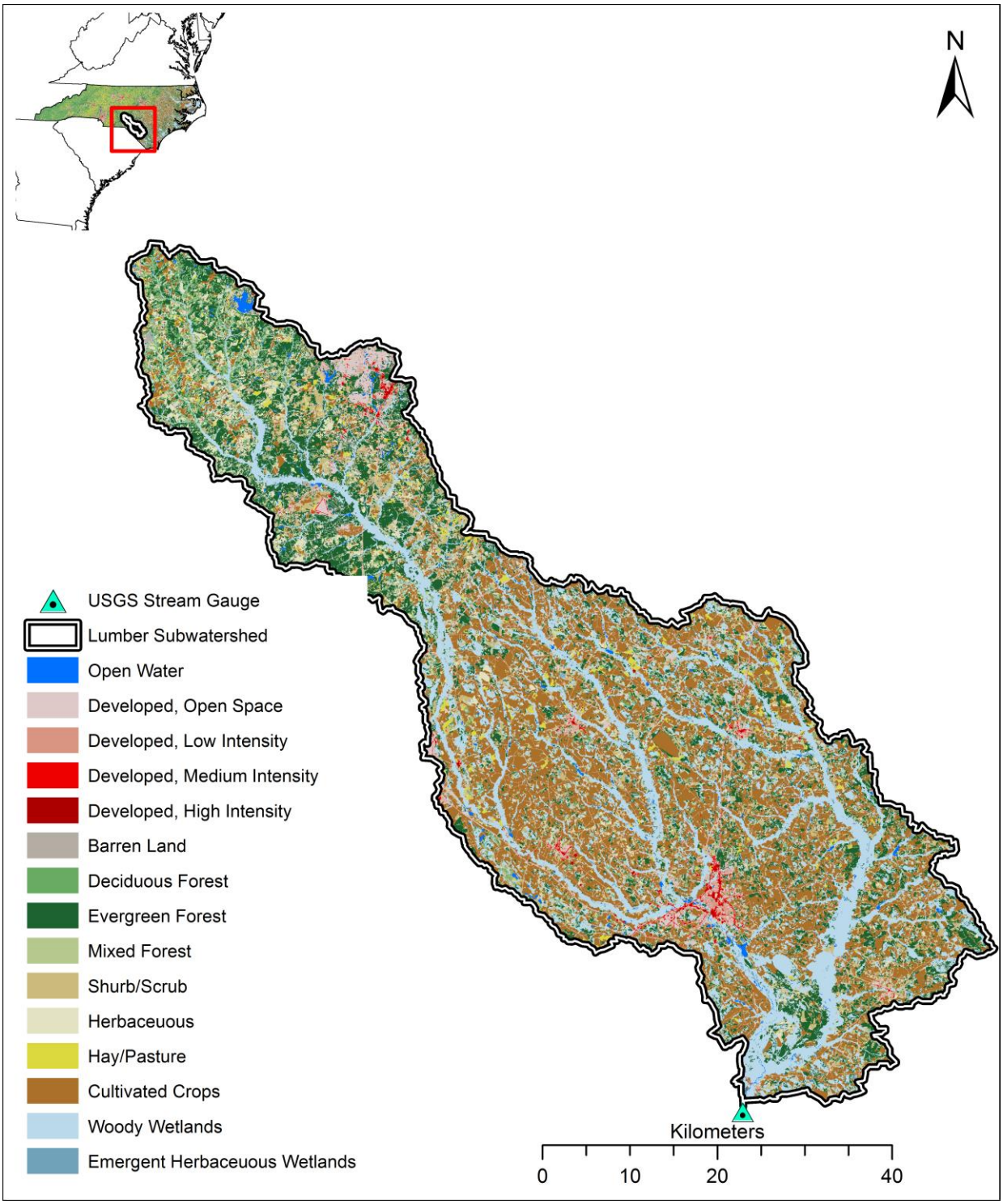

Figure 12. Land cover map of the Lumber watershed. Shades of Red indicate developed lands, shades of green indicate forested lands, browns and yellows represent shrubs or agricultural lands, and blues represent water systems. Teal triangles indicate the locations of the USGS stream gauge stations selected in this study.

Neuse River Basin

The second largest river basin in the study with a discharge area of 15701 square kilometers, the Neuse River basin, contains the Neuse River which is the longest river in North Carolina and is also the widest river in North America (N.C.DENR Office of Environmental Education and Public Affairs). This 2-million year old river used to begin at the joining of the Eno and Flat rivers, but now begins as it spills over the Falls Lake Reservoir Dam near Raleigh. While the Neuse River Basin is the second largest river basin in the current study, the streams of this watershed span only 5486 kilometers, less than the French Broad River Basin (Table 1). The tributaries that make up this basin include the Eno, Little, and Trent rivers, as well as the Crabtree, Swift, and Contentnea creeks. As the Neuse river travels from a portion of the Piedmont into the Coastal plains, the streamflow of the river slows as it widens near New Bern and becomes a tidal estuary before emptying into the Pamlico Sound and later into the Atlantic (N.C.DENR Office of Environmental Education and Public Affairs). The Neuse River Basin is split, with nearly half in CNC and half in ENC (Fig. 8). Therefore, this river basin has both the clay piedmont soils and the sandy coastal soils. It is also one of the more urbanized regions in North Carolina with 1,687,462 residents mainly concentrated in the Triangle area (Chapel Hill, Durham, and Raleigh). The Neuse River is subjected to large amounts of nitrogen and phosphorus due to fertilizer and animal waste introduced to the river system by runoff from urban areas, farming, and animal operations (N.C.DENR Office of Environmental Education and Public Affairs).

Neuse Watershed

The Neuse watershed provides a good representation of the entire Neuse River Basin (Fig. 13). This watershed includes 92 percent of the total Neuse River Basin population and includes some of the more urbanized areas from the full river basin including Durham, Raleigh, Goldsboro, and New Bern. The decreased discharge area of this watershed also gives it the greatest population density (Table 2). This is well-illustrated in the northwestern portion of the Neuse watershed where there is a broad region of developed land cover associated with Durham and Raleigh (Fig. 13). A characteristic of this watershed that was mainly illustrated in the mountainous watersheds is the concentration of urbanization near the stream networks. These higher concentrations of urban landscapes and impervious surfaces near stream networks in combination with a relatively flat terrain and fairly porous soils will provide some interesting comparisons with other watersheds in the study.

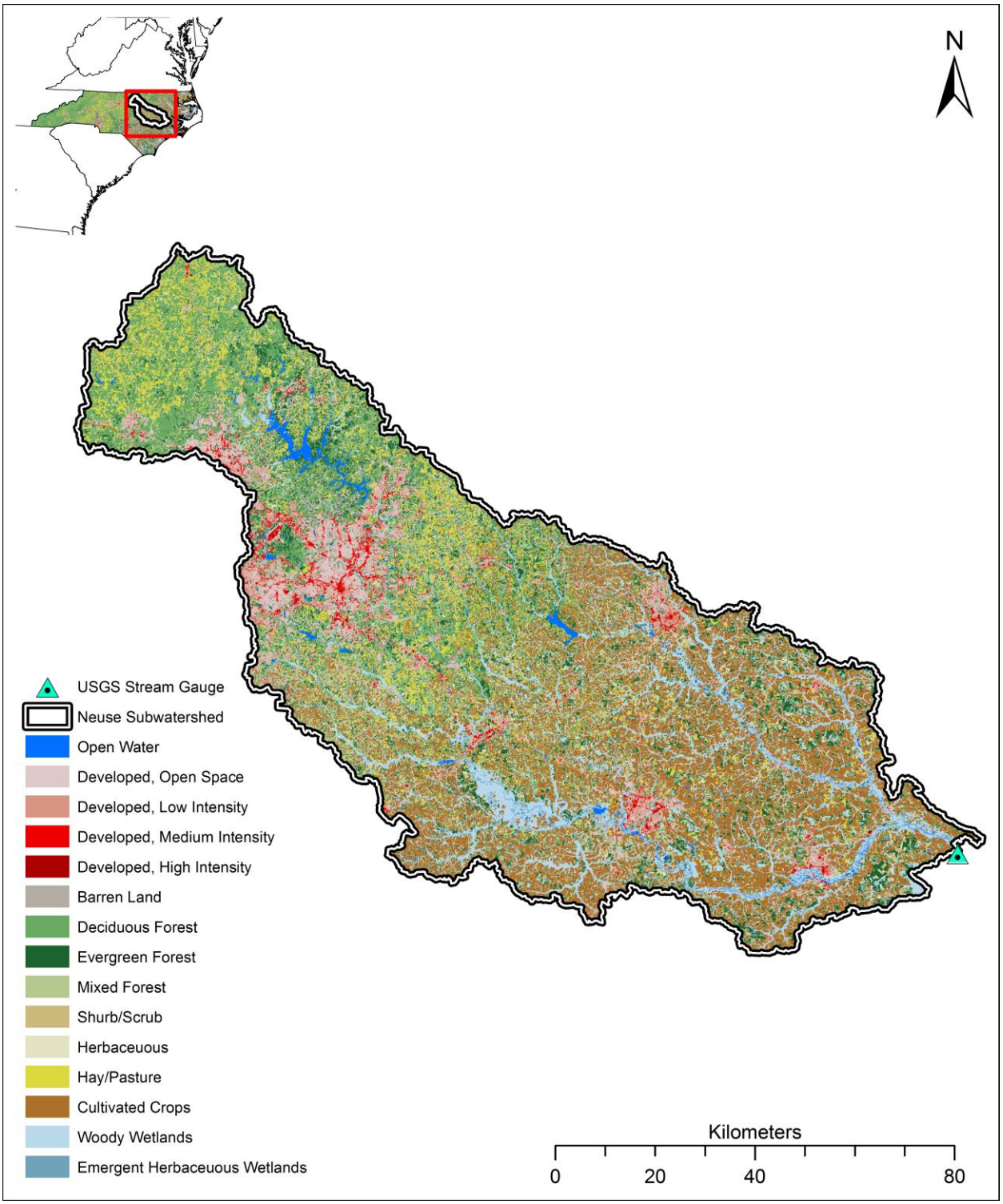

Figure 13. Land cover map of the Neuse watershed. Shades of Red indicate developed lands, shades of green indicate forested lands, browns and yellows represent shrubs or agricultural lands, and blues represent water systems. Teal triangles indicate the locations of the USGS stream gauge stations selected in this study.

3.3 USGS Stream Gauge Data

Discharge data came from the U.S Geological Survey (USGS) stream gauge stations (Table 4). Data from the USGS stations is freely available online and provides regular information about a stream's discharge rate, stream velocity, and stream height. However, while there are numerous USGS gauging stations across the country, many are only partial record stream gauges, activated only under certain conditions, and others have been decommissioned before or during the timeframe of the current study. Therefore, stream gauges were deemed appropriate for use in this study if they 1) had a full data record from 1 January 2009 – 31 December 2012, 2) measured discharge rates regularly, and 3) fell along the main river in each of the river basins. The final gauges selected in this study met all of the requirements, but were also the nearest stream gauge stations to the North Carolina and South Carolina borders.

Watershed	Site Name	Site Number	Site Latitude	Site Longitude	Drainage Area (km^2)
French Broad	French Broad at Hot Springs, NC	3454500	35°53'23.7"	82°49'15.6"	4272.83
Broad	Broad River Near Boiling Springs, NC	2151500	35°12'39"	81°41'51"	2154.82
Yadkin-Pee Dee	Pee Dee River Near Rockingham, NC	2129000	34°56'45"	79°52'11"	16865.34
Lumber	Lumber River at Boardman, NC	2134500	34°26'33"	78°57'37"	3184.04
Neuse	Neuse River Near Fort Barnwell, NC	2091814	35°18'50"	77°18'10"	10256.72

Table 4. USGS selected stream gauge stations

3.4 ArcGIS

A main goal of this study is to show an application of the precipitation organization climatology. It was determined that a GIS, specifically ArcGIS, would provide the best framework to apply this climatology. This is because ArcGIS has a suite of spatial tools available that allow for more detailed spatial analyses of this climatology. In the current study, ArcGIS software was used to explore the spatial and temporal patterns of the precipitation modes of organization as well as to investigate the different hydrological impacts of the different modes of organization. The following section reviews the process of integrating and analyzing the precipitation organization climatology in ArcGIS.

3.4.1 Data Conversion

The first step in the process was converting the NetCDF files into GIS format. This was done by converting the array of precipitation data in each of the NetCDF files into raster format using the ArcGIS tool, *Make NetCDF Raster Layer*; where a raster is a matrix of pixels where each pixel contains a value representing information such as elevation, temperature, precipitation, satellite imagery, etc. However, the new rasters' metadata for both the cell size and the starting XY point were incorrectly defined during the conversion. Additionally, the spatial reference datum was lost during the raster conversion. Multiple platforms including ArcGIS toolbox, NCL, NetCDF Viewer, and NCDC Weather and Climate Toolkit were used as a medium to try and resolve the loss of this spatial information in the conversion process; however, none were able to resolve the issue. Therefore, the newly created rasters were exported as text files using

the *Raster to ASCII* tool. From here, a python text editing script went through each of the ASCII files and corrected the spatial information in each file. A second ArcGIS script then converted the corrected ASCII files back to rasters using the *ASCII to Raster* tool.

3.4.2 Watershed Delineation

Sub-regions from the main NC river basins were created (Fig. 14) because the discharge regions that flowed into the stream gauges selected in this study did not always correspond with the watersheds defined by the USGS in the Watershed Boundary Dataset (WBD). This is due to the fact that the stream gauges selected in this study are not the final discharge point of the main rivers associated with each of the five river basins. Therefore, some of the streams that feed into the main river had not yet connected with the main river prior to the stream gauges selected. To accurately depict the regions that contributed to the discharge rates at the stream gauges sites selected, those areas that drain into the streams which then empty into the main river after the stream gauge station needed to be omitted. The following section reviews the steps taken to delineate the five sub watersheds used in this study.

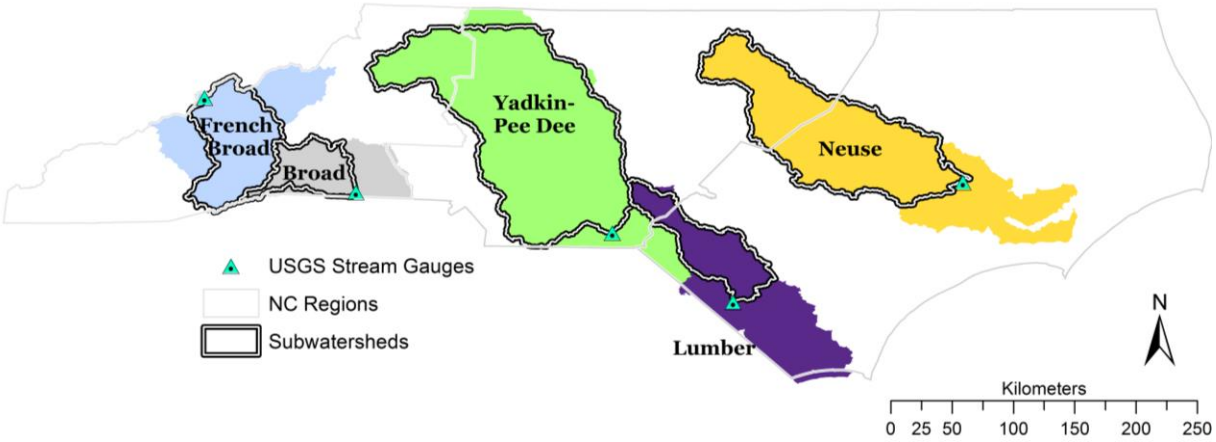

Figure 14. The five river basins selected in the study with the watersheds created from each basin overlaid (bold white outline). The three main regions of North Carolina are depicted by the grey lines and USGS stream gauge stations are denoted by the teal triangles.

An 80 foot Digital Elevation Model (DEM) layer from the North Carolina Department of Transportation (NCDOT) was used for the watershed delineation. This DEM layer was created using Light Detection And Ranging (LIDAR) data from the North Carolina Floodplain Mapping Program and is projected in the North Carolina State Plan NAD83 projection. The first step in the watershed delineation was to use the ArcGIS *Fill* tool to remove any imperfections (i.e. sinks) in the DEM. This corrects for errors and false sinks caused by things like quarries, large construction projects, or glaciated potholes (Chang 2012). Next, the flow directions of the rain water based on the DEM data were determined using the *Flow Direction* tool. With this new flow direction layer, it was then possible to use the *Flow Accumulation* tool to determine where the water moves downhill and accumulates. This tool uses the flow direction raster to count how many cells upstream of a certain cell of interest flow into that cell (Fig. 15).

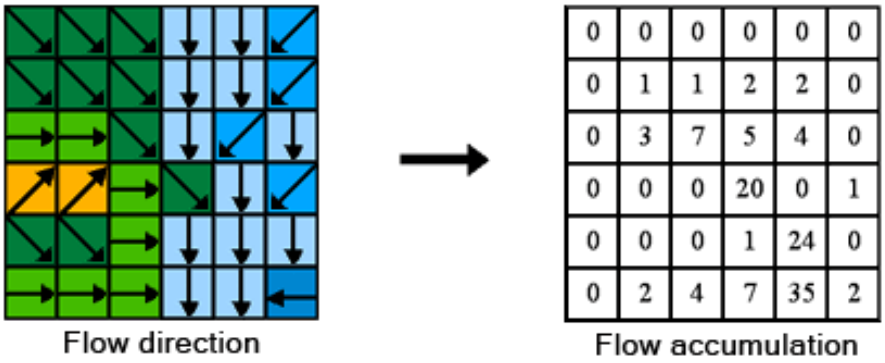

Figure 15. Diagram of how flow accumulation raster is calculated from flow direction raster. Image courtesy of ArcGIS Resource Center: http://help.arcgis.com/en/arcgisdesktop/10.0/help/index.html#//009z00000062000000.htm

Therefore, cells that have a high accumulation will generally correspond to stream channels, and cells with values of zero are typically mountain peaks or ridgelines. This new flow accumulation raster represents where streams would form based on the DEM. The streams created in this process were then compared to a shapefile of North Carolina stream networks from the NC Department of Environment and Natural Resources Division of Water Quality (NCDENR Division of Water Quality). There were obvious differences between the stream network layers, likely due to imperfections left even after applying the *Fill* tool due to the relatively low resolution of the DEM layer. The blame is put on the DEM for the differences because some obvious streams were either broken into separate streams or were left out entirely. Multiple attempts were made to adjust the parameters in the ArcGIS tools previously used to match the two layers, and the use of higher resolution DEM layers was considered; however, it was discovered that the NC stream network layer from the NCDENR Division of Water Quality could be integrated into the current DEM layer through a process called ‘Stream Burning’, and this new layer would provide the most realistic representation of the stream networks

(Chang 2012; Kenny and Matthews 2005; Simley 2004). The first step in this stream burning was to convert the NC stream network layer from the NCDENR Division of Water Quality to raster format and reclassify the data as either 1 (stream) or 0 (no stream). Following, the *Raster Calculator* was employed to burn in the stream network and to adjust the raster so that flow would be forced toward the actual streams. This was done using the equation below.

Con([hydro_mag_ras] = 1, [nc_ele], [nc_ele] + "Max Elevation") (2.1)

Where hydro_mag_ras is the stream network raster layer, nc_ele is the NCDOT DEM layer, and the "Max Elevation" was actually replaced with the Maximum Elevation in the DEM (6676 feet). This equation is a conditional statement that first assesses whether a cell in the stream network layer has a value of 1. If it does, then it will keep the current elevation of the DEM. However, if the cell has a value of 0, it will add the maximum elevation of the DEM layer to that cell. While this alters the elevation of the layer, it does not do anything in the processing of watersheds because this method raises everything but the actual streams by a constant value, which forces those cells not associated with a stream network to flow toward a stream network.

With the stream network information burned into the new DEM layer, the watershed delineation process was then rerun using the new elevation layer. The final step of the watershed delineation process was defining each of our selected USGS stream gauges as the final points to where discharge flows. To do this, the USGS stream gauges were defined as the pour points in the *Watershed* tool, where pour points are geographically defined final points of interest where water flows to. The watersheds delineated from this process represent the discharge from each of the five

river basins, French Broad, Broad, Yadkin-Pee Dee, Lumber, and Neuse River Basins, that flows into the USGS stream gauges selected in this study (Fig. 14, Table 4).

3.4.3 Local Statistics of Precipitation within the Watersheds

Zonal Statistics is an ArcGIS tool that allows the user to calculate descriptive statistics from values in a raster layer that fall within the boundaries of a specified polygon. In this study, we were interested in information like how much precipitation falls each season in each of the five watersheds. Therefore, an ArcGIS tool was created to calculate precipitation statistics for each day in the four year dataset across the five watersheds (Appendix A). In this tool, precipitation values were extracted from each daily precipitation raster layer; these layers were created in the NetCDF to raster conversion process. The five watershed shapefiles were defined as the five different polygon boundaries in the *Zonal Statistics* tool and acted as bounds for the values extracted from the daily precipitation rasters. The information was then exported to multiple tables and combined in Excel. Once in Excel, it was possible to conduct different analyses over any time frame of interest. For example, the statistics computed from this tool can provide information about the seasonal precipitation totals that fell within each of the five watersheds (Fig. 16). The flowchart in Figure 17 provides an overview of the steps involved in extracting the precipitation information necessary to compare the watershed precipitation input to the stream gauge discharge.

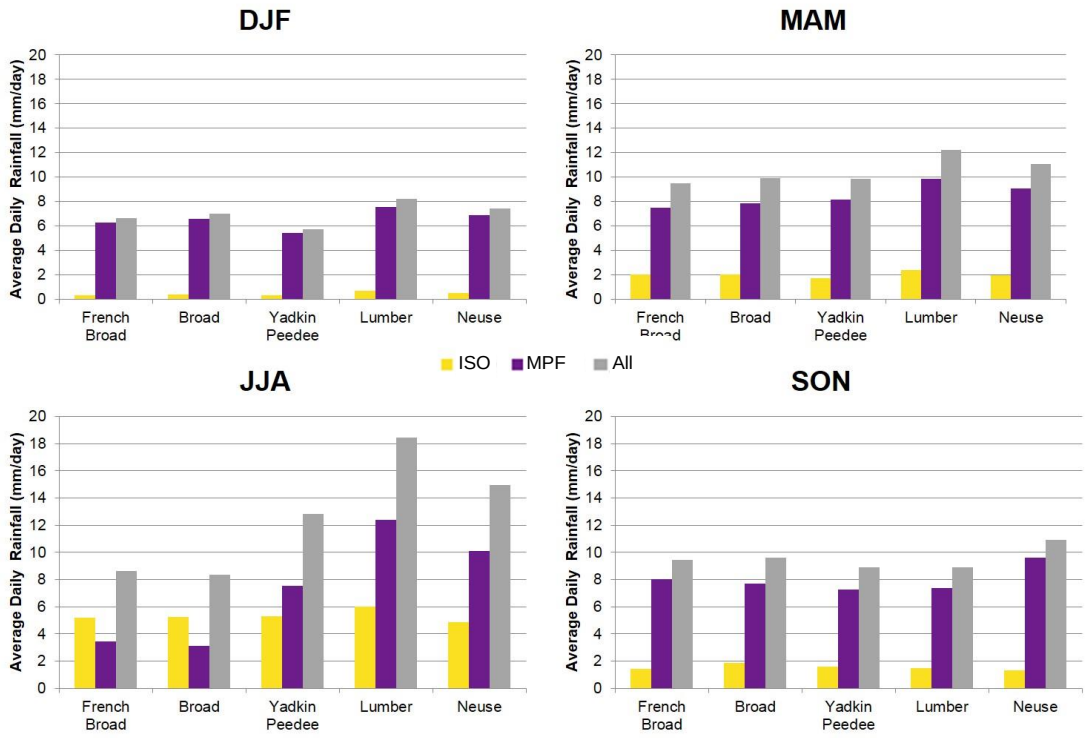

Figure 16. Daily averaged seasonal precipitation for each of the five watersheds. Gold bars represent average daily precipitation contribution by isolated convection. Purple bars is the average daily precipitation from MPF, and gray bars is the total average daily precipitation.

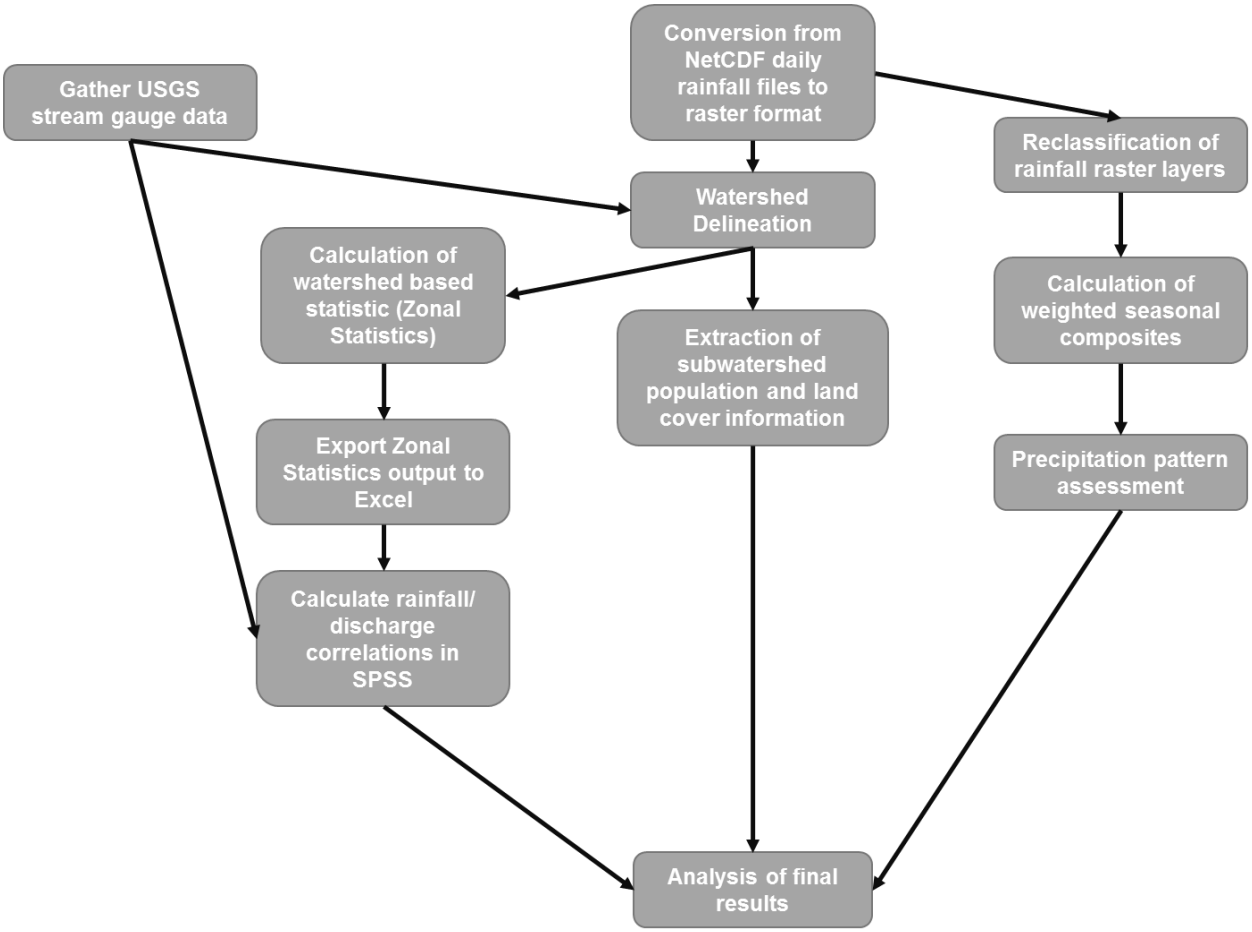

Figure 17. Flowchart of the steps involved in the preparation of the data for comparison of precipitation and discharge correlations, analyses of land cover data and census data, and precipitation pattern analyses.

3.5 Watershed Precipitation and Discharge Correlations

Initial hydrographs (shown later) suggested that there may be a correlation between the precipitation and discharge, and there also appeared to be some lag between when the time the rain event took place and when the peak discharge occurred. Therefore, we investigated the correlations between precipitation modes of organization and stream discharge. Organizing the stream gauge and precipitation data in Excel for each of the watersheds simplified the analysis of this correlation using IBM's

SPSS statistical software package. However, it was first necessary to conduct unit conversions for both the USGS stream discharge data and the precipitation data so that values could be compared directly. The USGS stream discharge data units were in cubic feet per second. Therefore, those values were all converted to total cubic meters of discharge per day using equation 2.2.

$$[\frac{ft^3}{s}][\frac{86400s}{d}][\frac{0.0283168m^3}{1ft^3}] \quad (2.2)$$

The precipitation data was in units of mm/day. To compare these values to stream discharge required that we calculate the daily volumetric precipitation for each of the watersheds. We used equation 2.3 to calculate the daily total volumetric rain input to each watershed by multiplying the daily precipitation by the watershed area.

$$[\frac{mm}{d}][\frac{.001m}{mm}][B_a] \quad (2.3)$$

(Where B_a is the basin area, or in our case the watershed discharge area)

After these conversions were made, daily scatterplots of daily discharge and daily precipitation were created for each watershed. Additionally, precipitation and discharge correlations were analyzed using Pearson correlations at four different temporal schemes which included: (1) annual correlations for each of the four years of data separated, (2) seasonal correlations for each of the four years of data separated, (3) annual composite correlations using all four years of data, and (4) seasonal composite correlations using all four years of data. Because time lag between the rain event and the peak discharge was expected based on past literature, all of these correlations took into account the potential for up to a 12 day offset. However, the strength of the correlations in each watershed showed some variation in time lag

between the correlations analyzed. Therefore, we elected to assess the typical time lag for each basin by investigating the top ten percent of discharge events; in theory, those discharge events would correspond to storm events that produced a substantial amount of rain. The thresholds for the top ten discharge events for each watershed were selected from a Cumulative Distribution Function (CDF). Next, the data was again offset each day up to a 12 day offset, and all cases that did not meet or exceed the top ten percent threshold were omitted. The results of this analysis provided a better understanding of the typical time lag experienced in each of the five watersheds.

3.6 Precipitation Pattern Analysis

Another important piece of information was to analyze precipitation patterns associated with either MPF or isolated storm organization. It is possible that some years may have more precipitation farther from the stream gauges leading to greater lag time between the precipitation event and discharge, more infiltration of the water into the watershed, more time for evaporation of that rain water, and/or a decrease in the peak measured discharge. Additionally, extreme precipitation events that occurred over a short time period may produce high precipitation totals in the composites over an area where rain events are actually relatively rare. This would cause biases when attempting to visually assess precipitation patterns. To examine these possibilities, the daily precipitation raster layers were reclassified based on whether a pixel had any rain greater than 1 mm/day. All pixels with values greater than 1 mm/day were reclassified as 1 (rain occurred) and pixels with values less that 1 mm/day were reclassified as a 0 (no rain). Once reclassified, the *Cell Statistics* tool was used to sum up the days with raining pixels, cells with a value of 1, for the specified time period (e.g. annual or

seasonal composites). The output layer from this analysis provided information regarding the number of days each pixel experienced rain greater than 1 mm/day. From these maps, it was possible to visually assess the locations of the greatest rain reoccurrences. Additional weighted layers were also created using the 1 mm/day precipitation reclassified raster layers. These layers were created by multiplying the reclassified raster layers by the corresponding composite rain raster layers (eq. 2.4).

$$W_p = C_p * F_p \quad 2.4$$

(*Where W_p is the final weighted pixel value, C_p is the composite pixel value, and F_p is the frequency of daily rain, or the number of days rain occurred at the pixel)*

Therefore, this multiplies the total number of days that rain occurred at each pixel by the composite average daily rain at each pixel. This was done so that the daily rain contributions could be weighted by the number of days that rain occurs at each pixel providing additional information about the patterning, but still taking into account the total daily precipitation contributions.

Chapter 4

Results

The following section presents the main results found in the current study. It begins with a review of the visual products created from this precipitation climatology. Following, a more in-depth look into the distribution and frequency of the modes of organization and the potential correlations of their associated precipitation with discharge are analyzed.

4.1 Composite Reflectivity Mapping

Figure 18 provides a visual representation of the dataset. The four year composite reflectivity images are separated seasonally, and show the total daily precipitation contributions from the two modes of organization analyzed in the current study, MPF and isolated rain events. The winter months, December, January, and February (DJF) are in the top left of each four panel figure; spring months, March, April, and May (MAM), are in the top right; summer months, June, July, and August (JJA), are the bottom left panels; and the fall months, September, October, and November (SON) are the bottom right panels.

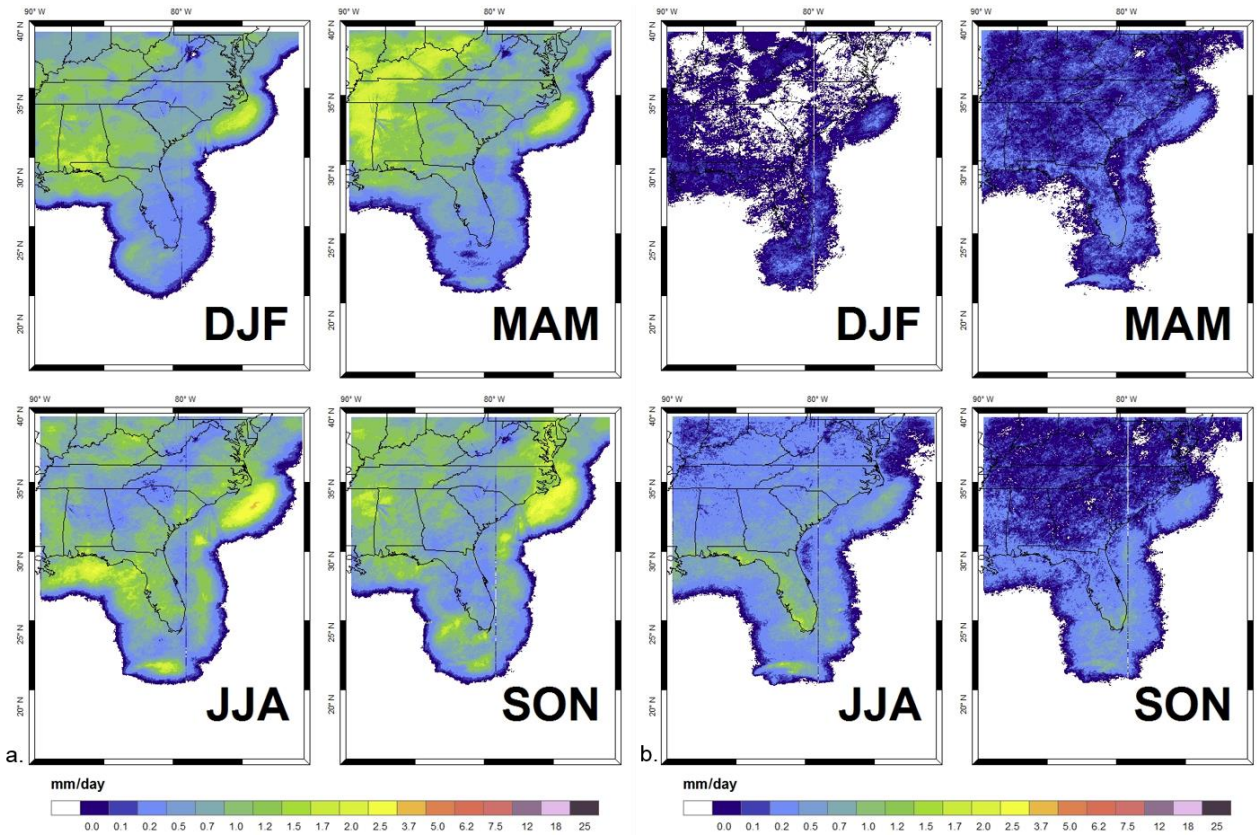

Figure 18. Seasonal composite reflectivity images of daily precipitation contributions from either MPF or Isolated precipitation where (a) is MPF precipitation and (b) is isolated precipitation.

Most apparent in Figure 18 are the differences between the precipitation distributions from the two precipitation modes of organization. Except for the summer months, MPF tend to have a much more homogenous appearance than isolated precipitation. There are also obvious differences in MPF activity between seasons. With the exception of the summertime, Florida sees little MPF precipitation. Also, there are greater amounts of MPF precipitation throughout the Ohio Valley and Southeast during the winter, spring and fall than in the summer. Another interesting feature is an area of consistently enhanced precipitation off the NC coast. Comparisons by Rickenbach et al.

(2014) using TRMM imagery confirms that this feature is a true area of enhanced precipitation, not a radar artifact.

As mentioned earlier, isolated convection has a much more heterogeneous precipitation distribution than the MCS seasonal precipitation. There is an increase in insolated precipitation during the summer and a decrease in isolated precipitation in the winter. In most seasons, and especially in the summer, there appears to be enhanced isolated convection along the Gulf of Mexico and Atlantic Ocean coastlines, suggesting that this boundary provides unique characteristics conducive to the development of isolated rain showers. Overall, it can already be said that there are fairly substantial seasonal variations in both MPF and isolated activity and it appears that isolated precipitation totals are greatest in the summer while there is a decrease in MPF precipitation totals during the summer.

North Carolina Precipitation

Figure 19 provides the same information as Figure 18, but zoomed into North Carolina.

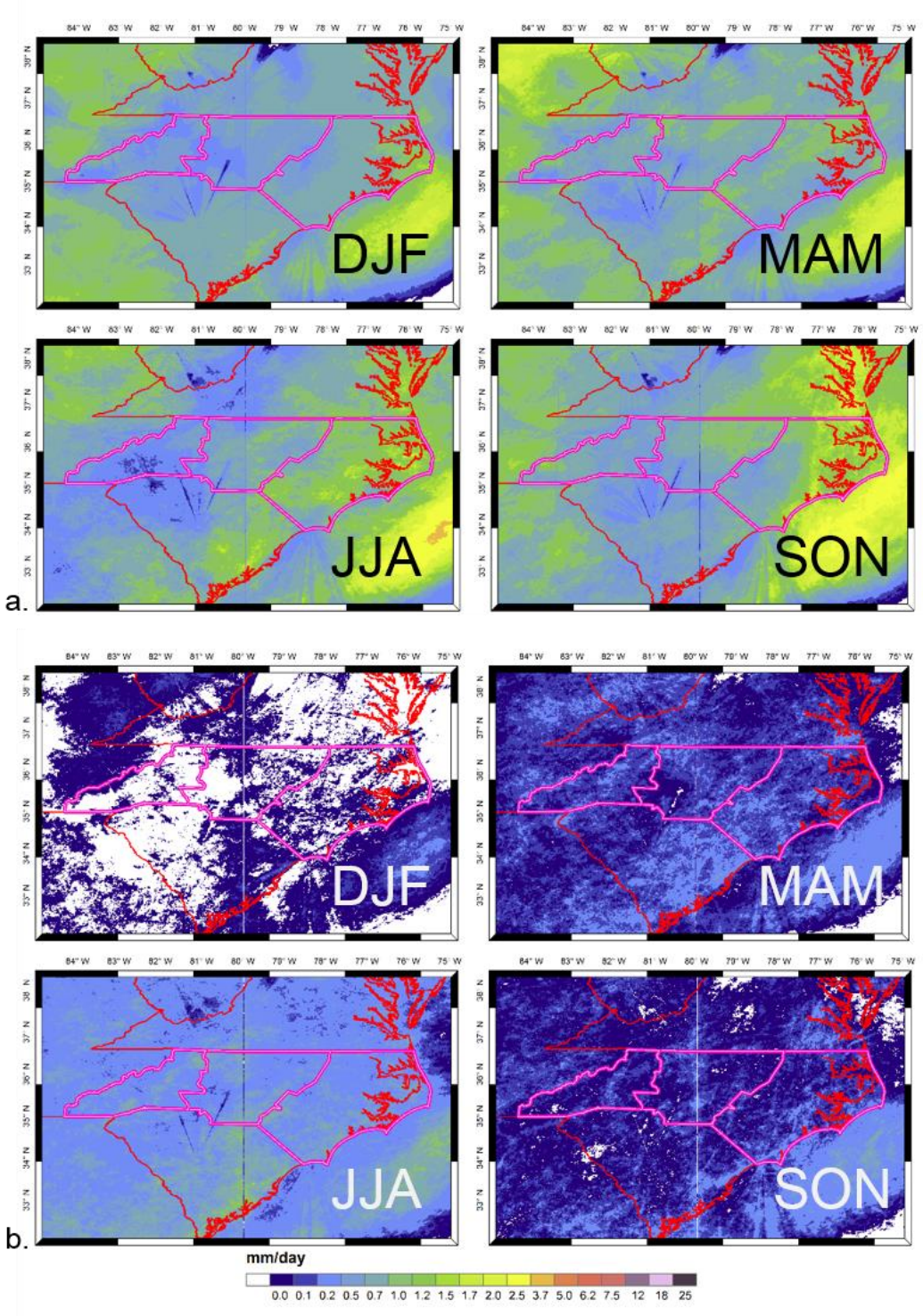

Figure 19. Seasonal composite reflectivity images of daily precipitation contributions from either MPF or Isolated precipitation where (a) is MPF precipitation and (b) is isolated precipitation.

Similar to the composite images for the entire Southeast U.S., the differences between MPF and isolated precipitation organization across North Carolina are quickly apparent. Again, the seasonal precipitation composite of MPF has a much more homogenous appearance than the more heterogeneous look of isolated precipitation. The summer is the only time that there is a more homogenous look to the isolated precipitation distribution. Figure 19 also shows the three main geographical regions of North Carolina; WNC, CNC, and ENC. Some of the more notable contrasts across North Carolina in regard to MPF precipitation are between the WNC and ENE regions. While the precipitation patterns between the two regions appear to be similar during the winter months, there is a region of increased daily precipitation totals along the middle portion of the ENC region in the spring. In the summer and fall months, ENC appears to receive a much greater amount of precipitation from MPF than WNC. Figure 20 provides the average daily precipitation across these regions generated from ArcGIS Zonal Statistics.

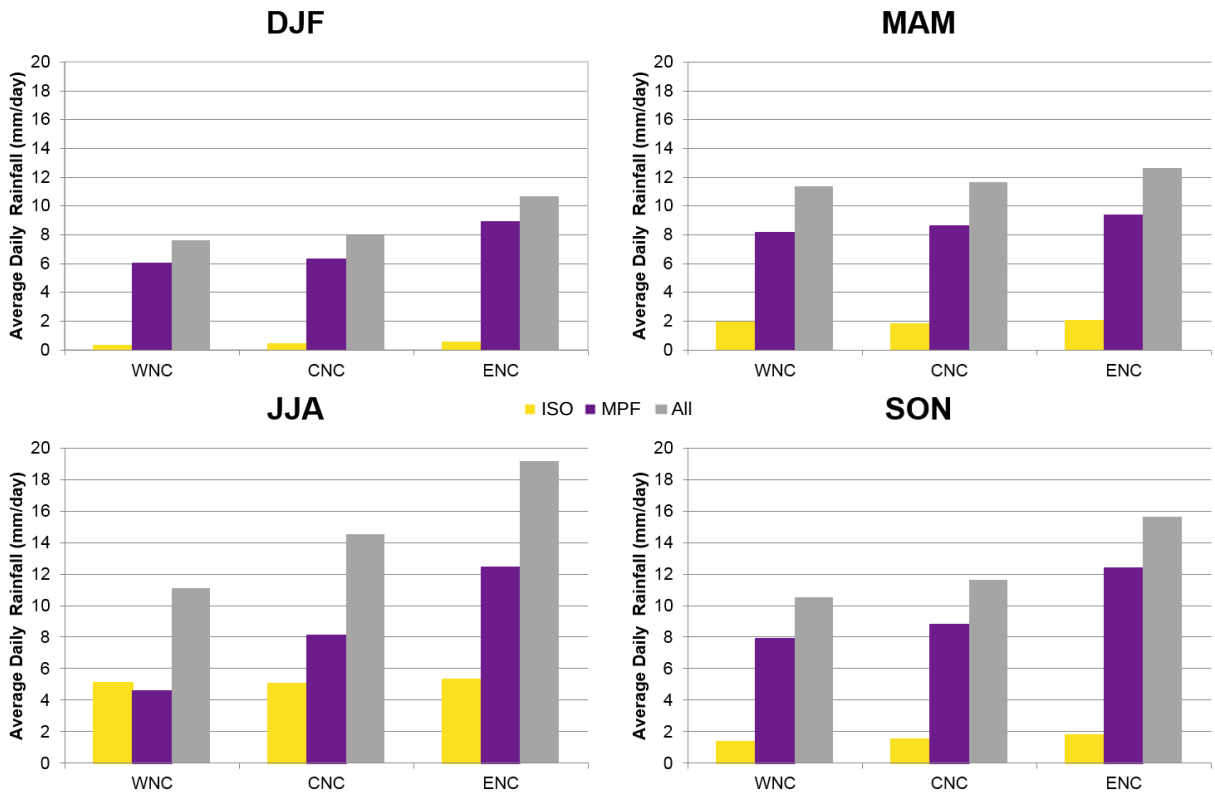

Figure 20. Seasonal composite average daily precipitation across the three regions of North Carolina. Gold bars represent isolated precipitation, purple bars are MPF precipitation, and gray is total precipitation.

Figure 20 shows that seasonal MPF precipitation is fairly consistent, but there is an obvious seasonal cycle in isolated precipitation. There is an increase in daily isolated precipitation in the summertime across the entire state with a decrease in isolated activity in the winter. This is expected because isolated convection tends to be enhanced in the summertime when there is greater heating, moisture, and therefore instability at lower levels allowing for widespread short-lived thunderstorms.

It is interesting to compare the precipitation contributions from MPF and isolated convection during each season (Fig. 20). For all regions and during most seasons, there is typically greater average daily MPF precipitation than isolated precipitation; however, the summertime brings about unique conditions for WNC. In the summer, this region

actually receives greater average daily precipitation from isolated events than MPF events. This is consistent with the physical processes in the mountain region during summer when increased low level instability, in conjunction with orographic lift produced by the rough terrain, enhances the potential for localized convection (Bleasdale and Chang 1972; Basist et al. 1994; Konrad 1996; Prudhomme and Reed 1998; Rowe et al. 2008).

4.2 Precipitation and Hydrology Connections

From these temporal and spatial differences in precipitation within and between the different precipitation modes of organization, it was hypothesized that these differences may be apparent when examining the hydrological response in North Carolina. Initial hypotheses regarding the correlations between the precipitation associated with the two and North Carolina watershed discharge were twofold: (1) isolated convection will produce steep peaks in discharge due to the high rates of runoff associated with the localized intense convection, (2) MPF precipitation will produce greater total discharge; however, peaks in stream discharge will not be as sharp or as dramatic as isolated precipitation--discharge will have a smoother appearance because of the longer duration and greater amounts of precipitation compared to isolated convection. Additionally, it was expected that we would see the correlations between isolated convection and discharge strongest in the summer while the correlations between MPF precipitation and discharge would be strongest in the winter.

4.2.1 Visual Assessment

Figure 21 and Figure 22 are hydrographs for the most western of the five watersheds, French Broad and Broad, and Figure 23 represents the Piedmont watershed, the Yadkin-Pee Dee. You will notice that these watersheds all appear to have very abrupt changes in discharge rates (gray line). These discharge curves are not smooth; they have steep changes in the slopes of these curves. These hydrographs suggest greater amounts of runoff, which is consistent with the steep terrain and rocky soils that tend to increase runoff potential and decrease the potential for rainwater infiltration. The bars in the image represent precipitation from MPF (purple) and isolated convection (gold). Simply following the peaks in precipitation and the peaks in discharge suggests possible correlations between the rain peaks and discharge peaks.

Moving toward the eastern watersheds (Figs. 24 & 25), the Neuse and the Lumber hydrographs have a much difference appearance than the mountains and Piedmont watersheds. These watersheds have a smoother appearance to the discharge. This is consistent with the sandier soils and the flatter terrain of these watersheds. These watersheds also show direct correlations between precipitation and discharge, although there appears to be more time between the rain event and the peak discharge than seen in the previous three watersheds.

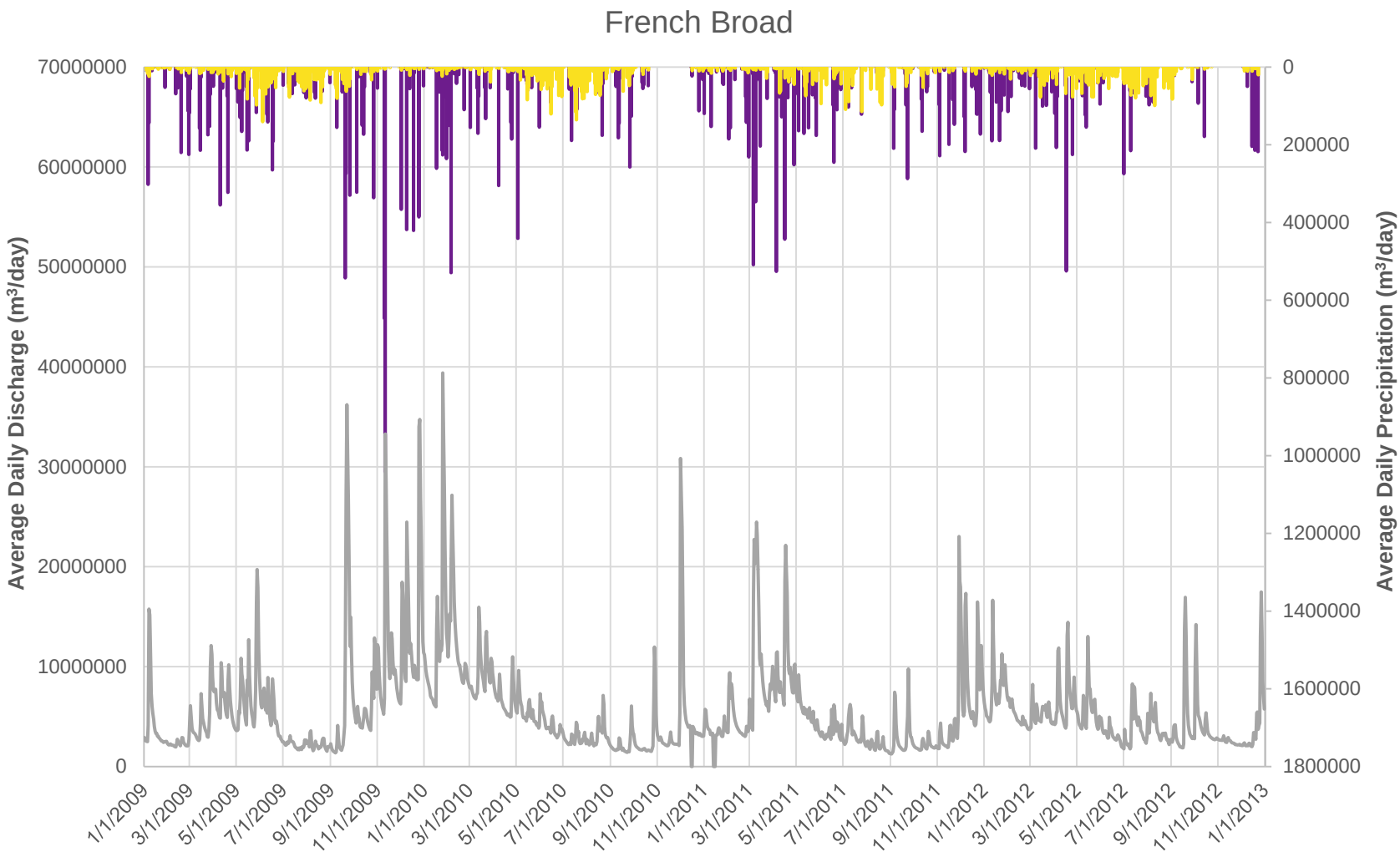

Figure 21. Hydrograph for the French Broad watershed. The gray curve is the average total daily discharge, purple bars are the average daily MPF volumetric precipitation, and gold bars are the average daily volumetric precipitation from isolated convection.

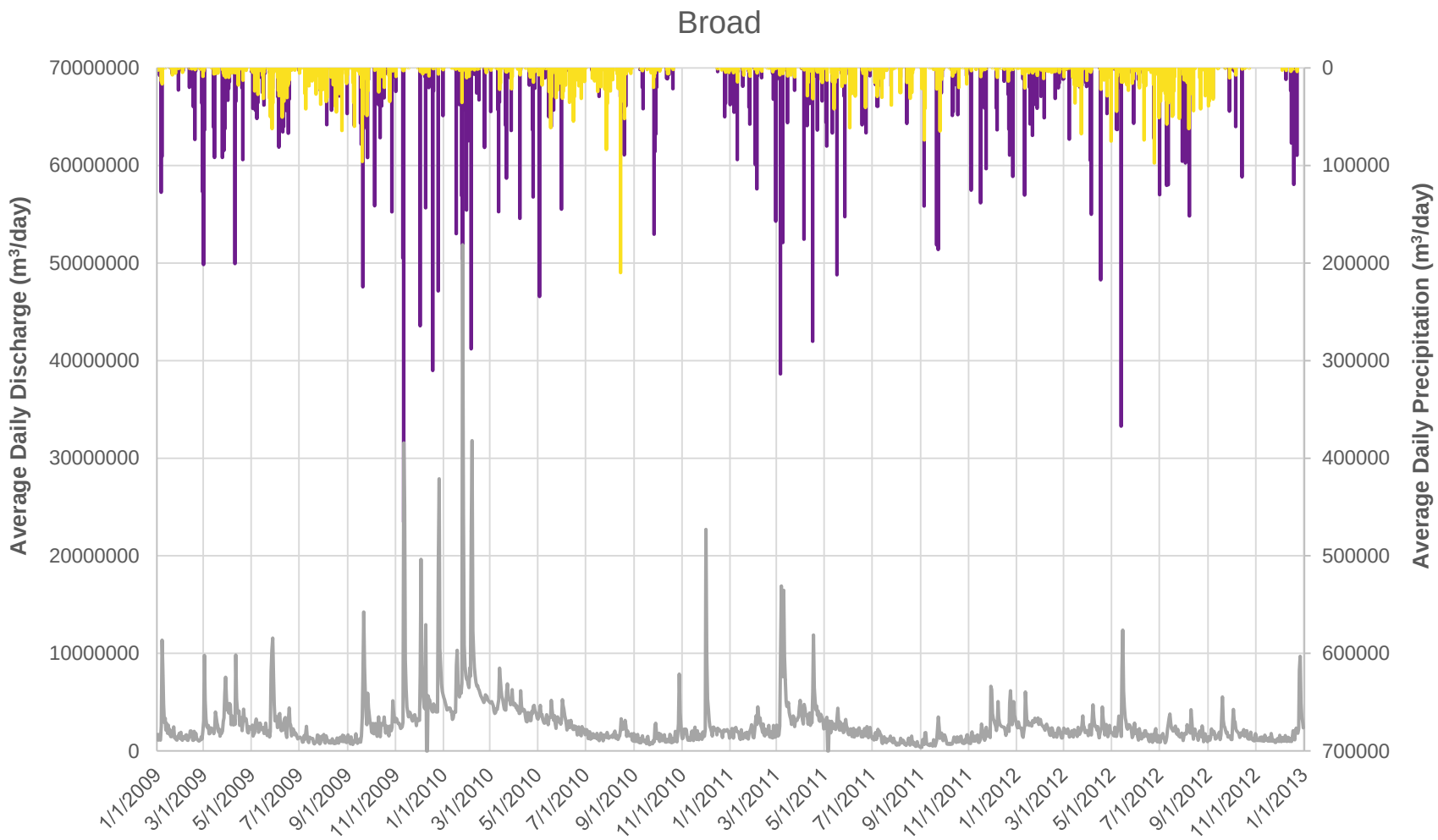

Figure 22. Hydrograph for the Broad watershed. The gray curve is the average total daily discharge, purple bars are the average daily MPF volumetric precipitation, and gold bars are the average daily volumetric precipitation from isolated convection.

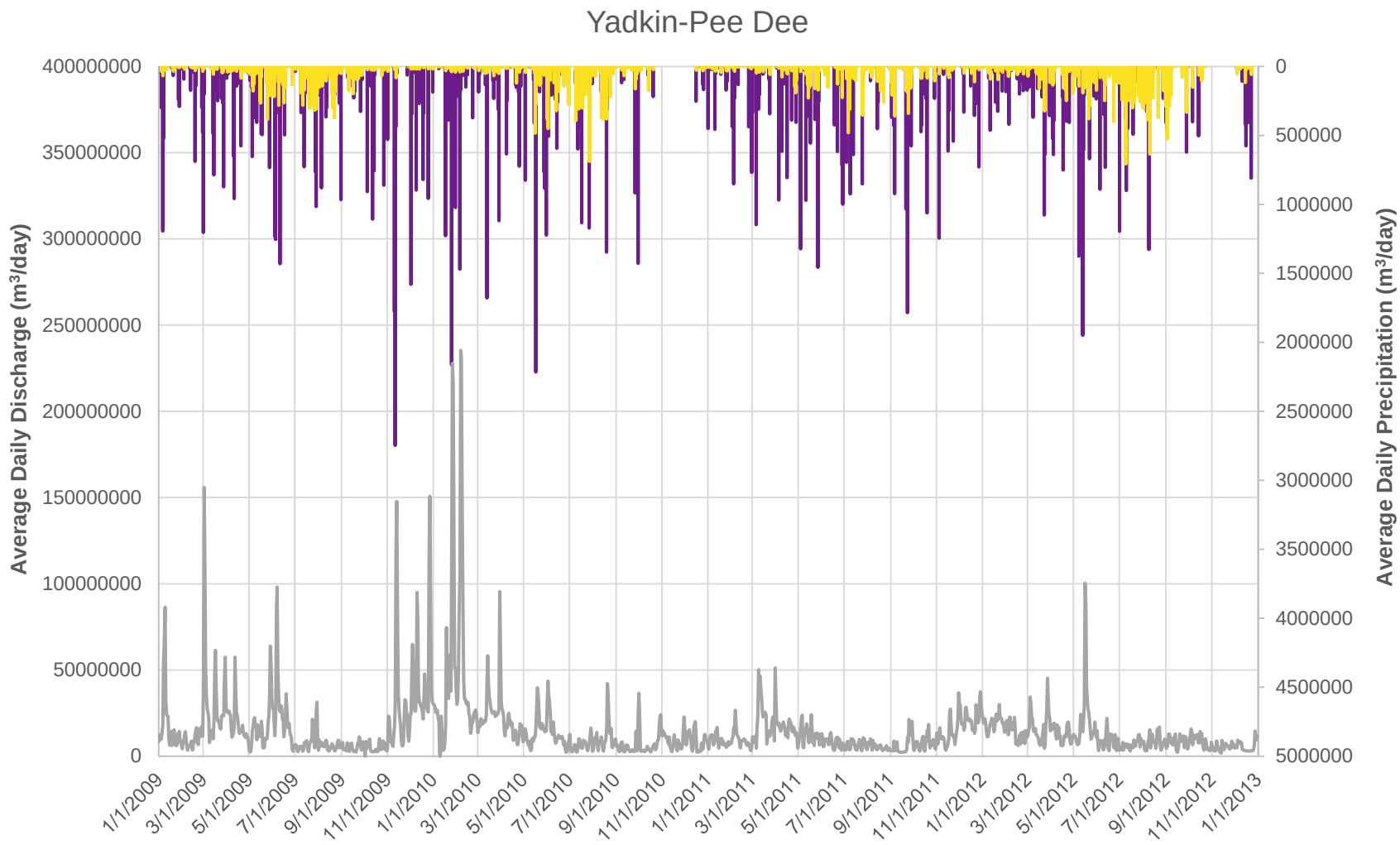

Figure 23. Hydrograph for the Yadkin-Pee Dee watershed. The gray curve is the average total daily discharge, purple bars are the average daily MPF volumetric precipitation, and gold bars are the average daily volumetric precipitation from isolated convection.

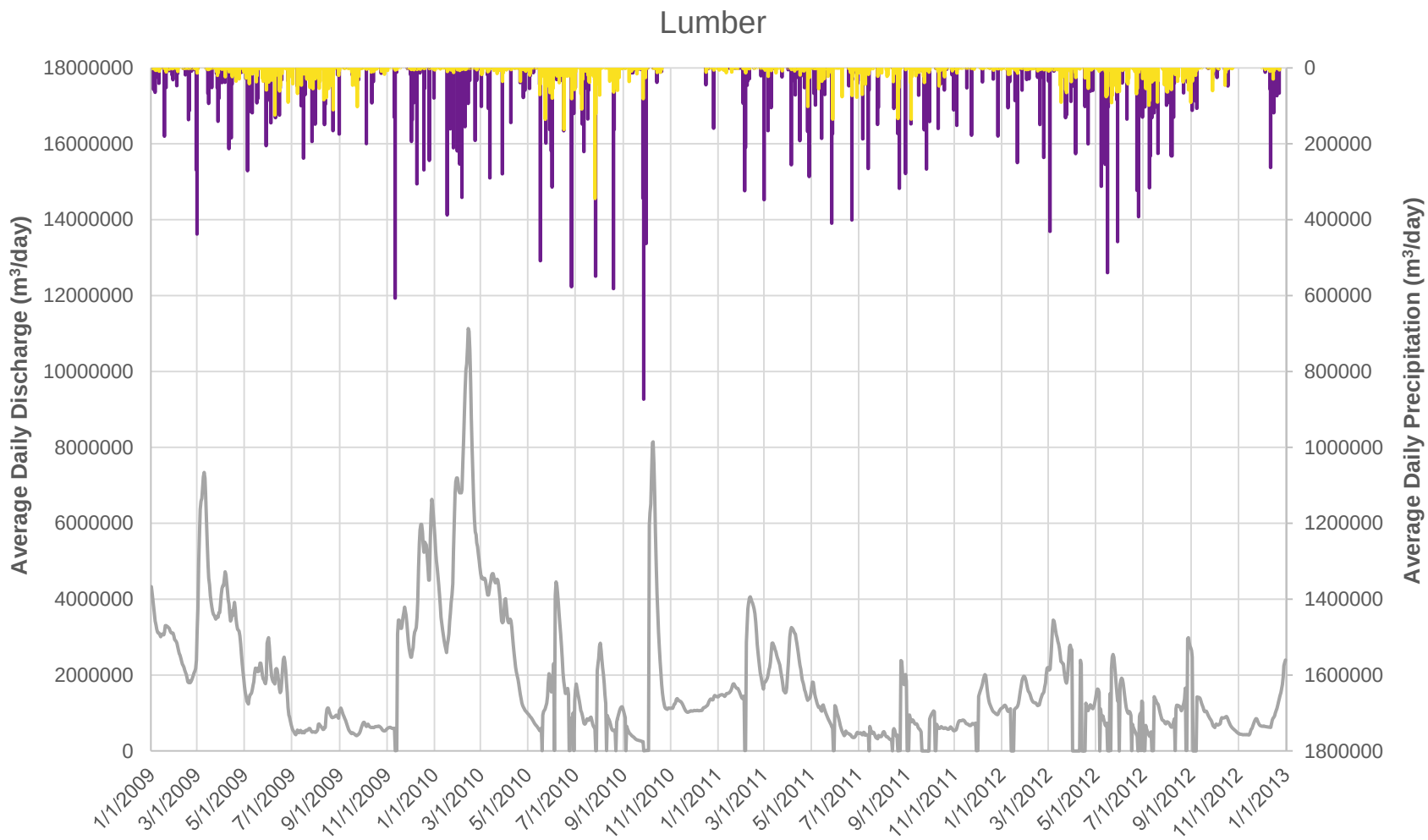

Figure 24. Hydrograph for the Lumber watershed. The gray curve is the average total daily discharge, purple bars are the average daily MPF volumetric precipitation, and gold bars are the average daily volumetric precipitation from isolated convection.

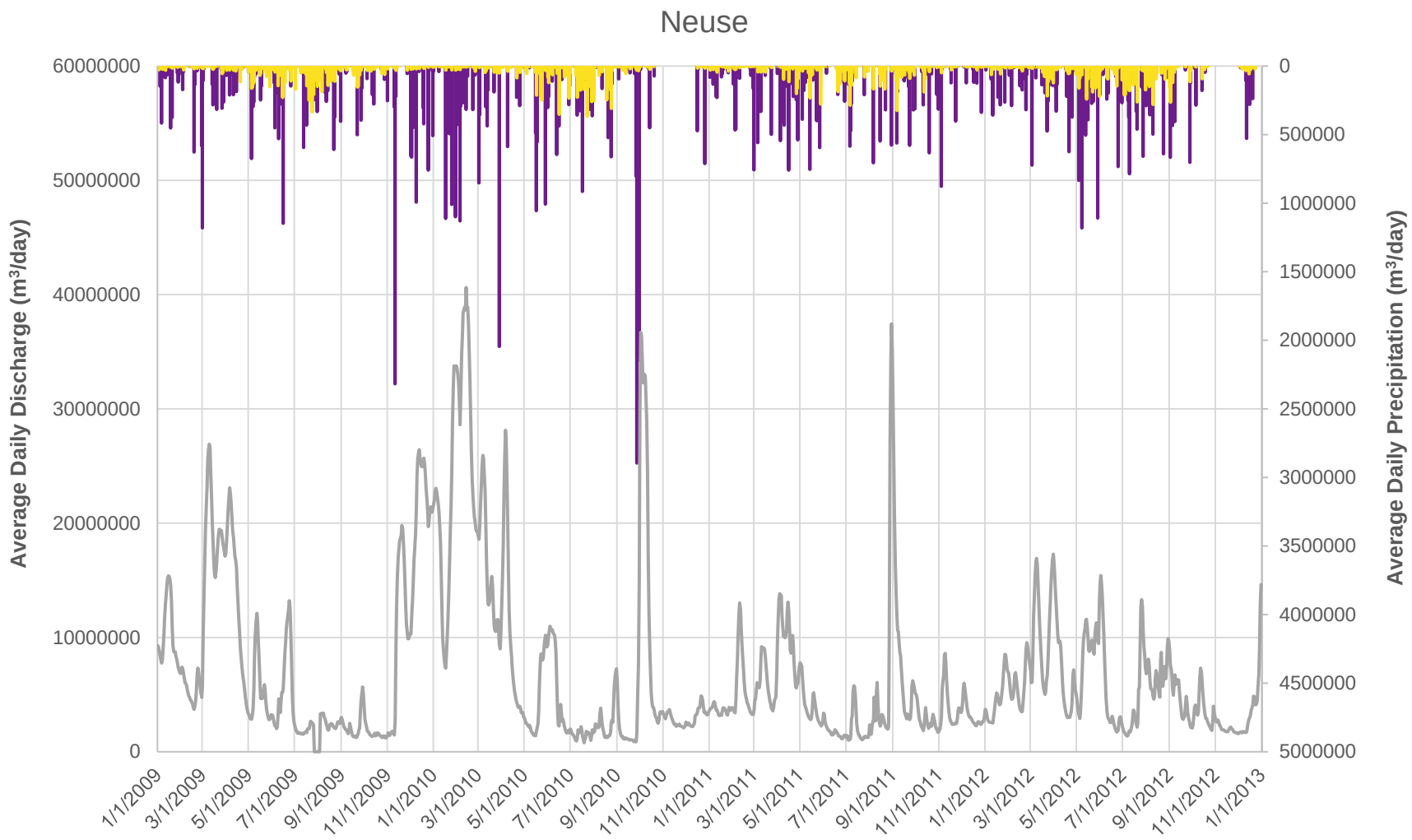

Figure 25. Hydrograph for the Neuse watershed. The gray curve is the average total daily discharge, purple bars are the average daily MPF volumetric precipitation, and gold bars are the average daily volumetric precipitation from isolated convection.

4.3 Precipitation-discharge Correlations

To investigate potential correlations between precipitation and discharge, multiple correlation analyses were conducted on each of these five watersheds. These correlations include an analysis of the correlations for the full dataset and an event based analysis where only ideal cases were hand selected for analysis to better understand the typical time lag in the precipitation-discharge correlation. Events were selected if there was steady and low discharge prior to a rain event and if there was little or no rain after the rain event (Fig. 26). Additionally, it was required that a corresponding peak in discharge occurred within 12 days of the rain event. Each of these analyses were broken down to investigate the correlations annually and seasonally (Tables 5-20). The following section presents the results from the investigation of these precipitation-discharge correlations.

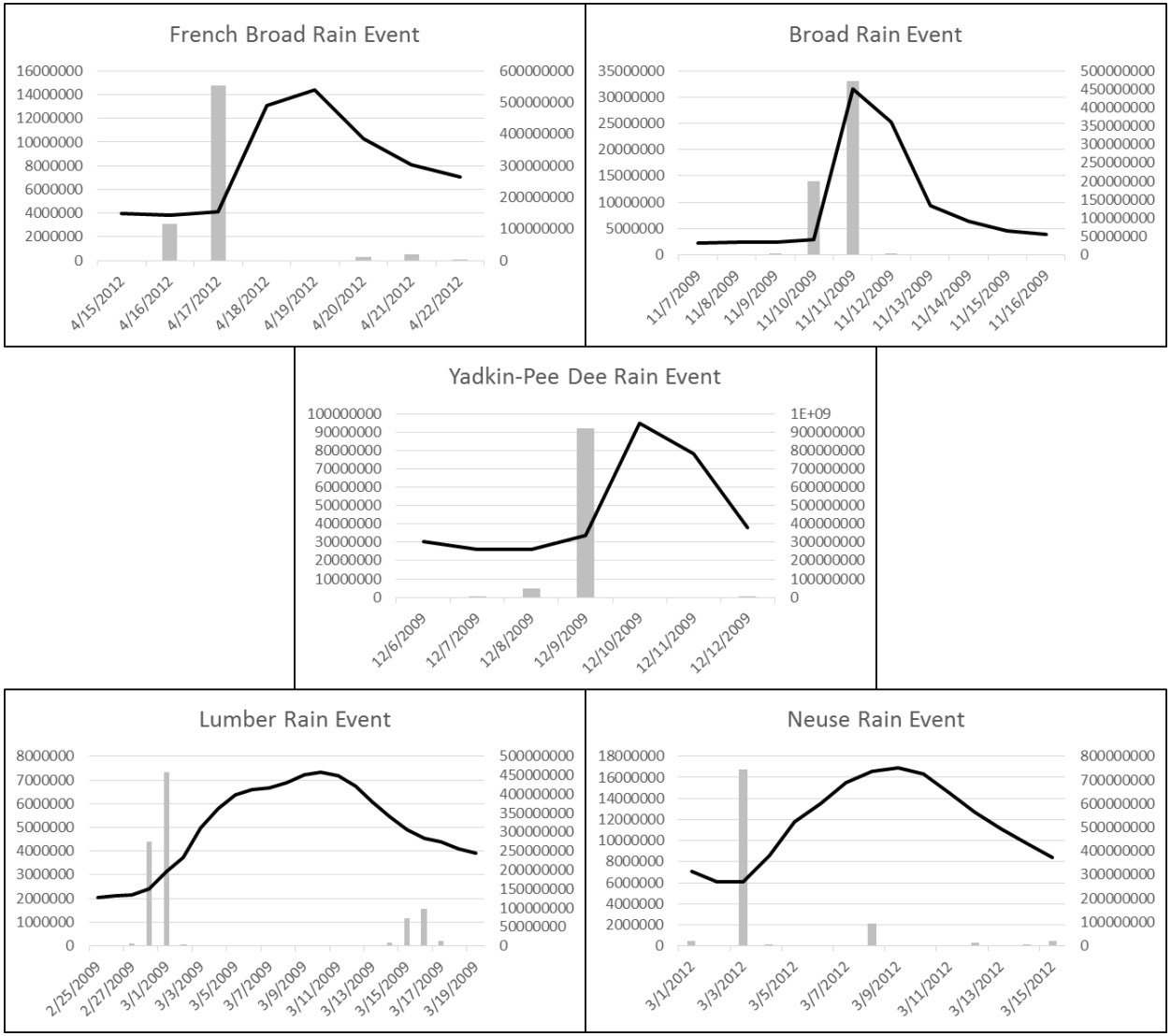

Figure 26. Example events selected from each watershed. The black line corresponds to discharge and the grey bars depict the total volumetric precipitation.

Table 5. 4-year precipitation-discharge correlations for all rain events. Daily rain is offset up to 12 days to allow for potential time lag in precipitation-discharge correlation.

	All Rain Events				
Daily Offset	French	Broad	Yadkin	Lumber	Neuse
Day 0	0.19**	0.24**	0.01	-0.10**	-0.01
Day +1	**0.39****	**0.44****	0.24**	-0.09**	0.03
Day +2	0.34**	0.22**	**0.29****	-0.07*	0.08**
Day +3	0.24**	0.12**	0.20**	-0.04	0.11**
Day +4	0.15**	0.09**	0.08**	0.02	0.17**
Day +5	0.09**	0.03	0.03	0.05	0.20**
Day +6	0.06*	0.03	-0.00	0.06*	**0.21****
Day +7	0.09**	0.10**	0.00	0.09**	0.20**
Day +8	0.08**	0.11**	0.03	0.10**	0.20**
Day +9	0.06*	0.02	0.03	0.11**	0.19**
Day +10	0.05	0.03	0.00	**0.11****	0.18**
Day +11	0.05	0.04	-0.02	0.10**	0.15**
Day +12	0.05	0.07*	0.02	0.09**	0.13**

** Correlation is significant at the 0.01 level (2-tailed)
* Correlation is significant at the 0.05 level (2-tailed)

Table 6. 4-year precipitation-discharge correlations for MPF rain events. Daily rain is offset up to 12 days to allow for potential time lag in precipitation-discharge correlation.

	MPF Rain Events				
Daily Offset	French	Broad	Yadkin	Lumber	Neuse
Day 0	0.23**	0.28**	0.04	-0.03	0.02
Day +1	**0.42****	**0.47****	0.28**	-0.02	0.07*
Day +2	0.36**	0.23**	**0.34****	0.01	0.11**
Day +3	0.26**	0.14**	0.23**	0.03	0.15**
Day +4	0.19**	0.12**	0.11**	0.09**	0.21**
Day +5	0.12**	0.06*	0.06*	0.11**	0.24**
Day +6	0.09**	0.06*	0.02	0.11**	**0.24****
Day +7	0.13**	0.14**	0.03	0.15**	0.24**
Day +8	0.12**	0.15**	0.06*	0.17**	0.24**
Day +9	0.10**	0.06*	0.06*	0.18**	0.23**
Day +10	0.10**	0.07*	0.03	**0.19****	0.21**
Day +11	0.10**	0.07**	0.01	0.18**	0.19**
Day +12	0.09**	0.10**	0.05	0.17**	0.16**

** Correlation is significant at the 0.01 level (2-tailed)
* Correlation is significant at the 0.05 level (2-tailed)

Table 7. 4-year precipitation-discharge correlations for isolated rain events. Daily rain is offset up to 12 days to allow for potential time lag in precipitation-discharge correlation.

	Isolated Rain Events				
Daily Offset	French	Broad	Yadkin	Lumber	Neuse
Day 0	-0.10**	-0.05	-0.10**	-0.15**	-0.16**
Day +1	-0.03	0.04	-0.06*	-0.15**	-0.15**
Day +2	-0.01	0.01	-0.04	-0.15**	-0.14**
Day +3	-0.03	-0.02	-0.04	-0.12**	-0.13**
Day +4	-0.06*	-0.05	-0.06*	-0.11**	-0.11**
Day +5	-0.10**	-0.08**	-0.08**	-0.09**	-0.10**
Day +6	-0.11**	-0.09**	-0.10**	-0.07*	-0.10**
Day +7	-0.11**	-0.08**	-0.11**	-0.07**	-0.10**
Day +8	-0.13**	-0.08**	-0.10**	-0.08**	-0.09**
Day +9	-0.15**	-0.10**	-0.09**	-0.08**	-0.10**
Day +10	-0.15**	-0.09**	-0.10**	-0.09**	-0.10**
Day +11	-0.15**	-0.08**	-0.12**	-0.08**	-0.11**
Day +12	-0.13**	-0.06*	-0.11**	-0.10**	-0.12**

** Correlation is significant at the 0.01 level (2-tailed)
* Correlation is significant at the 0.05 level (2-tailed)

Table 8. 4-year seasonal precipitation-discharge correlations for all rain events, MPF rain events, and isolated rain events. Rain events are offset up to 12 days to allow for potential time lag in precipitation-discharge correlation.

	French All				**French MPF**				**French Isolated**			
Daily Offset	DJF	MAM	JJA	SON	DJF	MAM	JJA	SON	DJF	MAM	JJA	SON
Day 0	0.31**	0.21**	0.21**	0.33**	0.38**	0.24**	0.15	0.45**	0.03	0.01	0.09	0.04
Day +1	**0.47****	**0.44****	**0.41****	**0.58****	**0.49****	**0.41****	**0.29****	**0.66****	**0.18****	0.07	0.23**	0.13
Day +2	0.39**	0.43**	0.37**	0.51**	0.41**	0.36**	0.23**	0.59**	0.18**	**0.17****	**0.24****	0.19*
Day +3	0.31**	0.29**	0.21**	0.43**	0.33**	0.26**	0.01	0.45**	0.17*	0.09	0.18**	**0.25****
Day +4	0.21**	0.19**	0.17**	0.30**	0.24**	0.19*	0.01	0.28**	0.12	-0.00	0.17**	0.24**
Day +5	0.12	0.10	0.16**	0.20**	0.15	0.13	0.06	0.16	0.03	-0.09	0.12*	0.20**
Day +6	0.08	0.06	0.15*	0.14	0.11	0.11	0.08	0.12	0.02	-0.10	0.07	0.14
Day +7	0.22**	0.05	0.12	0.14	0.30**	0.08	0.01	0.12	0.04	-0.04	0.11	0.09
Day +8	0.28**	-0.01	0.03	0.16*	0.36**	0.01	-0.03	0.17	0.03	-0.04	0.04	0.05
Day +9	0.25**	-0.04	-0.01	0.15	0.27**	0.03	-0.04	0.22*	0.03	-0.09	0.01	0.02
Day +10	0.20**	0.00	0.04	0.09	0.25**	0.10	0.04	0.17	-0.02	-0.08	0.03	-0.03
Day +11	0.17*	0.06	0.09	0.05	0.28**	0.16*	0.05	0.08	-0.02	-0.10	0.01	-0.00
Day +12	0.13	0.07	0.05	0.05	0.23**	0.16*	-0.01	0.05	0.08	-0.06	0.02	0.02

** Correlation is significant at the 0.01 level (2-tailed)
* Correlation is significant at the 0.05 level (2-tailed)

Table 9. 4-year seasonal precipitation-discharge correlations for all rain events, MPF rain events, and isolated rain events. Rain events are offset up to 12 days to allow for potential time lag in precipitation-discharge correlation.

	Broad All				**Broad MPF**				**Broad Isolated**			
Daily Offset	DJF	MAM	JJA	SON	DJF	MAM	JJA	SON	DJF	MAM	JJA	SON
Day 0	0.38**	0.10	0.08	0.45**	0.42**	0.10	0.06	0.60**	0.06	0.02	0.05	-0.00
Day +1	**0.56****	**0.50****	0.27**	**0.62****	**0.54****	**0.48****	0.25**	**0.65****	**0.46****	0.10	**0.21****	0.11
Day +2	0.32**	0.32**	**0.32****	0.31**	0.33**	0.30**	**0.35****	0.43**	0.27**	0.09	0.16**	0.14
Day +3	0.19*	0.15*	0.18**	0.21*	0.35**	0.17*	0.21*	0.32**	0.08	0.03	0.12	0.12
Day +4	0.13	0.17*	0.14*	0.19*	0.13	0.25**	0.17	0.17	0.08	-0.05	0.11	0.08
Day +5	0.07	0.03	0.10	0.10	0.07	0.06	0.08	0.10	0.02	-0.10	0.07	0.01
Day +6	0.13	0.00	0.09	0.12	0.20	0.09	0.18*	0.20	0.07	-0.18**	0.04	-0.01
Day +7	0.36**	0.10	0.10	0.21*	0.38**	0.15	0.20*	0.24*	0.09	-0.08	0.05	0.12
Day +8	0.41**	-0.00	0.09	0.16	0.37**	0.03	0.11	0.21*	-0.00	-0.05	0.09	0.03
Day +9	0.19*	-0.05	0.08	0.06	0.13	-0.02	0.08	0.18	-0.00	-0.11	0.10	-0.06
Day +10	0.11	0.04	0.00	0.01	0.29**	0.04	-0.00	0.02	-0.02	-0.05	0.05	-0.02
Day +11	0.10	-0.02	0.12	-0.03	0.39**	-0.01	0.16	-0.01	-0.03	-0.07	0.08	-0.01
Day +12	0.25**	-0.01	0.13*	0.03	0.33**	0.07	0.19*	0.01	0.23**	-0.09	0.05	0.08

** Correlation is significant at the 0.01 level (2-tailed)
* Correlation is significant at the 0.05 level (2-tailed)

Table 10. 4-year seasonal precipitation-discharge correlations for all rain events, MPF rain events, and isolated rain events. Rain events are offset up to 12 days to allow for potential time lag in precipitation-discharge correlation.

	Yadkin All				**Yadkin MPF**				**Yadkin Isolated**			
Daily Offset	DJF	MAM	JJA	SON	DJF	MAM	JJA	SON	DJF	MAM	JJA	SON
Day 0	0.14*	-0.04	0.04	0.14	0.25**	-0.06	0.07	0.11	-0.03	-0.08	-0.01	0.01
Day +1	**0.45****	0.22**	0.30**	0.39**	**0.53****	0.22**	0.38**	0.39**	0.07	0.02	0.03	0.02
Day +2	0.44**	0.30**	**0.34****	**0.58****	0.44**	0.26**	**0.40****	**0.60****	0.11	0.07	0.05	0.04
Day +3	0.27**	**0.33****	0.25**	0.43**	0.25**	**0.26****	0.27**	0.43**	0.07	0.09	0.07	0.02
Day +4	0.12	0.20**	0.11	0.26**	0.08	0.18*	0.20**	0.23*	0.01	0.07	0.02	0.03
Day +5	0.14*	0.06	0.01	0.24**	0.10	0.09	0.12	0.21*	0.01	-0.02	-0.02	0.07
Day +6	0.08	0.00	0.02	0.25**	0.06	0.08	0.07	0.27**	-0.03	-0.07	-0.03	0.06
Day +7	0.12	-0.01	0.05	0.06	0.14	0.10	0.09	0.17	-0.03	-0.10	-0.05	-0.05
Day +8	0.21**	0.06	0.11	-0.04	0.27**	0.06	0.11	-0.01	-0.01	-0.07	0.02	-0.06
Day +9	0.23**	0.04	0.09	-0.09	0.32**	0.04	0.10	-0.10	-0.04	-0.06	0.05	-0.08
Day +10	0.21**	-0.02	0.06	-0.10	0.28**	-0.06	0.08	-0.1	-0.05	-0.08	0.04	-0.10
Day +11	0.18**	-0.01	-0.00	-0.00	0.27**	-0.05	0.03	0.01	-0.05	-0.09	-0.02	-0.06
Day +12	0.29**	-0.02	-0.01	0.04	0.43**	-0.01	-0.01	0.06	-0.01	-0.06	0.01	-0.09

** Correlation is significant at the 0.01 level (2-tailed)
* Correlation is significant at the 0.05 level (2-tailed)

Table 11. 4-year seasonal precipitation-discharge correlations for all rain events, MPF rain events, and isolated rain events. Rain events are offset up to 12 days to allow for potential time lag in precipitation-discharge correlation.

	Lumber All				**Lumber MPF**				**Lumber Isolated**			
Daily Offset	DJF	MAM	JJA	SON	DJF	MAM	JJA	SON	DJF	MAM	JJA	SON
Day 0	0.13*	-0.18**	-0.15*	-0.13	0.20*	-0.17*	-0.20*	-0.15	-0.1	-0.21**	-0.05	-0.08
Day +1	0.18**	-0.16**	-0.14*	-0.15*	0.25**	-0.12	-0.19*	-0.18	-0.07	-0.20**	-0.07	-0.06
Day +2	0.23**	-0.11	-0.05	-0.16*	0.31**	-0.13	-0.08	-0.21*	-0.06	-0.21**	-0.05	-0.05
Day +3	0.26**	-0.04	-0.06	-0.06	0.34**	-0.01	-0.12	-0.11	-0.04	-0.18**	0.06	-0.12
Day +4	0.30**	-0.01	0.10	0.12	0.38**	0.02	0.04	0.09	-0.03	-0.14*	0.15**	-0.10
Day +5	0.32**	0.06	0.15**	0.19*	0.41**	0.08	0.10	0.17	-0.03	-0.11	0.16**	-0.05
Day +6	0.32**	0.06	**0.18****	0.18*	0.44**	0.11	0.12	0.17	-0.01	-0.10	**0.16****	-0.07
Day +7	0.31**	0.06	0.15*	0.39**	0.45**	0.11	0.13	0.40**	0.00	-0.10	0.15**	-0.05
Day +8	0.32**	0.08	0.11	0.51**	0.46**	0.10	0.09	0.50**	0.02	-0.13*	0.14*	0.08
Day +9	0.33**	0.09	0.12*	**0.54****	0.48**	0.10	0.12	**0.52****	0.02	-0.16**	0.13*	0.08
Day +10	**0.34****	0.13*	0.12*	0.54**	0.50**	0.10	0.08	0.50**	0.03	-0.15*	0.15*	0.08
Day +11	0.33**	0.11	0.12*	0.54**	**0.50***	0.11	0.02	0.51**	0.03	-0.13*	0.14*	0.09
Day +12	0.32**	0.06	0.07	0.52**	0.49**	0.07	0.05	0.52**	0.03	-0.13*	0.08	0.07

** Correlation is significant at the 0.01 level (2-tailed)
* Correlation is significant at the 0.05 level (2-tailed)

Table 12. 4-year seasonal precipitation-discharge correlations for all rain events, MPF rain events, and isolated rain events. Rain events are offset up to 12 days to allow for potential time lag in precipitation-discharge correlation.

	Neuse All				**Neuse MPF**				**Neuse Isolated**			
Daily Offset	DJF	MAM	JJA	SON	DJF	MAM	JJA	SON	DJF	MAM	JJA	SON
Day 0	0.18**	-0.09	-0.02	0.00	0.26**	-0.05	0.07	-0.01	-0.03	-0.15**	-0.16**	0.03
Day +1	0.22**	-0.08	0.02	0.15*	0.32**	-0.03	0.09	0.18*	-0.02	-0.17**	-0.12*	0.03
Day +2	0.25**	-0.05	0.01	0.29**	0.35**	0.01	0.02	0.35**	-0.00	-0.16**	-0.09	0.05
Day +3	0.27**	-0.01	0.08	0.38**	0.37**	0.05	0.17*	0.45**	0.01	-0.12*	-0.06	0.05
Day +4	0.30**	0.06	0.16**	0.48**	0.40**	0.12	0.23**	0.55**	0.02	-0.05	0.01	0.04
Day +5	0.31**	0.11	**0.21****	**0.52****	0.42**	0.19**	**0.27****	**0.59****	0.04	-0.01	0.04	0.05
Day +6	0.32**	0.15*	0.19**	0.50**	0.42**	0.22**	0.22**	0.58**	0.05	-0.01	0.05	0.04
Day +7	0.32**	0.16**	0.15**	0.47**	0.42**	**0.23****	0.15	0.55**	0.07	-0.01	0.04	0.01
Day +8	0.34**	**0.16****	0.11	0.44**	0.43**	0.22**	0.07	0.51**	0.07	-0.03	0.04	-0.00
Day +9	0.34**	0.14*	0.11	0.42**	0.44**	0.20**	0.04	0.49**	0.07	-0.04	0.06	-0.03
Day +10	**0.35****	0.11	0.08	0.40**	0.44**	0.16*	-0.00	0.46**	0.07	-0.06	0.09	-0.05
Day +11	0.34**	0.08	0.06	0.37**	**0.45****	0.12	0.02	0.40**	0.08	-0.09	0.06	-0.02
Day +12	0.32**	0.05	0.06	0.31**	0.45**	0.09	0.07	0.32**	0.07	-0.11	0.04	-0.01

** Correlation is significant at the 0.01 level (2-tailed)
* Correlation is significant at the 0.05 level (2-tailed)

Table 13. Event-based precipitation-discharge correlations for all rain events. Daily rain is offset up to 12 days to allow for potential time lag in precipitation-discharge correlation.

	All Rain Events				
Daily Offset	French	Broad	Yadkin	Lumber	Neuse
Day 0	0.17**	0.29**	-0.13	-0.32**	-0.24**
Day +1	**0.44****	**0.58****	0.25**	-0.22	-0.11
Day +2	0.37**	0.18*	**0.33****	-0.05	0.01
Day +3	0.16**	0.00	0.15	0.01	0.13
Day +4	0.05	-0.01	-0.02	0.08	0.25**
Day +5	-0.01	-0.09	-0.08	0.14	0.32**
Day +6	0.00	-0.07	-0.12	0.13	0.33**
Day +7	0.12	0.14	-0.07	0.11	**0.34****
Day +8	0.09	0.22**	0.16	0.13	0.33**
Day +9	0.02	-0.01	0.21*	0.12	0.30**
Day +10	-0.02	-0.01	0.10	0.11	0.27**
Day +11	0.04	0.01	0.01	0.07	0.21**
Day +12	0.09	0.16	0.14	0.06	0.14

** Correlation is significant at the 0.01 level (2-tailed)
* Correlation is significant at the 0.05 level (2-tailed)

Table 14. Event-based precipitation-discharge correlations for MPF rain events. Daily rain is offset up to 12 days to allow for potential time lag in precipitation-discharge correlation.

	MPF Rain Events				
Daily Offset	French	Broad	Yadkin	Lumber	Neuse
Day 0	0.19**	0.31**	-0.11	-0.27*	-0.21**
Day +1	**0.46****	**0.57****	0.29**	-0.17	-0.08
Day +2	0.37**	0.16*	**0.36****	-0.01	0.04
Day +3	0.17**	0.00	0.17*	0.05	0.16*
Day +4	0.05	-0.01	-0.00	0.13	0.27**
Day +5	0.00	-0.08	-0.06	0.19	0.34**
Day +6	0.01	-0.05	-0.10	0.18	0.36**
Day +7	0.13*	0.16	-0.04	0.16	**0.37****
Day +8	0.11	0.24**	0.20*	0.19	0.35**
Day +9	0.04	0.01	0.23**	0.17	0.32**
Day +10	0.00	0.01	0.12	0.16	0.29**
Day +11	0.07	0.02	0.04	0.13	0.23**
Day +12	0.11	0.16	0.16	0.12	0.16*

** Correlation is significant at the 0.01 level (2-tailed)
* Correlation is significant at the 0.05 level (2-tailed)

Table 15. Event-based precipitation-discharge correlations for isolated rain events. Daily rain is offset up to 12 days to allow for potential time lag in precipitation-discharge correlation.

	Isolated Rain Events				
Daily Offset	French	Broad	Yadkin	Lumber	Neuse
Day 0	-0.09	0.01	-0.23**	-0.35**	-0.30**
Day +1	0.01	**0.25****	-0.13	-0.32**	-0.27**
Day +2	0.06	0.13	-0.08	-0.25*	-0.22**
Day +3	0.01	0.01	-0.09	-0.26*	-0.17*
Day +4	-0.03	-0.04	-0.13	-0.23*	-0.12
Day +5	-0.08	-0.11	-0.17	-0.21	-0.11
Day +6	-0.07	-0.13	-0.18*	-0.21	-0.10
Day +7	-0.03	-0.05	-0.20*	-0.23*	-0.07
Day +8	-0.07	-0.06	-0.12	-0.26*	-0.08
Day +9	-0.13*	-0.12	-0.09	-0.25*	-0.07
Day +10	-0.14*	-0.10	-0.15	-0.25*	-0.11
Day +11	-0.11	-0.05	-0.19*	-0.28**	-0.17*
Day +12	-0.04	0.07	-0.13	-0.28*	-0.16*

** Correlation is significant at the 0.01 level (2-tailed)
* Correlation is significant at the 0.05 level (2-tailed)

Table 16. Event-based seasonal precipitation-discharge correlations for all rain events, MPF rain events, and isolated rain events. Rain events are offset up to 12 days to allow for potential time lag in precipitation-discharge correlation.

	French All				**French MPF**				**French Isolated**			
Daily Offset	DJF	MAM	JJA	SON	DJF	MAM	JJA	SON	DJF	MAM	JJA	SON
Day 0	0.23	0.03	0.39*	0.24	0.24*	0.03	0.41*	0.25	-0.16	0.04	0.08	-0.05
Day +1	**0.50****	**0.36****	**0.46****	**0.55****	**0.51****	**0.34****	**0.43****	**0.55****	0.08	0.23**	0.21	0.09
Day +2	0.33**	0.36**	0.05	0.48**	0.34**	0.33**	0.06	0.47**	0.08	**0.32****	-0.03	0.16
Day +3	0.08	0.04	-0.21	0.32*	0.08	0.01	-0.20	0.31*	-0.03	0.18*	-0.10	0.19
Day +4	-0.05	-0.06	-0.29	0.19	-0.05	-0.08	-0.28	0.18	-0.02	0.03	-0.12	0.21
Day +5	-0.05	-0.13	-0.08	0.10	-0.05	-0.12	-0.12	0.08	-0.05	-0.10	0.08	0.18
Day +6	-0.01	-0.02	0.07	0.04	-0.01	-0.00	0.07	0.02	-0.04	-0.04	0.02	0.21
Day +7	0.43**	0.02	0.08	0.06	0.44**	-0.02	0.05	0.05	0.13	0.22*	0.09	0.13
Day +8	0.39**	0.00	0.13	0.02	0.39**	-0.04	0.09	0.03	0.05	0.21*	0.14	-0.03
Day +9	0.28*	-0.07	0.24	-0.08	0.28*	-0.08	0.21	-0.06	0.02	0.09	0.18	-0.11
Day +10	0.01	-0.00	-0.04	-0.03	0.02	0.01	-0.12	-0.02	-0.06	-0.10	0.06	-0.06
Day +11	0.05	0.12	-0.02	0.10	0.06	0.13	-0.11	0.15	-0.01	-0.05	0.08	0.02
Day +12	0.16	0.17	-0.14	0.11	0.14	0.17*	0.01	0.07	0.28*	0.03	-0.22	0.17

** Correlation is significant at the 0.01 level (2-tailed)
* Correlation is significant at the 0.05 level (2-tailed)

Table 17. Event-based seasonal precipitation-discharge correlations for all rain events, MPF rain events, and isolated rain events. Rain events are offset up to 12 days to allow for potential time lag in precipitation-discharge correlation. Some correlations cannot be computed (N/A) because of lack of available events.

	Broad All				**Broad MPF**				**Broad Isolated**			
Daily Offset	DJF	MAM	JJA	SON	DJF	MAM	JJA	SON	DJF	MAM	JJA	SON
Day 0	0.41**	0.00	N/A	0.50*	0.43**	-0.03	N/A	0.55*	0.00	0.26*	N/A	-0.14
Day +1	**0.64****	**0.64****		**0.78****	**0.62****	**0.61****		**0.79****	**0.57****	**0.43****		0.06
Day +2	0.10	0.33**		0.26	0.10	0.31**		0.23	0.13	0.24*		0.17
Day +3	0.01	-0.00		-0.02	0.01	-0.02		-0.02	-0.02	0.08		0.01
Day +4	0.00	0.03		-0.10	-0.00	0.03		-0.09	0.02	-0.05		-0.06
Day +5	-0.10	-0.08		-0.16	-0.1	-0.07		-0.16	-0.12	-0.11		-0.03
Day +6	-0.05	-0.07		-0.16	-0.05	-0.04		-0.15	-0.02	-0.22		-0.14
Day +7	0.29*	0.07		-0.26	0.29*	0.07		-0.23	0.19	0.04		-0.27
Day +8	0.41**	0.03		-0.27	0.42**	0.00		-0.29	0.00	0.24*		-0.25
Day +9	0.04	-0.05		-0.30	0.04	-0.05		-0.26	0.00	-0.01		-0.31
Day +10	-0.04	0.04		-0.04	-0.04	0.07		0.12	-0.06	-0.11		-0.18
Day +11	0.06	-0.06		-0.05	0.06	-0.05		-0.04	-0.01	-0.09		-0.05
Day +12	0.24	0.09		0.01	0.22	0.13		-0.05	0.28	-0.09		0.14

** Correlation is significant at the 0.01 level (2-tailed)
* Correlation is significant at the 0.05 level (2-tailed)

Table 18. Event-based seasonal precipitation-discharge correlations for all rain events, MPF rain events, and isolated rain events. Rain events are offset up to 12 days to allow for potential time lag in precipitation-discharge correlation.

	Yadkin All				**Yadkin MPF**				**Yadkin Isolated**			
Daily Offset	DJF	MAM	JJA	SON	DJF	MAM	JJA	SON	DJF	MAM	JJA	SON
Day 0	-0.05	-0.28*	0.26	-0.09	-0.05	-0.25*	0.22	-0.10	-0.17	-0.31*	0.28	0.26
Day +1	0.46**	0.17	**0.71****	0.44	0.46**	0.21	**0.71****	0.43	0.24	-0.14	0.46	0.30
Day +2	**0.47****	0.30*	0.47	**0.75****	**0.47****	0.32*	0.42	**0.76****	0.35*	0.03	0.46	-0.04
Day +3	0.13	**0.31***	-0.09	0.46	0.12	0.31*	-0.19	0.48	0.16	0.12	0.26	-0.11
Day +4	-0.12	0.14	-0.36	0.12	-0.13	0.14	-0.39	0.13	0.01	0.05	-0.06	-0.12
Day +5	-0.08	-0.11	-0.26	-0.07	-0.09	-0.10	-0.26	-0.06	0.14	-0.13	-0.09	-0.15
Day +6	-0.17	-0.171	-0.03	-0.29	-0.17	-0.15	-0.16	-0.30	-0.07	-0.21	0.41	-0.29
Day +7	-0.08	-0.17	-0.26	-0.30	-0.08	-0.15	-0.25	-0.30	0.01	-0.24	-0.13	-0.31
Day +8	0.11	0.17	0.10	-0.17	0.11	0.22	0.06	-0.16	0.08	-0.06	0.13	-0.24
Day +9	0.17	0.16	0.46	-0.14	0.17	0.16	0.36	-0.13	0.09	0.09	0.47	-0.18
Day +10	0.06	-0.03	0.27	-0.15	0.06	-0.03	0.20	-0.13	-0.04	-0.02	0.30	-0.31
Day +11	0.02	-0.03	-0.46	0.06	0.02	-0.03	-0.43	0.06	-0.09	-0.06	-0.30	0.01
Day +12	0.20	0.03	-0.43	0.18	0.21	0.03	-0.54*	0.16	0.04	0.04	-0.24	0.44

** Correlation is significant at the 0.01 level (2-tailed)
* Correlation is significant at the 0.05 level (2-tailed)

Table 19. Event-based seasonal precipitation-discharge correlations for all rain events, MPF rain events, and isolated rain events. Rain events are offset up to 12 days to allow for potential time lag in precipitation-discharge correlation. Some correlations cannot be computed (N/A) because of lack of available events.

	Lumber All				**Lumber MPF**				**Lumber Isolated**			
Daily Offset	DJF	MAM	JJA	SON	DJF	MAM	JJA	SON	DJF	MAM	JJA	SON
Day 0	-0.44**	-0.41	-0.34	N/A	-0.43**	-0.38	-0.33	N/A	-0.43**	-0.49*	-0.29	N/A
Day +1	-0.24	-0.44*	-0.41		-0.26	-0.42	-0.34		-0.21	-0.43*	-0.42	
Day +2	-0.02	-0.28	0.09		-0.02	-0.22	0.17		-0.10	-0.52*	-0.09	
Day +3	0.05	-0.03	0.54*		0.05	0.02	0.55*		-0.01	-0.65**	0.42	
Day +4	0.15	0.12	0.42		0.15	0.17	0.36		0.06	-0.52*	0.34	
Day +5	0.19	0.21	0.12		0.19	0.25	0.07		0.07	-0.39	0.13	
Day +6	0.12	0.25	0.12		0.13	0.28	0.12		0.05	-0.27	0.07	
Day +7	0.07	0.30	0.09		0.07	0.31	0.07		0.05	-0.09	0.08	
Day +8	0.10	0.36	0.00		0.10	0.36	0.01		0.02	0.32	0.00	
Day +9	0.13	0.34	-0.09		0.13	0.34	-0.03		-0.03	0.28	-0.14	
Day +10	0.17	0.21	-0.17		0.17	0.22	-0.11		-0.03	-0.14	-0.15	
Day +11	0.17	0.09	-0.34		0.17	0.13	-0.32		-0.03	-0.41*	-0.17	
Day +12	0.12	0.06	-0.27		0.13	0.10	-0.32		-0.04	-0.52**	-0.01	

** Correlation is significant at the 0.01 level (2-tailed)
* Correlation is significant at the 0.05 level (2-tailed)

Table 20. Event-based seasonal precipitation-discharge correlations for all rain events, MPF rain events, and isolated rain events. Rain events are offset up to 12 days to allow for potential time lag in precipitation-discharge correlation.

	Neuse All				Neuse MPF				Neuse Isolated			
Daily Offset	DJF	MAM	JJA	SON	DJF	MAM	JJA	SON	DJF	MAM	JJA	SON
Day 0	-0.34	-0.32**	-0.37	-0.20	-0.33	-0.27*	-0.32	-0.20	-0.27	-0.42**	-0.41*	-0.26
Day +1	-0.26	-0.29*	-0.28	0.01	-0.26	-0.25*	-0.23	0.01	-0.13	-0.41**	-0.35	-0.11
Day +2	-0.16	-0.2	-0.11	0.18	-0.16	-0.16	-0.08	0.18	-0.08	-0.36**	-0.16	0.06
Day +3	0.00	-0.07	0.01	0.32	0.00	-0.04	0.02	0.32	0.07	-0.31**	-0.05	0.20
Day +4	0.17	0.03	0.08	0.48**	0.16	0.06	0.08	0.48**	0.17	-0.22	0.05	0.31
Day +5	0.29	0.12	0.10	**0.55****	0.28	0.15	0.10	**0.55****	0.29	-0.15	0.07	0.34
Day +6	0.32	0.18	0.11	0.52**	0.31	0.20	0.11	0.52**	0.35	-0.10	0.07	0.32
Day +7	0.27	0.23*	0.18	0.49**	0.25	0.25*	0.17	0.49**	0.44*	-0.09	0.14	0.28
Day +8	0.01	0.24*	0.26	0.50**	-0.01	0.27*	0.28	0.45**	0.32	-0.09	0.13	0.23
Day +9	-0.11	0.20	0.37	0.42*	-0.11	0.23*	0.35	0.43*	0.03	-0.10	0.28	0.21
Day +10	-0.14	0.14	0.28	0.41*	-0.14	0.17	0.27	0.41*	-0.01	-0.14	0.17	0.20
Day +11	0.02	0.03	0.18	0.35*	0.01	0.06	0.18	0.36	0.11	-0.22	0.07	0.04
Day +12	-0.06	-0.06	0.11	0.30	-0.07	-0.04	0.11	0.30	0.05	-0.20	0.05	0.09

** Correlation is significant at the 0.01 level (2-tailed)
* Correlation is significant at the 0.05 level (2-tailed)

4.3.1 Four Year Annual Correlations

From the analysis of all rain, either MPF, isolated, or both, it is apparent that correlations are strongest for different daily offsets depending on the watershed (Tables 5-7). In the French Broad and Broad watersheds, the strongest all precipitation-discharge correlations (r_{all}=0.39, p<0.01 & r_{all}=0.44, p<0.01) occur with a one day offset. As for the Yadkin-Pee Dee, the strongest all precipitation-discharge correlation (r_{all}=0.29, p<0.01) occurs with a two day offset. This is much different than the ENC watersheds where the Lumber and Neuse find the strongest correlations at a ten day offset (r_{all}=0.11, p<0.01) and six day offset (r_{all}=0.21, p<0.01).

It is interesting how consistent the correlations from the all precipitation-discharge correlations are to the MPF precipitation-discharge correlations. Again, the French Broad and Broad watersheds have the strongest precipitation-discharge correlations with a one day offset (r_{mpf}=0.42, p<0.01 & r_{mpf}=0.47, p<0.01). An important difference between MPF precipitation-discharge correlations and all precipitation-discharge correlations is the change to higher positive correlations. Both the French Broad and the Broad experienced an increase in the strength of this correlation from the all precipitation-discharge correlations and the MPF precipitation-discharge correlations. This increased strength in the correlations are also seen in the Yadkin-Pee Dee with a two day offset (r_{mpf}=0.34, p<0.01), the Lumber with a ten day offset (r_{mpf}=0.19, p<0.01), and the Neuse at a six day offset (r_{mpf}=0.24, p<0.01).

It was surprising to find that when analyzing the annual isolated precipitation-discharge correlations using all four years of data, there are no strong correlations between the two.

4.3.2 Four Year Seasonal Correlations

These correlations were then analyzed seasonally to investigate whether there were important seasonal differences in the correlations of precipitation from these modes of precipitation organization and discharge (Tables 8-12). For the French Broad watershed (Table 8), the analysis found that there is substantial seasonal variability in the precipitation-discharge correlations for these modes of precipitation organization. For the all precipitation-discharge correlations, the one day offset still appears to be the typical timeframe where the strongest correlations occurs (DJF: r_{all}=0.47, p<0.01; MAM: r_{all}=0.44, p<0.01; JJA: r_{all}=0.41, p<0.01; SON: r_{all}=0.58, p<0.01). The greatest differences in the precipitation-discharge correlations are found when MPF and isolated precipitation are separated. For MPF precipitation, the stronger correlations between precipitation and discharge are still found with a one day offset, but are better correlated in the winter (r_{mpf}=0.49, p<0.01), spring (r_{mpf}=0.41, p<0.01), and fall (r_{mpf}=0.65, p<0.01); whereas the summer has a much weaker (r_{mpf}=0.29, p<0.01) precipitation-discharge correlation. This is a much different story for the isolated precipitation-discharge correlations. For isolated events, the precipitation-discharge correlations are strongest in the summer (r_{iso}=0.24, p<0.01) with a two day offset and in the fall (r_{iso}=0.25, p<0.01) with a three day offset. These correlations are weakest in the winter (r_{iso}=0.18, p<0.01) and spring (r_{iso}=0.17, p<0.01).

In the Broad watershed (Table 9) the all precipitation-discharge correlations are still strongest in the winter (r_{all}=0.56, p<0.01), spring (r_{all}=0.50, p<0.01), and fall ($r=_{all}$.62, p<0.01) with a one day offset; however, it seems that an offset of two days has the strongest precipitation-discharge correlation in the summer months (r_{all}=0.32, p<0.01).

This same signal is also found for MPF precipitation-discharge correlations where summer (r_{mpf}=0.54, p<0.01), spring (r_{mpf}=0.48, p<0.01), and fall (r_{mpf}=0.65, p<0.01) are strongest with a one day offset, but summer is strongest with a two day offset (r_{mpf}=0.35, p<0.01). More seasonal differences arise with isolated precipitation-discharge correlations. The strongest correlations arise with a one day offset in the winter (r_{iso}=0.46, p<0.01) with the weakest correlations in the spring and fall. In the summer, the isolated precipitation-discharge correlation (r_{iso}=0.21, p<0.01) is comparable to what was found in the French Broad watershed.

Precipitation-discharge correlations in the Yadkin-Pee Dee watershed (Table 10) prove to be even more scattered when broken down seasonally. Where the majority of precipitation-discharge correlations in the mountain watersheds were strongest with a one day offset, the strongest correlations in the Yadkin-Pee Dee range from a single day offset up to a three day offset depending on the season and precipitation organization. In the winter, the strongest all and MCS precipitation-discharge correlations occur with a one day offset ($r_{all=0.}$45, p<0.01; r_{mpf}=0.53, p<0.01) and there were no significant wintertime isolated precipitation-discharge correlations. In the spring, a three day offset corresponds to the strongest all and MPF precipitation-discharge correlations (r_{all}=0.33, p<0.01; r_{mcs}=0.262, p<0.01). In the summer (r_{all}=0.34, p<0.01; r_{mpf}=0.405, p<0.01) and fall (r_{all}=0.40, p<0.01; r_{mpf}=0.60, p<0.01), these precipitation-discharge correlations are strongest with a two day offset. Again, for spring, summer, and fall, there are no significant correlations between isolated precipitation and discharge.

In the Lumber watershed, the precipitation-discharge correlations are much weaker across the board. Additionally, it is much harder to identify a typical time offset where the strongest correlations occur (Table 11). In the winter months, significant correlations exist for all daily offsets with the strongest all precipitation-discharge correlations occurring around a ten day offset (r_{all}=0.34, p<0.01). The same is true for MPF precipitation-discharge correlations (r_{mpf}=0.50, p<0.01). Similar results are found in the fall, although strongest precipitation-discharge correlations occur with a nine day offset (r_{all}=0.54, p<0.01; r_{mpf}=0.52, p<0.01). These correlations are much different for the spring and summer months where there are no significant correlations in the spring and weak all precipitation-discharge correlations (r_{all}=0.18, p<0.01) in the summer with a six day offset. The isolated precipitation-discharge correlation results are either negative meaning the data is likely contaminated from past rain events or are not significant at the 99th percentile pursued in this study.

The Neuse watershed is similar to the Lumber watershed in that it is challenging to determine a typical time offset where the precipitation-discharge correlations are strongest (Table 12). In the winter months, significant correlations again exist for all daily offsets and the strongest correlations in the Neuse watershed occur with a 10 day offset (r_{all}=0.34, p<0.01) and an eleven day offset (r_{mpf}=0.45, p<0.01). This correlation is much different in the fall. The strongest precipitation-discharge correlations occur with a five day offset for both all (r_{all}=0.52, p<0.01) and MPF (r_{mpf}=0.59, p<0.01) precipitation-discharge correlations. Whereas the Lumber watershed either had no significant or very weak correlations between the spring and summertime precipitation and discharge, statistically significant correlations were present in the Neuse watershed. For all

precipitation, the correlations were strongest in the spring with a seven day offset (r_{all}=0.16, p<0.01) and in the summer with a five day offset (r_{all}=0.21, p<0.01). Similar correlations exist for MPF precipitation where the spring correlations are strongest with a seven day offset (r_{mpf}=0.23, p<0.01) and in the summer with a five day offset (r_{mpf-}=0.27, p<0.01). For isolated precipitation-discharge correlations, it was also found that the Neuse watershed yielded results that were either physically impossible or not significant at the 99th percentile.

4.3.3 Event-based Correlations

The previous analysis provided information regarding the general correlations and potential time lags between precipitation events and discharge event. However, annual correlations were slightly weaker than may be expected, suggesting that there may be too much noise when analyzing all four years of data. Additionally, seasonal correlations were often inconclusive in identifying the typical time lags between rain events and discharge events experienced in each of the watersheds. The following event-based analysis hones in on ideal events where there seem to be obvious connections between precipitation and discharge as a means to better understand the precipitation-discharge correlations. These ideal events where characterized by little or no rain prior to a rain event, then a rain event occurs with an associated discharge response within 12 days and little to no rain occurs between the main rain event and the discharge. Table 21 shows the number of ideal events that were selected from each watershed while Appendix B provides a full list of the event dates selected for each watershed.

All Events	French	Broad	Yadkin	Lumber	Neuse
Number of Events	39	19	18	5	12
DJF Degrees of Freedom (N-2)	59-73	43-56	30-42	39	21-31
MAM Degrees of Freedom (N-2)	130-136	70-71	60-61	22-24	74-75
JJA Degrees of Freedom (N-2)	28-34	0-1	13	13-14	24-25
SON Degrees of Freedom (N-2)	50-58	15	13	N/A	30-32

Table 21. Number of all rain events included in event-based analysis. Range of degrees of freedom represents the range from day 0 offset to day +12 offset.

4.3.4 Annual Event-based Correlations

In the annual event-based analysis, we find similar results as found in the full four year dataset annual analysis, although, the signals are more apparent in these event-based analyses (Tables 13-20). In the French Broad and Broad watershed, the strongest all precipitation-discharge correlations (r_{all}=0.44, p<0.01 & r_{all}=0.58, p<0.01) occur with a one day offset. The Yadkin-Pee Dee experiences the strongest all precipitation-discharge correlation (r_{all}=0.33, p<0.01) with a two day offset. In this analysis, there were no significant correlations found in the Lumber watershed. As for the Neuse, the strongest correlation for all precipitation-discharge correlations occurred with a seven day offset (r_{all}=0.21, p<0.01).

Similar results hold true for MPF precipitation-discharge correlations. The French Broad and Broad watersheds have the strongest precipitation-discharge correlations with a one day offset (r_{mpf}=0.46, p<0.01 & r_{mpf}=0.57, p<0.01). The Yadkin-Pee Dee finds that its strongest correlations occur with a two day offset (r_{mpf}=0.36, p<0.01). Again, there were no significant correlations found in the Lumber watershed. As for the Neuse

watershed, a seven day offset produced the strongest precipitation-discharge correlations (r_{mpf}=0.37, p<0.01).

For isolated precipitation-discharge correlations, only the Broad watershed resulted in a potentially realistic correlation with a one day offset (r_{iso}=0.25, p<0.01).

4.3.5 Seasonal Event-based Correlations

These event-based correlations get especially interesting when broken down seasonally. In the French Broad watershed, seasonal differences between all precipitation-discharge correlations and MPF precipitation-discharge correlations are not as substantial as the seasonal contrasts in the isolated precipitation-discharge correlations. For all rain, strongest correlations occur with a one day offset for all seasons (DJF: r_{all}=0.50, p<0.01; MAM: r_{all}=0.36, p<0.01; JJA: r_{all}=0.46, p<0.01; SON: r_{all}=0.55, p<0.01). The same offset is true for MPF precipitation-discharge correlations (DJF: r_{mcs}=0.51, p<0.01; MAM: r_{mpf}=0.34, p<0.01; JJA: r_{mpf}=0.43, p<0.01; SON: r_{mpf}=0.55, p<0.01). Shifting focus to isolated precipitation-discharge correlations, the only significant correlations occur during the spring months. This isolated-precipitation discharge correlation is strongest with a two day offset (r_{iso}=0.32, p<0.01).

Before discussing the results from the Broad watershed precipitation-discharge correlations, it should be noted that there were inadequate ideal events in the summer months to produce precipitation-discharge correlations (Table 17). However, there was sufficient data to provide useful information for all other seasons. Similar to the full dataset analysis, the strongest all precipitation-discharge correlations occur with a one day offset (DJF: r_{all}=0.64, p<0.01; MAM: r_{all}=0.64, p<0.01; JJA: r_{all}=0.64, p<0.01; SON: r_{all}=0.78, p<0.01). MPF precipitation-discharge correlations show a similar pattern with a

one day offset (DJF: r_{mpf}=0.62, p<0.01; MAM: r_{mpf}=0.61; SON: r_{mpf}=0.79, p<0.01). Possibly more interesting are the much stronger isolated precipitation-discharge correlations in the winter (r_{iso}=0.57, p<0.01) and spring (r_{iso}=0.43, p<0.01) with a one day offset compared to the full dataset analysis.

Correlations in the Yadkin-Pee Dee watershed are slightly different in this event-based analysis compared to the full four year dataset (Tables 10 & 18). The strongest all and MPF precipitation-discharge correlations are associated with a two day offset in the winter ($r_{all=0.}$47, p<0.01; r_{mpf}=0.47, p<0.01) and in the fall ($r_{all=0.}$75, p<0.01; r_{mpf}=0.76, p<0.01). In the summer, the strongest correlations correspond to a one-day offset (r_{all}=0.71, p<0.01; r_{mpf}=0.71, p<0.01). Again, for spring, summer, and fall, there are no significant correlations between isolated precipitation and discharge.

As with the Broad watershed, the Lumber watershed does not have enough ideal events to produce correlations for any of the precipitation modes of organization in the fall. Additionally, there are inadequate ideal events to produce correlations at a 99 percent significance level for all other seasons in this seasonal event based analysis.

While in a similar situation, the Neuse watershed did provide some interesting information regarding the fall all precipitation and MPF precipitation-discharge correlations (Table 20). The results from this event based analysis suggest that a five day offset corresponds to the strongest correlations (r_{all}=0.55, p<0.01; r_{mpf}=0.55, p<0.01), although it should be noted that these correlations are relatively strong from the four day offset through the ten day offset.

Chapter 5

Discussion of Results

The following section will expand on the results from both the full dataset and the event-based analyses, and will provide suggestions for reasons why there is so much spatial and temporal variability found in the precipitation-discharge correlations. The focus of this section will be on three potential influential factors including: (1) the characteristics of the watershed, (2) the seasonal distribution of the precipitation, and (3) the precipitation organization from which the precipitation originated.

5.1 Watershed Characteristics

The French Broad and the Broad watersheds have some of the strongest correlations with the shortest time lags. Both of these watersheds also happen to be located in the mountains region of North Carolina (Fig. 6). This mountainous terrain results in increased isolated convection, especially in the summer (Fig. 20), due to the enhanced low level instability and orographic uplift. This likely plays into why these watersheds are the only two out of the five in the current study that have statistically significant correlations between isolated precipitation and discharge. However, other characteristics in these mountainous watersheds must be influencing this correlation because a strong correlation between isolated precipitation and discharge is also found in the fall for the French Broad watershed and in the winter for the Broad watershed. Additionally, the relatively strong MPF precipitation-discharge correlations and short time lags between MPF precipitation and discharge in these two watersheds is likely

influenced by the high concentration of impermeable rocks and steep terrain, both of which decrease water infiltration and increase precipitation runoff.

Precipitation-discharge correlations are weaker in the Piedmont watershed--the Yadkin-Pee Dee--and there is also a longer time lag between rain events and the associated discharge. This watershed has less relief than the prior two mountainous watersheds (Fig. 7). Therefore, terrain is not as much of a factor in the enhancement and acceleration of precipitation runoff, although the Yadkin-Pee Dee does have greater concentrations of developed lands and agricultural lands (Fig. 11). The impermeable and packed surfaces, along with the loss of friction due to the loss of vegetation, enhance precipitation runoff and decrease rainwater infiltration (Hollis 1975, USDA NRCS 1986). In addition, the Yadkin-Pee Dee watershed has a relatively high concentration of clay in its soil (Fish et al. 1957) which also resists rainwater infiltration and therefore enhances runoff. The combination of these factors not only reflects why the Yadkin-Pee Dee watershed has a longer time lag between a rain event and discharge than the mountainous watersheds, but also why this time lag is not as long as the coastal watersheds.

The two coastal watersheds, the Lumber and the Neuse, have very interesting time lags associated with the precipitation-discharge correlations. While there is a specific time lag where the precipitation-discharge correlation associated with each watershed is strongest, the precipitation-discharge correlation is still significant for several days prior to and following the lag time with the highest correlation. This was a curious finding, although one that can be explained by the characteristics of these two watersheds. Both have much sandier soils that allow for greater rainwater infiltration.

Additionally, both watersheds have very little relief and are nearly flat (Fig. 7). These two factors contribute to less runoff, greater rain water infiltration, and slower progression of rainwater through the stream network. Moreover, an interesting contrast exists between these two coastal watersheds. The Neuse watershed typically had less of a time lag than the Lumber watershed. This is surprising because, as shown in Table 2, the area of the Lumber watershed in this study is substantially less than the Neuse watershed. A potential reason for this discrepancy is the greater concentration of developed lands in the Neuse watershed (Fig. 13), than in the Lumber watershed (Fig. 12). Therefore, the Neuse watershed has a greater concentration of impermeable surfaces (Table 3) which enhance runoff and could decrease the time lag in the Neuse watershed.

5.2 Seasonal Precipitation Distributions

It has been shown by Konrad (1996) that seasonal analyses of correlations between precipitation and surface characteristics can conclude much different results than annual analyses. This was expected and was also found in the current study. Reasons for these differences between seasonal and annual analyses likely result from seasonal changes in patterns of atmospheric circulation and heating. Additionally, we know that the type of precipitation and the modes of precipitation organization activity from which this precipitation originates has strong seasonal variability. The question that remains in the current study is whether this seasonal variability in precipitation-discharge correlations could also be a product of the changes in where the precipitation falls within the watershed throughout the year. Figure 27 provides some insight into this question.

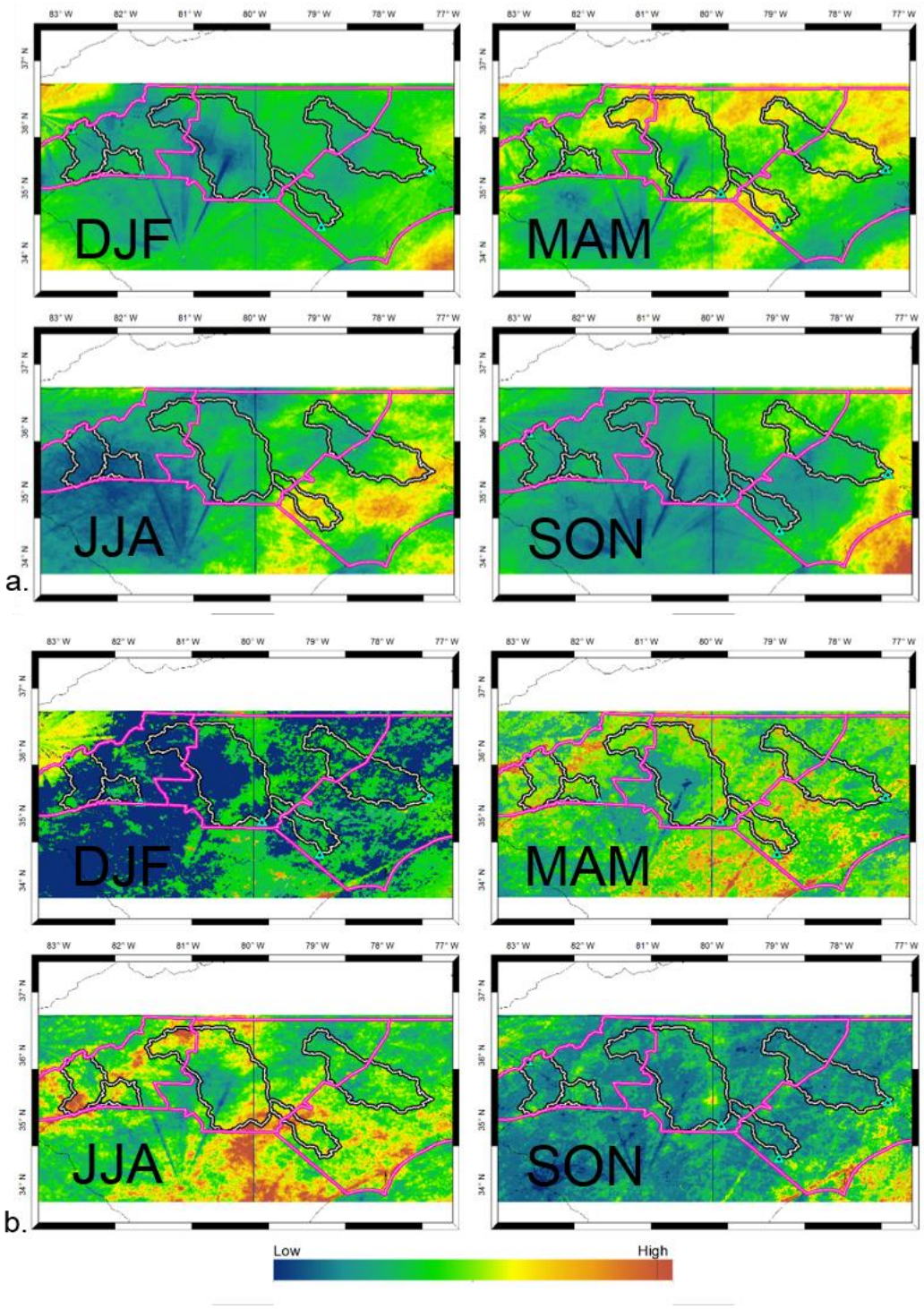

Figure 27. Weighted seasonal composites of daily precipitation contributions from either MPF or isolated precipitation where (a) is MPF precipitation and (b) isolated precipitation

Figure 27 takes into account both how much daily average precipitation occurs as well as how often it rains at each pixel. This weights the composite reflectivity images so that an area that experiences a single, heavy rain event (e.g. tropical cyclone landfall) will have a similar appearance to an area that experiences many lighter rain events throughout the year. Therefore, Figure 27a provides some extra insight into how much and how often rain is occurring at each pixel and gives some idea about seasonal precipitation patterns across North Carolina. Some other features, like radar beam blockage effects, are more obvious in this image.

For MPF precipitation, distinct seasonal patterns of precipitation distributions across North Carolina become apparent. In the winter, the distribution is fairly homogenous. In the spring, there are areas of greater MPF precipitation activity in the northern portions of the Yadkin-Pee Dee and Neuse watersheds. There is also increased MPF precipitation activity over the Lumber watershed. In the summer and fall, enhanced MPF precipitation activity appears to be shifted to the coastal regions. This enhanced MPF precipitation activity actually occurs in the southeastern portion of the Lumber and Neuse watersheds, closer to the location of these watersheds' stream gauges. Examining both figure 27a and the correlations for these coastal watersheds (Tables 11, 12, 19 & 20) helps to explain why these two watersheds experience a shorter precipitation-discharge time lag in the fall than they do in the winter.

The enhanced isolated precipitation due to orographic lift in WNC is apparent in the summer (Fig. 27b). This enhanced summer precipitation in the mountains region may help explain why the French Broad and Broad watersheds have significant isolated precipitation-discharge correlations in the summer. It is also interesting to examine the

Broad watershed in Figure 27b along with the strong precipitation-discharge correlations found in the Broad (Tables 9 & 15). In JJA, Figure 27b identifies two regions of enhanced weighted daily precipitation in the western portion of the Broad watershed. Keeping this in mind and looking back at Figure 10, these enhanced regions of weighted daily precipitation seem to coincide with two of the large open water sources in the watershed. The potential thermodynamic relationship between the two is beyond the scope of this study, but does suggest that more of the isolated precipitation during the summer in the Broad watershed occurred over open water and therefore fed directly into the stream network to the stream gauge station. Even so, the surface and soil characteristics are likely a greater player in these precipitation-discharge correlations because Figure 27b alone cannot explain why the French Broad and Broad watersheds have strong precipitation-discharge correlations in winter despite less amounts of isolated precipitation than in the summer. This conclusion is consistent with Hewlett et al. (1977) that land surface characteristics dominate hydrological response.

5.3 Precipitation Organization Characteristics

It is quickly apparent looking at these previous precipitation-discharge correlations (Tables 5-20) that MPF precipitation-discharge correlations are typically stronger than isolated precipitation-discharge correlations. This contradicts the initial hypothesis of this project that isolated precipitation would produce sharper discharge peaks due to the substantial precipitation they produce over a short period leading to greater amounts of runoff. While contrasting initial expectations in this study, this result does concur with results found by Hewlett et al. (1977) suggesting that storm intensity is not an important contributor when assessing stream flow. Therefore, the longer duration

and greater total storm precipitation from MPF events likely explains why MPF precipitation-discharge correlations are typically stronger than isolated precipitation-discharge correlations.

Chapter 6

Conclusions

This thesis presented the process of constructing a new precipitation organization dataset for the Southeastern United States, the integration of this dataset into a GIS framework, and an analysis of North Carolina watershed precipitation-discharge correlations to study how two different modes of precipitation organization influence regional hydrology.

The main goal of this study was to assess whether it was of hydrological importance to separate precipitation based on its storm origination, either MPF or isolated storms. To investigate this question, a methodology for bringing netCDF formatted meteorological data into a GIS framework was developed. This methodology was used to convert a 4-year climatology of precipitation organization into GIS format so that it could be used in a more interdisciplinary scope. Using ArcGIS, annual and seasonal precipitation distributions were examined across the Southeast U.S. and across North Carolina. Because seasonal differences were apparent in MPF and isolated precipitation composites, and due to the drastic differences between MPF and isolated daily average precipitation, the value in separating these two modes of precipitation organization for a hydrological application in North Carolina was assessed.

Results from this work support past literature suggesting that watershed characteristics cause the greatest variations to precipitation-discharge correlations. This is first shown through the strengths and general pattern of the correlations in the watersheds. Where the French Broad (r_{all}=0.39) and Broad (r_{all}=0.44) watersheds experience relatively strong correlations with a one to two day offset, the Lumber

watershed has a relatively weak correlation (r_{all}=.11) that stays fairly consistent from a seven day up to a twelve day offset. This is similar in the Neuse watershed where relatively weak correlations (r_{all}=0.21) are similar from a four day up to a ten day offset. The main differences between these four watersheds include the topography and the soil composition. The French Broad and Broad watersheds are mountainous and therefore have steep slopes which help accelerate runoff. Additionally, the soils resist rainwater infiltration due to the high concentration of rock. In contrast, the Lumber and Neuse watersheds are coastal watersheds and therefore are relatively flat. This allows more time for rainwater to infiltrate the surface. Aiding in this infiltration of rainwater are the much sandier and pervious soils. The mountain watershed characteristics act to accelerate runoff and decrease time lags between rain events and discharge response, whereas the coastal watershed characteristics promote a much slower and gradual response between rain events and the discharge response leading to the long, drawn out time lags.

It was also determined that daily total discharge is dependent more on MPF precipitation than isolated precipitation. This is exemplified by the correlations for all of the watersheds where, besides the mountain watersheds, there are no significant isolated precipitation-discharge correlations. The mountainous watersheds further exemplify this conclusion in the seasonal analyses. In the summer, the majority of total precipitation for both the French Broad and Broad watersheds originated from isolated convection (Fig. 16). This is the opposite in the winter for the two watersheds when the majority of total precipitation comes from MPF events. Correlations comparing these two seasons shows that the stronger correlations occur in the winter for both the

watersheds, and that for all seasons the correlations for the total precipitation are most similar to the MPF precipitation-discharge correlations. This contrasts initial expectations that isolated precipitation would produce the stronger correlations with a shorter time lag. However, this result does support past literature that suggests the intensity of the precipitation is not as important as other variables, like precipitation duration, in explaining the discharge response.

The scale of this analysis is likely too broad to analyze the more localized nature of isolated convection. It is therefore suggested that future work investigate at higher time and space resolutions (e.g. county level) to assess the potential differences in MPF precipitation-discharge and isolated precipitation-discharge correlations. This would be best accomplished with well-chosen case studies. It would also be advantageous to investigate differences in runoff characteristics between these two modes of precipitation organization at a higher resolution.

Another factor not considered in the current study, but one that could have an important impact on watershed discharge, is the antecedent moisture of the watershed. This preexisting wetness or dryness of the watershed can have important implications for the flow response of the stream network. Therefore, precipitation-discharge correlations may be better explained if antecedent moisture has been taken into account.

While the current four year dataset may not be sufficient to assess potential long-term hydrological differences between these two modes of precipitation organization it is expected that this dataset will be extended, potentially back to 1996. This extended dataset will allow future work to assess with more rigor the seasonal

variations, interannual variations, precipitation-discharge correlations, and potential connections with the modes of precipitation organization.

The results from this work provide important information that can be used in future hydrological applications. Understanding that MPF precipitation drives the precipitation-discharge correlations may lead to better assessment of seasonal water availability based on our knowledge of the total seasonal precipitation contributions from each precipitation organization. For example, the decreased MPF activity and increased isolated activity in the summer suggests decreased stream discharge and potentially decreased summertime water availability. The finding that watershed characteristics have a greater impact on precipitation-discharge correlations than the location, type, and total precipitation is important in land use decisions. This work shows that increases in impervious surfaces will likely increase runoff and stream discharge by decreasing the ability for rain water to infiltrate the surface. Therefore, it is imperative to consider the type and location of future development in the context of its potential implications on the hydrology of the watershed.

The next steps of this work will build upon these initial precipitation-discharge results by using the climatology of precipitation organization to better assess flood risk. With this climatology of precipitation organization, flood risk assessments for different watersheds across the Southeast U.S. can be conducted. This could provide additional information regarding what areas are prone to flooding beyond our current knowledge base by producing seasonal flood risk maps. Because it has been shown in the current study that there are differences in precipitation-discharge correlations between MPF and isolated events, seasonal flood risk maps should also include the separation of

MPF and isolated precipitation. This new approach to composited flood risk mapping could aid in the assessment of flood prone areas based on season and daily precipitation characteristics.

Overall, the current study provides a methodological platform and a new GIS-based precipitation organization climatology that will be a valuable resource for future interdisciplinary work. This methodology provides insight into new ways of bringing meteorological information into a GIS framework and synthesizing meteorological data into a more interdisciplinary realm by overcoming the challenges of integrating NetCDF data into ArcGIS. The ability to correctly display the climatology of precipitation organization in ArcGIS opens up new research avenues to a greater variety of end users. Results from this work support much of what has been found in past literature, but also introduce new information about the different hydrological impacts MPF and isolated storms have on North Carolina watersheds. This work will be beneficial to a variety of applications including water resource management, agriculture planning, hydrologic prediction, climate prediction, and hazards mitigation. Additionally, this work has demonstrated how the use of GIS in meteorological research aids in the interdisciplinary nature of the research by extending the applicability and reach of the work.

REFERENCES

Adler, R. F., G. Gu, and G. J. Huffman, 2011: Estimating climatological bias errors for the global precipitation climatology project (GPCP). *J. Appl. Meteor. Climatol.,* **51**, 84-99.

Amatya, D. M., G. M. Chescheir, R. W. Skaggs, and G. P. Fernandez, 2002: Hydrology of poorly drained coastal watersheds in eastern North Carolina. *Proc. ASAE/CIGR Congress Annual Intl Meeting.*

----------, G. Sun, R. Skaggs, G. Chescheir, and J. Nettles, 2006: Hydrologic effects of global climate change on a large drained pine forest. Proc. Proceedings of the International Conference, 12.

Ashley, S. T., W. S. Ashley, 2008: Flood fatalities in the United States. *J. Appl. Meteor. Climatol.,* **47**, 805-818.

Austin, P. M., 1987: Relation between measured radar reflectivity and surface precipitation. *Mon. Wea. Rev.,* **115**, 1053-1070.

Baigorria, G., J. W. Jones, and J. J. O'Brien, 2007: Understanding precipitation spatial variability in southeast USA at different timescales. *Int. J .Climate.,* **27**, 749-760.

Baik, J., Y. Kim, and H. Chun, 2001: Dry and moist convection forced by an urban heat island. *J. Appl. Meteor.,* **40**, 1462-1475.

Basist, A., G. D. Bell, and V. Meentemeyer, 1994: Statistical relationships between topography and precipitation patterns. *J. Climate,* **7**, 1305-1315.

Biemans, H., R. Hutjes, P. Kabat, B. Strengers, D. Gerten, and S. Rost, 2009: Effects of precipitation uncertainty on discharge calculations for main river basins. *J. Hydrometeorol*., **10**, 1011-1025.

Bjerknes, J., 1919: On the structure of moving cyclones. *Mon. Wea. Rev*., **47**, 95-99.

Bleasdale, A., & Chan, Y. K. 1972: Orographic influences on the distribution of precipitation. *Distribution of precipitation in mountainous areas*, ***2***, 322-332.

Boyles, R. P., S. Raman, 2003: Analysis of climate trends in North Carolina (1949-1998). *Environ. Int.*, **29**, 263-275.

Brooks, H. E., D. J. Stensrud, 2000: Climatology of Heavy Rain Events in the United States from Hourly Precipitation Observations. *Mon. Wea. Rev.,* **128**, 1194-1201.

Browning, K. A., 1985: Conceptual models of precipitation systems. *ESA Journa*l (ISSN 0379-2285), **9**, 157-180.

----------,N. M. Roberts, 1994: Structure of a frontal cyclone. *Q. J. R. Meteor. Soc*., **120**, 1535-1557

Brunsdon, C., S. Fotheringham, and M. Charlton, 1998: Geographically weighted regression. *Journal of the Royal Statistical Society: Series D (The Statistician)*, **47**, 431-443.

Carlson, T. N., 1980: Airflow through midlatitude cyclones and the comma cloud pattern. *Mon. Wea. Rev*., **108**, 1498-1509.

----------, S. Traci Arthur, 2000: The impact of land use—land cover changes due to urbanization on surface microclimate and hydrology: a satellite perspective. *Global Planet Change,* **25**, 49-65.

Chang, K., 2012: Introduction to geographic information systems. McGraw-Hill New York.

Chen, F., R. Avissar, 1994: Impact of land-surface moisture variability on local shallow convective cumulus and precipitation in large-scale models. *J. Appl. Meteor.,* **33**, 1382-1401.

Chen, T.-C., S.-Y. Wang, M.-C. Yen, and A. J. Clark, 2008: Are tropical cyclones less effectively formed by easterly waves in the western North Pacific than in the North Atlantic? *Mon. Wea. Rev.,* **136**, 4527–4540.

Churchill, D. D., R. Houze, 1984: Development and structure of winter monsoon cloud clusters on 10 December 1978. *J. Sci.,* **41**, 933-960.

Córdova, J. R., I. Rodríguez-Iturbe, 1985: On the probabilistic structure of storm surface runoff. *Water Resour. Res*., **21**, 755-763.

Cova, T. J., 1999: GIS in emergency management. *Geographical information systems*, **2**, 845-858.

Cunningham, R. M. 195I: Some observations of natural precipitation processes. **32**, 334-343

Curriero, F. C., J. A. Patz, J. B. Rose, and S. Lele, 2001: The association between extreme precipitation and waterborne disease outbreaks in the United States, 1948-1994. *Am. J. Public Health*, **91**, 1194-1199.

Curtis, S., 2006: Developing a climatology of the south's ‘other' storm season: ENSO impacts on winter extratropical cyclogenesis. *Southeastern Geographer*, **46**, 231-244.

Curtis, S., T. W. Crawford, and S. A. Lecce, 2007: A comparison of TRMM to other basin-scale estimates of precipitation during the 1999 Hurricane Floyd flood. *Nat. Haz.,* **43**, 187-198.

Davis, R. E., R. Dolan, 1993: Nor'easters. *Am. Sci.* 428-439.

Eichler, T., W. Higgins, 2006: Climatology and ENSO-related variability of North American extratropical cyclone activity. *J. Climate.,* **19**, 2076-2093.

Emanuel, K., 2003: Tropical cyclones. *Annu. Rev. Earth Planet Sci.,* **31**, 75-104.

Epstein, E. S., A. G. Barnston, 1990: A precipitation climatology of 5-day periods. *J. Climate*, **3**, 218-236.

Field, P. R., R. Wood, 2007: Precipitation and cloud structure in midlatitude cyclones. *J. Climate*, **20**, 233-254.

Fish, R. E., H. E. LeGrand, and G. A. Billingsley, 1957: Water Resources of the Yadkin-Pee Dee River Basin, North Carolina. US Government Printing Office,

Geerts, B., 1998: Mesoscale convective systems in the southeast United States during 1994-95: A survey. *Wea. For*, **13**, 860-869.

Goel, N., R. Kurothe, B. Mathur, and R. Vogel, 2000: A derived flood frequency distribution for correlated precipitation intensity and duration. *J. Hydrology*, **228**, 56-67.

Goldenberg, S. B., C. W. Landsea, A. M. Mestas-Nunez, and W. M. Gray, 2001: The recent increase in Atlantic hurricane activity: Causes and implications, *Science*, **293**, 474–479.

Gourley, J. J., Y. Hong, Z. L. Flamig, L. Li, and J. Wang, 2009: Intercomparison of precipitation estimates from radar, satellite, gauge, and combinations for a season of record precipitation*. J. Appl. Meteor. Climatol*., **49**, 437-452.

Graybeal, D. Y., D. J. Leathers, 2006: Snowmelt-related flood risk in Appalachia: first estimates from a historical snow climatology. J*. Appl. Meteor. Climatol.,* **45**, 178-193.

Guirguis, K. J., R. Avissar, 2008: A precipitation climatology and dataset intercomparison for the western United States. *J. Hydrometeor.,* **9**, 825-841.

Gunes, A., J. Kovel, 2000: Using GIS in emergency management operations. *J. Urban Plann. Dev*., **126**, 136-149.

Hewlett, J., J. Fortson, and G. Cunningham, 1977: The effect of precipitation intensity on storm flow and peak discharge from forest land. *Water Resour. Res.,* **13**, 259-266.

Hewlett, J., J. Fortson, and G. Cunningham, 1984: Additional tests on the effect of precipitation intensity on storm flow and peak flow from wild-land basins. *Water Resour. Res.,* **20**, 985-989.

Hollis, G., 1975: The effect of urbanization on floods of different recurrence interval. *Water Resour. Res.,* **11**, 431-435.

Horton, E., 2012: North Carolina Regional Vegetation. Ncpedia,

Houze, R. A., 1989: Observed structure of mesoscale convective systems and implications for large-scale heating. *Q.J.R. Meteor. Soc*., **115**, 425-461.

----------, 1993: *Cloud Dynamics*. Academic Press, San Diego, 573 pp.

----------, 1997: Stratiform precipitation in regions of convection: A meteorological paradox? *Bull. Amer. Meteor. Soc.,* **78**, 2179-2226.

----------, A., B. Smull, and P. Dodge, 1990: Mesoscale Organization of Springtime Rainstorms in Oklahoma. *Mon. Wea. Rev*., **118**, 613-654, doi:10.1175/1520-0493(1990)118<0613:MOOSRI>2.0.CO;2.

----------, P. V. Hobbs, 1982: Organization and structure of precipitating cloud systems. *Adv. Geophys.,* **24**, 225-315.

IPCC, 2007: Contribution of Working Group I to the Fourth Assessment Report of the Intergovernmental Panel on Climate Change. Solomon, S., D. Qin, M. Manning, Z. Chen, M. Marquis, K.B. Averyt, M. Tignor and H.L. Miller (eds.), Cambridge University Press, Cambridge, United Kingdom and New York, NY, USA.

Kalnay, E., M. Kanamitsu, R. Kistler, W. Collins, D. Deaven, L. Gandin, M. Iredell, S. Saha, G. White, J. Woollen, Y. Zhu, M. Chelliah, W. Ebisuzaki, W. Higgins, J. Janowiak, K. Mo, C. Ropelewski, J. Wang, A. Leetmaa, R. Reynolds, R. Jenne, and D. Joseph, 1996: The NCEP/NCAR 40-year reanalysis project. *Bull. Amer. Meteor. Soc*., **77**, 437-471.

Kane Jr, R., C. Chelius, and J. Fritsch, 1987: Precipitation characteristics of mesoscale convective weather systems. *J. Appl. Meteorol*., **26,** 1345-1357.

Kao, S., R. S. Govindaraju, 2007: Probabilistic structure of storm surface runoff considering the dependence between average intensity and storm duration of precipitation events. *Water Resour. Res*., **43**.

Keighton, S., L. Lee, B. Holloway, D. Hotz, S. Zubrick, J. Hovis, G. Votaw, L. B. Perry, G. Lackmann, and S. E. Yuter, 2009: A collaborative approach to study northwest flow snow in the southern Appalachians. *Bull. Amer. Meteor. Soc*., **90**, 979-991

Knight, D. B., R. E. Davis, 2009: Contribution of tropical cyclones to extreme precipitation events in the southeastern United States. *J. Geophys. Res*., **114**, D23102.

Konrad, C. E., 1996: Relationships between precipitation event types and topography in the Southern Blue Ridge Mountains of the southeastern USA. *Int. J. Climatol*., **16**, 49-62.

Krajewski, W. F., J. A. Smith, 2002: Radar hydrology: precipitation estimation. *Adv. Water Resour.,* **25**, 1387-1394, doi:10.1016/S0309-1708(02)00062-3.

Kucera, P. A., W. F. Krajewski, and C. B. Young, 2004: Radar beam occultation studies using GIS and DEM technology: An example study of Guam. *J. Atmos. Ocean Technol.,* **21**, 995-1006.

Kurothe, R., N. Goel, and B. Mathur, 1997: Derived flood frequency distribution for negatively correlated precipitation intensity and duration. *Water Resour. Res*., **33**, 2103-2107.

La Torre Torres, D. M. Amatya, G. Sun, and T. J. Callahan, 2011: Seasonal precipitation–runoff relationships in a lowland forested watershed in the southeastern USA. *Hydrol. Process.*, **25**, 2032-2045.

Leary, C. and R. A. Houze, 1979: The structure and evolution of convection in a tropical cloud cluster. *J. Atmos. Sci.,* **36,** 437-457.

Lu, J., G. Sun, S. G. McNulty, and D. M. Amatya, 2005: A comparison of six potential evapotranspiration methods for regional use in the southeastern United States. *J. American Water Res. Assoc.*, **41**, 621-633.

Markewich, H., M. Pavich, and G. Buell, 1990: Contrasting soils and landscapes of the Piedmont and Coastal Plain, eastern United States. *Geomorphology*, **3**, 417-447.

McCabe, G. J., M. P. Clark, and M. C. Serreze, 2001: Trends in Northern Hemisphere surface cyclone frequency and intensity. *J. Climate,* **14**, 2763-2768.

Mennis, J., 2006: Mapping the results of geographically weighted regression. *Cartographic Journal*, **43**, 171-179.

Miller, D. K., 2012: Near-term effects of the lower atmosphere in simulated northwest flow snowfall forced over the Southern Appalachians. *Wea. For.*, **27**, 1198-1216.

Missouri Stream Team Program, 2009: Chapter 3 Stream Discharge. Introduction to Volunteer Water Quality Monitoring Training Notebook, Anonymous.

Mote, T. L., D. W. Gamble, S. J. Underwood, and M. L. Bentley, 1997: Synoptic-scale features common to heavy snowstorms in the southeast United States. *Wea. For.*, **12**, 5-23.

Munroe, R., T. Crawford, and S. Curtis, 2013: Geospatial analysis of space–time patterning of ENSO forced daily precipitation distributions in the Gulf of Mexico. *The Professional Geographer*,

N.C.DENR Office of Environmental Education and Public Affairs, River Basin Interactive Map. [Available online at http://www.eenorthcarolina.org/riverbasins-interactive.html].

North Carolina Department of Public Instruction, "Geography of North Carolina," North Carolina Department of Public Instruction. [Available online at http://www.ncpublicschools.org/curriculum/socialstudies/elementary/studentsampler/20geography]. cited 2014

Naoum, S., I. Tsanis, 2004: Orographic precipitation modeling with multiple linear regression. *J. Hydrol. Eng*., **9**, 79-102.

Nesbitt, S. W., R. Cifelli, and S. A. Rutledge, 2006: Storm morphology and precipitation characteristics of TRMM precipitation features. *Mon. Wea. Rev.,* **134**, 2702-2721.

Nguyen, L. T., A. T. DeGaetano, 2011: A Climatology of 500-hPa Closed Lows and Associated Precipitation in the Northeastern United States. *J. Appl. Meteor*. Climatol. **51**, 3-15.

Nieto-Ferreira R., L. Hall, T.M. Rickenbach, 2013: A Climatology of the Structure, Evolution, and Propagation of Midlatitude Cyclones in the Southeast United States. *J. Climate*, **26**, 8406–8421.

Nunes Correia, F., F. Castro Rego, M. Da Grača Saraiva, and I. Ramos, 1998: Coupling GIS with hydrologic and hydraulic flood modelling. *Water Res. Manage*., **12**, 229249

Oki, T., S. Kanae, 2006: Global hydrological cycles and world water resources. *Science,* 313**,** 1068-1072

Overeem, A., I. Holleman, and A. Buishand, 2009: Derivation of a 10-year radar-based climatology of precipitation. *J. Appl. Meteor. Climatol.,* **48**, 1448-1463.

Palecki, M. A., J. R. Angel, and S. E. Hollinger, 2005: Storm precipitation in the United States. Part I: meteorological characteristics. *J. Appl. Meteor.,* **44**, 933-946.

Parker, M. D., D. A. Ahijevych, 2007: Convective episodes in the East-Central United States. *Mon. Wea. Rev.,* **135**, 3707-3727, doi:10.1175/2007MWR2098.1.

----------, R. Johnson, 2000: Organizational modes of midlatitude mesoscale connective systems. *Mon. Wea. Rev.,* **128**, 3413-3436.

Prat, O. P., & Nelson, B. R. (2013). Precipitation contribution of tropical cyclones in the southeastern United States from 1998 to 2009 using TRMM satellite data. *J. Climate,* **26(3**), 1047-1062.

Prudhomme, C., D. W. Reed, 1998: Relationships between extreme daily precipitation and topography in a mountainous region: a case study in Scotland. *Int. J. Climatol.,* **18**, 1439-1453.

Qi, S., G. Sun, Y. Wang, S. McNulty, and J. M. Myers, 2009: Streamflow response to climate and landuse changes in a coastal watershed in North Carolina. *Trans ASABE*, **52**, 739-749.

Rauber, R. M., L. S. Olthoff, M. K. Ramamurthy, D. Miller, and K. E. Kunkel, 2001: A synoptic weather pattern and sounding-based climatology of freezing precipitation in the United States east of the Rocky Mountains. *J. Appl. Meteor*., **40**, 1724-1747.

Rickenbach, T. M., R. Nieto-Ferreira, C. M. Zarzar, and B. Nelson, 2014: A seasonal and diurnal climatology of precipitation organization in the southeastern United States. *Submitted Quart. J. Roy. Meteor. Soc.*

----------, R. Nieto-Ferreira, R. P. Barnhill, and S. W. Nesbitt, 2012: Seasonal and regional differences in the precipitation and intensity of isolated convection over South America. *Int. J. Climate.*

----------, S. Rutledge, 1998: Convection in TOGA COARE: Horizontal scale, morphology, and precipitation production. *J. Atmos. Sci.,* **55**, 2715-2729.

Rowe, A. K., S. A. Rutledge, T. J. Lang, P. E. Ciesielski, and S. M. Saleeby, 2008: Elevation-dependent trends in precipitation observed during NAME. *Mon. Wea. Rev*., **136**, 4962-4979.

Rutledge, S. A., P. Hobbs, 1983: The mesoscale and microscale structure and organization of clouds and precipitation in midlatitude cyclones. VIII: A model for the “seeder-feeder” process in warm-frontal rainbands. *J. Atmos. Sci.,* 40, 1185-1206.

Schultz, D. M., C. F. Mass, 1993: The occlusion process in a midlatitude cyclone over land. *Mon. Wea. Rev*., **121**, 918-940.

Senkbeil, J., D. Brommer, I. Comstock, and T. Loyd, 2012: Hydrometeorological application of an extratropical cyclone classification scheme in the southern United States. *Theoretical and Applied Climatology*, **109**, 27-38.

Shepherd, J. M., A. Grundstein, and T. L. Mote, 2007: Quantifying the contribution of tropical cyclones to extreme precipitation along the coastal southeastern United States. *Geophys. Res. Lett*., **34**.

----------, H. Pierce, and A. J. Negri, 2002: Precipitation modification by major urban areas: Observations from spaceborne rain radar on the TRMM satellite. J. Appl. Meteor., **41**, 689-701.

----------, S. J. Burian, 2003: Detection of urban-induced precipitation anomalies in a major coastal city. Earth Interact., **7**, 1-17.

Shipley, S. T., 2005: GIS Applications in Meteorology, or Adventures in a Parallel Universe. *Bull. Amer. Meteor.* Soc., **86**, 171-173.

----------, I. A. Graffman, and J. K. Ingram, 2000: GIS applications in climate and meteorology. Proc. Proc., ESRI Annual User Conf.

Squires, M. F., 2010: Development a GIS Snowstorm Database. Proc. AGU Fall Meeting Abstracts, 1406.

Steiner, M., R. A. Houze, and S. E. Yuter, 1995: Climatological characterization of three-dimensional storm structure from operational radar and rain gauge data. *J. Appl. Meteor.,* **34**, 1978-2007.

Stensrud, D. J., H. E. Brooks, J. Du, M. S. Tracton, and E. Rogers, 1999: Using ensembles for short-range forecasting. *Mon. Wea. Rev*., **127**, 433-446.

Sui, C., C. Tsay, and X. Li, 2007: Convective–stratiform precipitation separation by cloud content. *J. of Geophysical* Research, **112**, D14213.

Sui, D. Z., R. C. Maggio, 1999: Integrating GIS with hydrological modeling: practices, problems, and prospects. *Comput. Environ. Urban Syst.,* **23**, 33-51.

Sun, G., A. Noormets, M. Gavazzi, S. McNulty, J. Chen, J. Domec, J. King, D. Amatya, and R. Skaggs, 2010: Energy and water balance of two contrasting loblolly pine plantations on the lower coastal plain of North Carolina, USA. *For. Ecol. Manage.,* **259**, 1299-1310.

Sun, X., and A. P. Barros, 2009: An Evaluation of the Statistics of Precipitation Extremes in Rain Gauge Observations, and Satellite-Based and Reanalysis Products Using Universal Multifractals. *J. Hydrometeor*, **11**, 388-404.

Thielen, J., W. Wobrock, A. Gadian, P. Mestayer, and J. Creutin, 2000: The possible influence of urban surfaces on precipitation development: a sensitivity study in 2D in the meso-γ-scale*. Atmos. Res*., **54**, 15-39.

U. S. Census Bureau, cited 2013: Population distribution and change, 2010 Census

U.S Census Bureau, 2011: 2010 census of population and housing, demographic profile summary file: Technical documentation.

United States Dept. of Agriculture, Natural Resource Conservation Service (USDA, NRCS). (1986). "Urban hydrology for small watershed, TR-55." Rep. No. PB87-101580, 2nd Ed., Springfield, Va.

United States Dept. of Agriculture, Natural Resource Conservation Service (USDA, NRCS). (2005). "Physical soil properties." Web soil survey, ⟨ http://websoilsurvey.nrcs.usda.gov/app/WebSoilSurvey.aspx ⟩ (July 12, 2005).

Vasic, S., C. A. Lin, I. Zawadzki, O. Bousquet, and D. Chaumont, 2007: Evaluation of precipitation from numerical weather prediction models and satellites using values retrieved from radars. *Mon. Wea. Rev*., **135**, 3750-3766.

Wallace, J. M., J. M. Wallace, and P. V. Hobbs, 2006: Atmospheric science: an introductory survey. Vol. **92**, Academic press.

Wilhelmi, O. V., J. C. Brunskill, 2003: Geographic Information Systems in Weather, Climate, and Impacts. *Bull. Amer. Meteor. Soc*., **84**, 1409-1414

----------, R. E. Morss, 2013: Integrated analysis of societal vulnerability in an extreme precipitation event: A Fort Collins case study. *Environ. Sci. Policy,* **26**, 49-62.

Wu, W., D. Kitzmiller, and S. Wu, 2012: Evaluation of radar precipitation estimates from the national mosaic and multisensor quantitative precipitation estimation system and the wsr-88d precipitation processing system over the conterminous United States. *J. Hydrometeor*., **13**, 1080-1093.

Xie, H., X. Zhou, E. R. Vivoni, J. M. Hendrickx, and E. E. Small, 2005: GIS-based NEXRAD Stage III precipitation database: automated approaches for data processing and visualization. *Comput. Geosci*., **31**, 65-76.

Yang, S., E. A. Smith, 2008: Convective-stratiform precipitation variability at seasonal scale from 8 years of TRMM observations: implications for multiple modes of diurnal variability*. J. Climate*, **21**, 4087-4114.

Yuan, M., 2005: Beyond Mapping in GIS applications to environmental analysis. Bull. *Amer. Meteor. Soc*., **86**, 169-170.

Zachary Bean, E., W. Frederick Hunt, and D. Alan Bidelspach, 2007: Evaluation of four permeable pavement sites in eastern North Carolina for runoff reduction and water quality impacts. J*.Irrig.Drain.Eng.,* **133**, 583-592.

Zhang, J., K. Howard, C. Langston, S. Vasiloff, B. Kaney, A. Arthur, S. Van Cooten, K. Kelleher, D. Kitzmiller, and F. Ding, 2011: National mosaic and multi-sensor QPE (NMQ) system: description, results, and future plans. *Bull. Amer. Meteor. Soc*., **92**, 1321-1338.

Zhang, X., R. Srinivasan, 2009: GIS-Based Spatial Precipitation Estimation: A Comparison of Geostatistical Approaches1. JAWRA *Journal of the American Water Resources Association*, **45**, 894-906.

APPENDIX A: ArcGIS Tools Developed

1. Convert NetCDF file to ASCII File

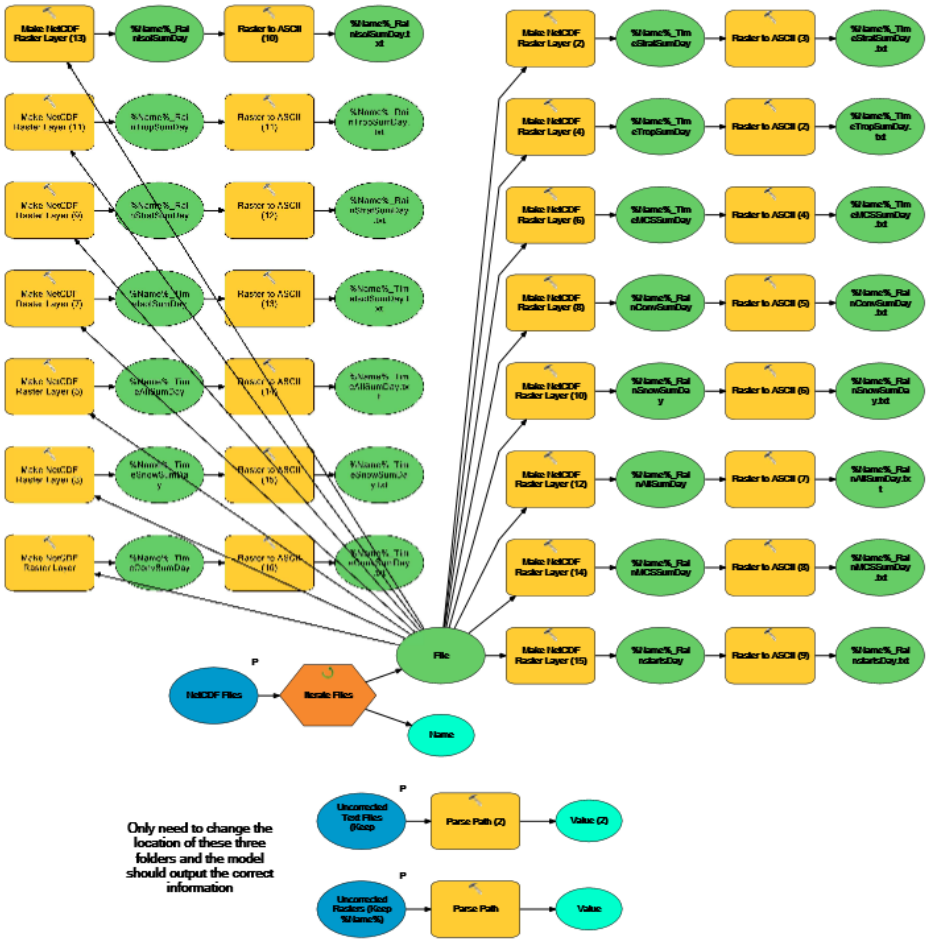

2. Convert ASCII File to Raster

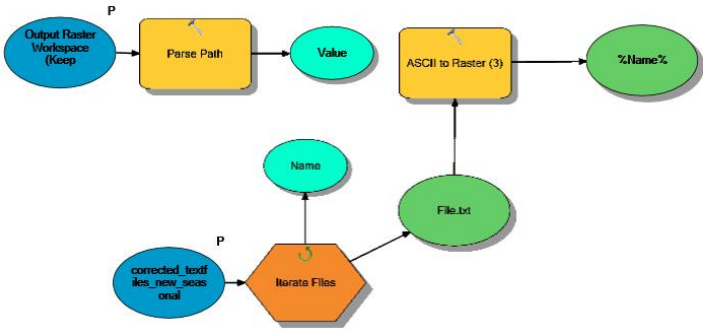

3. Reclassify Raster

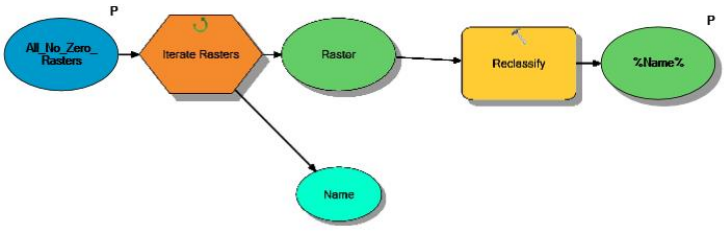

4. Regional Zonal Statistics

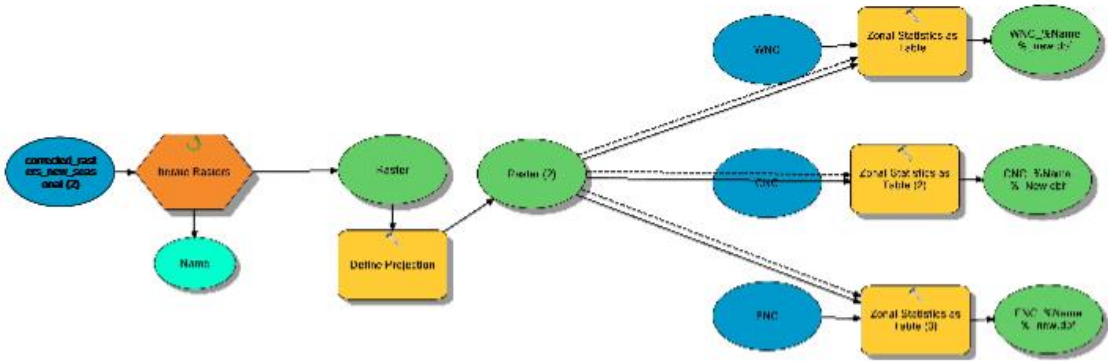

5. Watershed Zonal Statistics

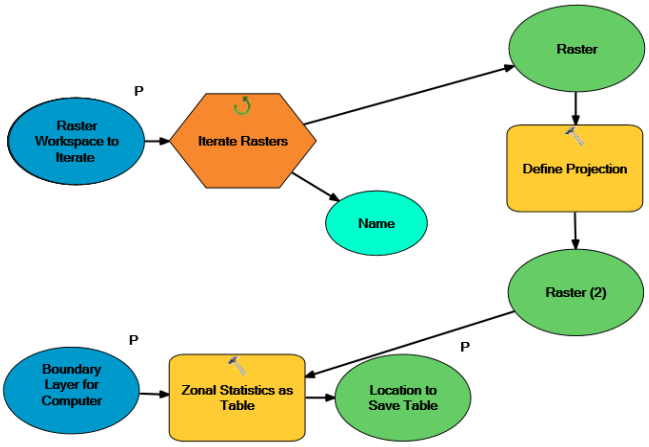

APPENDIX B: Event Based Analysis Dates

Events	French	Broad	Yadkin	Lumber	Neuse
1	1/4/2009 - 1/10/2009	1/4/2009 - 1/12/2009	1/3/2009 - 1/10/2009	2/25/2009 - 3/19/2009	1/3/2009 - 1/18/2009
2	2/25/2009 - 2/28/2009	2/24/2009 - 3/5/2009	2/24/2009 - 3/4/2009	12/23/2009 - 1/8/2010	2/26/2009 - 3/12/2009
3	12/6/2009 - 12/12/2009	12/6/2009 - 12/12/2009	12/6/2009 - 12/12/2009	2/3/2011 - 2/22/2011	2/4/2011 - 2/17/2011
4	12/23/2009 - 12/27/2009	12/22/2009 - 12/30/2009	12/24/2009 - 12/30/2009	5/27/2009 - 6/2/2009	5/5/2009 - 5/19/2009
5	1/14/2010 - 1/20/2010	1/13/2010 - 1/20/2010	1/24/2010 - 2/9/2010	6/13/2009 - 6/27/2009	3/1/2010 - 3/10/2010
6	2/3/2010 - 2/8/2010	1/23/2010 - 1/28/2010	3/23/2012 - 3/28/2012		3/29/2010 - 4/11/2010
7	1/31/2011 - 2/7/2011	2/4/2010 - 2/9/2010	3/13/2009 - 3/19/2009		3/1/2012 - 3/15/2012
8	12/3/2011 - 12/11/2011	1/9/2012 - 1/16/2012	3/24/2009 - 4/1/2009		3/22/2012 - 4/2/2012
9	12/19/2011 - 12/31/2011	3/23/2009 - 3/31/2009	4/9/2009 - 4/13/2009		6/14/2009 - 6/29/2009
10	1/9/2012 - 1/17/2012	4/7/2009 - 4/14/2009	3/9/2010 - 3/18/2010		7/3/2011 - 7/14/2011
11	3/1/2009 - 3/4/2009	5/27/2009 - 6/3/2009	3/28/2010 - 4/2/2010		9/23/2010 - 10/14/2010
12	3/14/2009 - 3/31/2009	3/8/2010 - 3/16/2010	5/16/2010 - 5/24/2010		11/2/2011 - 11/15/2011
13	4/1/2009 - 4/13/2009	3/27/2010 - 3/31/2010	5/13/2012 - 5/20/2012		
14	4/18/2009 - 4/24/2009	3/3/2011 - 3/8/2011	6/8/2012 - 6/16/2012		
15	5/27/2009 - 5/31/2009	3/9/2011 - 3/17/2011	7/27/2009 - 8/1/2009		
16	3/9/2010 - 3/20/2010	4/15/2011 - 4/20/2011	11/7/2009 - 11/15/2009		
17	3/21/2010 - 4/1/2010	5/10/2012 - 5/20/2012	9/28/2010 - 10/3/2010		
18	4/22/2010 - 5/6/2010	9/17/2009 - 9/23/2009			
19	3/4/2011 - 3/8/2011	11/7/2009 - 11/16/2009			
20	4/3/2011 - 4/7/2014				
21	4/14/2011 - 4/18/2011				
22	4/26/2011 - 5/1/2011				
23	4/1/2012 - 4/9/2012				
24	4/15/2012 - 4/22/2012				
25	4/24/2012 - 4/30/2012				
26	5/13/2012 - 5/19/2012				
27	6/1/2009 - 6/5/2009				
28	6/14/2009 - 6/25/2009				
29	6/14/2010 - 6/19/2010				
30	8/19/2010 - 8/26/2010				
31	6/17/2011 - 6/21/2011				
32	9/18/2009 - 9/30/2009				
33	10/26/2009 - 10/30/2009				
34	11/8/2009 - 11/17/2009				
35	9/25/2010 - 10/2/2010				
36	9/2/2011 - 9/9/2011				
37	9/21/2011 - 9/30/2011				
38	11/2/2011 - 11/7/2011				

Winter Spring Summer Fall